AN EXPERIMENTAL INVESTIGATION OF SURFACE IONIZATION

by

Miles Joel Dresser

A Dissertation Submitted to the
Graduate Faculty in Partial Fulfillment of
The Requirements for the Degree of
DOCTOR OF PHILOSOPHY

Major Subject: Physics

Approved:

Signature was redacted for privacy.

In Charge of Major Work

Signature was redacted for privacy.

Head of Major Department

Signature was redacted for privacy.

Dean of Graduate College

Iowa State University
Of Science and Technology
Ames, Iowa

1964

I. INTRODUCTION

A. Surface Ionization

When atoms or molecules are allowed to come into the proximity of the surface of a metal, a certain fraction of these atoms will give up or take an electron from the surface before being re-evaporated and thus become ions. This process of ionization of atoms in the presence of metal surfaces is known as surface ionization (SI). Studies of surface ionization have been made in both high and low electric fields. The high field studies are in fields of 10^6 volts/cm or greater (1,2). In the low field studies, the phenomena is found to be independent of the electric field and therefore the fraction of atoms converted into ions is studied as a function of surface temperature (3,4,5,6). This work will be restricted to the low field phenomena.

Several techniques exist for placing atoms in the vicinity of an incandescent surface. The atoms may be coated onto the surface before it is heated to incandescence. There may be atoms of a surrounding gas, or, as was done for this study, they may be part of a molecular beam directed onto the surface. After the ionization, a low electric field is applied externally to draw the ions from the surface to a collector, where the magnitude of the ion current can be measured to indicate the number of atoms that were ionized. In this work the hot surface was a thin metal ribbon and,

in order to get significant ion current, this ribbon was heated to somewhere between 1100-3300°K.

Surface ionization is characterized by a number α which is the ratio of the number of ions n_+ leaving the surface per second (or ion flux) to the flux n_o of neutral particles leaving the surface. The number α is called the degree of ionization $\alpha = n_+/n_o$. Another number frequently used to characterize SI is β, the ionization efficiency. This number is the ratio of n_+ to the flux of atoms impingent on the surface n:

(1) $$\beta = n_+/n.$$

Since $n = n_+ + n_o$, it follows that

(2) $$\beta = \alpha/(1 + \alpha).$$

If $\alpha << 1$, $\beta \approx \alpha$ and if $\alpha >> 1$ then $\beta \approx 1$.

B. Established Facts of Surface Ionization

1. Introduction

The phenomena of surface ionization was observed by Langmuir in 1923 (7) and explained in 1924 by Langmuir and Kingdon (3). The subsequent fifteen years produced many studies of the SI of the alkali metals, principally on tungsten. The two principal techniques of study were the bulb method (3,6,7) and the atomic beam method (5). The bulb method has the disadvantage that strong photoelectric currents mask the ion current at high temperatures. Kaminsky (8) has written an excellent review of SI including tables which

summarize most of the studies to date.

2. Major experimental contributions

Surface ionization has been studied heavily by Russian laboratories since 1945. Two excellent monographs on SI, particularly concerning the contributions of the Russians, have been written by Dobretsov (9), and Zandberg and Ionov (2). In studying the ionization of sodium on tungsten, Romanov and Starodubtsev (10) have demonstrated the need for high vacuum conditions. Zandberg and Ionov (2) have attempted to demonstrate the existence of thermal equilibrium and do so within the admittedly poor limits of error of their experiment. Zandberg and Ionov have further emphasized the necessity of using a more sophisticated approach to the interpretation of data taken from polycrystalline surfaces. Zemal has undertaken such an approach for SI by tungsten (11). Szhenov (12) has studied surface ionization of concurrent beams of the alkali earths on tungsten and oxidized tungsten.

In 1956, Datz and Taylor (13,14) began a series of publications on the surface ionization of alkalis and alkali salts on W, Pt, Pt + 8% W. They were primarily looking for reflections of alkali metals by the different surfaces. For tungsten there was zero reflection but they found very significant reflection coefficients for the alkali metals on platinum. Werning (15) established the existence of chemical effects which altered the atom or ion density near the surface

and which thus affected the measured ion current. Reynolds (16) has studied the ionization of calcium and strontium by single crystal surfaces and from the temperature dependence of the current he ascertained the work function of the crystal plane using the known ionization potential of calcium, assuming the theory of Langmuir to be correct. He then used this method to measure the ionization potential of strontium.

3. Applications

Until recent years, the process of surface ionization has been used primarily as a source of ions for mass spectrometric and ion beam studies. In the last decade, its application to ion propulsion and to thermionic conversion has also been recognized and much development is directed along these lines. A review of the use of SI in ion beam studies is given by Ramsey (17) and a review for mass spectrometry is given by Inghram and Hayden (18). Mueller (19) has given an excellent bibliography and review of SI and its application to ion propulsion. The application of SI to thermionic conversion can be found in a report by Cayless (20).

C. Theories of Surface Ionization

1. Thermodynamic derivation

Although the phenomena of SI has been used heavily for nearly three decades, it has only been in the last ten years that any effort has been made to extend the verification of

theory by experiment beyond the alkali-tungsten systems. However, some slight improvements have been made to the theory so that it is now applicable to a slightly more general system. The general theory was first proposed by Langmuir and Kingdon (3). They used the equilibrium constant of Saha (21) for a gaseous mixture of atoms, ions, and electrons inside a box whose walls had work function ϕ. They could then calculate the equilibrium density of electrons in this box using the Richardson equation for thermionic emission, and thereby determine the ratio of ion to atom densities in the box.

Saha derived the equilibrium constant by considering that the atoms, ions, and electrons satisfy a reaction equation of the form $R^+ + e^- \rightleftarrows R^\circ$. In this equation R^+ and R° represent the ion and atom respectively. The law of mass action was used to derive the ratio of densities of ions n_+ and electrons n_e, to that of atoms n_o. Saha's result was

$$\frac{n_+ n_e}{n_o} = \frac{g_+ g_e}{g_o} \frac{(2\pi mkT)^{3/2}}{h^3} e^{-eV/kT}, \tag{3}$$

where g_+, g_e, and g_o are the statistical weights of the ionic, electronic, and atomic states; m is the atomic mass; h is Planck's constant; V is the first ionization potential; k is the Boltzman constant; and T the absolute temperature of the surface. Now $g_e = 2$ and g_+ and g_o are given by (2J+1) or (2L+1)(2S+1) depending on how the fine structure splitting energies compare to the kT of the ionizing surface. For this

work (2J+1) is appropriate with some small corrections to be discussed later. Landau and Lifschitz discuss the effects of angular momentum and spin of particles in a perfect gas and their application to this problem in sections 46 and 103 of their book, Statistical Physics (22). Langmuir took this result of Saha and calculated the value of n_o by the following arguments: If a gas of electrons inside a box, whose walls have work function ϕ, is in equilibrium, the flux of electrons into the wall must equal that of the electrons leaving the wall. From kinetic theory the flux of electrons striking a wall is given by $(1/4)\, n_e(8kT/\pi m)^{1/2}$, so that the flux that passes into the wall is given by $n_e(1-R)(kT/2\pi m)^{1/2}$ where R is the reflection coefficient for electrons striking the surface. The flux out of the wall must be that given by the Richardson equation for thermionic emission,

$$J_o = (1-R)(4\pi mek^2T^2/h^3)e^{-e\phi/kT}. \tag{4}$$

In this equation J_o is the saturation current density for zero electric field. The flux from the surface is seen to be J_o/e. Langmuir then equates these two fluxes to yield

$$n_e = 2(2\pi mkT/h^2)^{3/2}\, e^{-e\phi/kT}, \tag{5}$$

which is then substituted into Equation 3 to arrive at the Saha-Langmuir equation:

$$\alpha = n_+/n_o = (g_+/g_o)\, e^{e(\phi-V)kT}. \tag{6}$$

of particle and surface. When the particle is inside the critical distance Dobretsov assumes that the valence electron states of the adatom become part of the electron states of the metal and as such their probability of occupation can be predicted by Fermi Dirac statistics. It is also assumed that at x_k the spreading (if any) of the valence energy level is not great enough for there to be any error in considering it as a single energy and that all effects due to the core of the atom can be ignored.

To begin Dobretsov first considers the case of an atom with a single valence electron. The probability that the adatom can cross x_k as an atom is then the probability that the valence energy level E_a of the atom is occupied. From Fermi Dirac statistics the probability that the energy level E_a is occupied is $W_o(E_a)$:

$$W_o(E_a) = (1+e^{(E_a-E_o)/kT})^{-1}. \tag{7}$$

In this equation E_o is the Fermi energy of the metal measured relative to the same zero as E_a. The probability that the adatom crosses x_k as an ion is the probability that the level E_a is empty, $W_+(E_a)$:

$$W_+(E_a) = 1-W_o(E_a) = (1+e^{-(E_a-E_o)/kT})^{-1}. \tag{8}$$

An atom can be formed in two ways since the electron can have either spin up or spin down whereas the ion can be formed in only one way. The ratio of probabilities that the adatom can exceed x_k as an ion or atom is therefore

surface is reduced by $e\Phi_m$ when the surface is located in an electric field. In terms of our problem $s_+ - s_+' = e(eF/4\pi\varepsilon_o)^{1/2}$. As long as the field is homogeneous there can be no force on the atoms so we conclude that $s_o - s_o' = 0$.

Next Dobretsov considers the case of a divalent atom which when adsorbed on the surface of a metal has two electrons interacting with the surface and their two energy levels can be considered as part of the Fermi sea of the metal. When the adatom has one of its electrons localized near it, it is also assumed that there is no shift in the energy level for the other electron. The probability that there is an electron in each of the states of the adatom as it crosses x_k is the probability that the adatom crosses x_k as an atom:

$$W_o = (1+e^{(E_a-E_o)/kT})^{-2}. \tag{14}$$

Similarly the probability that the adatom exceeds x_k as an ion is the product of the probabilities that one level is occupied and the other is empty:

$$W_+ = 2(1+e^{(E_a-E_o)/kT})^{-1}(1+e^{-(E_a-E_o)/kT})^{-1}. \tag{15}$$

The 2 is present here because one state may be occupied and the second empty or the first state empty and the second state occupied. If the electron states are labeled 1 and 2 we see that an atom can be formed in two ways: it can be formed if state 1 has an electron of spin up and state 2 has spin down or, alternately, if state 1 has spin down and state 2 has spin up. However, for the ion we see that it can also be

formed in two ways since the occupied electron state can have either spin up or down. Therefore when we take the ratio of probabilities for an ion to that of an atom for two electrons involved in the adsorption process the effect due to the degeneracy of the valence electrons cancels out. The ratio of the probabilities at x_k is then

$$(16) \qquad (2W_+/2W_o)_{x_k} = (n_+/n_o)_{x_k} = 2\, e^{(E_a-E_o)/kT}.$$

The arguments which were presented in the one electron case may now be repeated and we find that the ratio of ions to atoms escaping from the surface in the absence of electric fields is

$$(17) \qquad \alpha = (n_+/n_o) = 2\, e^{e(\phi-V)/kT}.$$

Dobretsov leaves the argument at this point presuming that the coefficients are the proper statistical weights of the states. Indeed these are identical with the numbers we might calculate using the rule of $g = 2J+1$ for the case of s electrons in the valence orbits and completely filled shells below but it is not obvious that the two coefficients will be identical in general.

This theory can also be generalized for the case of excited states and Dobretsov corrects Equation 2 by replacing the coefficient (g_+/g_o) with a number A where A is defined as,

$$(18) \qquad A = Q_+/Q_o,$$

where,

$$Q_+ = g_+ + \sum_j g_+^j \, e^{-E_+^j/kT},$$

and

$$Q_o = g_o + \sum_j g_o^j \, e^{-E_o^j/kT}.$$

In this equation g^j and E^j refer to the statistical weight of the j'th excitation and its corresponding energy measured relative to the ground state of the atom. We see that this equation reduces to (g_+/g_o) if $E^j >> kT$.

Because this theory is not based on first principles the only test of the many assumptions is a thorough experimental investigation of the implications of each.

3. Reflections

Attempts have been made to improve the theory of SI for the case of nonequilibrium by the insertion of reflection coefficients. Copley and Phipps (5) wrote α in the form

$$\alpha = (1-r_+)(1-r_o)^{-1} A \, e^{e(\phi-V)/kT}, \tag{19}$$

where r_+ and r_o are the reflection coefficients for the ions and atoms. Datz and Taylor (13) add a reflection coefficient to β to exclude those atoms which are immediately reflected from the surface without coming into equilibrium. The expression for β is then

$$\beta = (1-r_i)\alpha/(1+\alpha), \tag{20}$$

where α is given by Equation 19 and r_i is the fraction of

incident atoms which are reflected from the surface before coming into equilibrium. The r_+ and r_o reflection coefficients refer to reflections at the surface barrier for atomic and ionic binding. In the case of equilibrium in a box the flux of atoms and ions crossing the barrier and going on to the surface is equal to that leaving the surface and crossing the barrier into space. The fraction of ions or atoms reflected at this surface going one way must be equal to the fraction of reflected atoms or ions going the other way. In an experiment of this sort there are no atoms or ions going toward the surface that manifest a distribution of energies equal to that expected from a Boltzman distribution centered about the surface temperature. Whereas in the case of equilibrium the effect of reflection cancels out, in the case of low intensity beams the effects of reflection at the surface barrier must be included. This reflection approach does not completely eliminate problems imposed by an equilibrium based theory since we must still assume that the atoms and ions come into thermal equilibrium while inside the surface barrier, but it does at least provide a correction that must be included. Unfortunately the experimental knowledge of such parameters is not known for most systems. It should be pointed out that the potential well in which the atom or ion is bound to the surface has a shape which does not have a strong dependence on temperature; hence, one must be careful not to experimentally ascribe strong temperature dependent variations to a reflection

coefficient.

4. Critique of the theory

Thermodynamic equilibrium. Thermodynamic equilibrium, as has been indicated before, is the assumption to which the greatest consideration must be given before one applies this theory to a given situation. This is the only major point at which the use of the thermodynamic derivation can be questioned and is one of several points of question in the statistical mechanical derivation. The only effort known to this writer of an attempt to establish the validity of an equilibrium argument in an experimental situation is in the work reported by Zandberg and Ionov (2). Unfortunately the experimental errors in this effort were too large to allow a conclusive result although there was an indication that the alkali tungsten system involved in that experiment was in thermal equilibrium.

Other considerations. Other considerations must be made in reference to the statistical mechanical derivation. First of course are the assumptions of the theory that have been presented earlier: that one can predict the occupancy of the valence electron states with the Fermi Dirac distribution function for a noninteracting system of free electrons is open to much question, and the simplified model of an atom makes the application of this theory to the heavier atoms and particularly the transition elements very tenuous. The

other point of question comes in the fact that as the ions leave the surface they must pass through an electron cloud which at elevated temperatures could be quite dense. Rough calculations indicate that this electron cloud in our field must extend out from the surface about 10^{-4} cm. It would seem that the ion-electron collision cross section in this gas should be quite significant and therefore the ions could be converted to atoms long after crossing x_k (which must be in the order of 10^{-7} cm). Because of these assumptions the only verification of this theory must come from experiment and perhaps systems such as those studied here can lead to a proper explanation of surface ionization.

D. Background of This Work

1. Introduction

In this laboratory, surface ionization has been used as an ionizing mechanism for a mass spectrometer which was used in studies of the cohesive energies of the rare earths by the Knudsen effusion method. A description of this technique is given by Johnson (23, 24). In performing studies of this kind, it is necessary to assume that the ionization efficiency β does not depend on the flux, n, of incident atoms. The theory developed in the previous section predicts that the degree of ionization α is given by

$$\alpha = (g_+/g_o)\, e^{e(\phi - V)/kT}. \tag{6}$$

We see that the assumption that β is independent of n is good as long as the Saha-Langmuir equation is valid.

2. Previous surface ionization studies at Ames

In addition to the secondary efforts such as those reported by Johnson (24) an explicit investigation of SI was begun in this laboratory by Harold Fox (4). Fox studied the surface ionization of Dy, Er, Ho, and Eu by W and Ir surfaces. The result of this study showed that the Saha-Langmuir equation did not fit the data in either the low or high temperature regions. It now seems apparent that the phenomena that were observed in these experiments were due in part to inadequately good vacuum conditions (in the range of 1-50 x 10^{-6} Torr) and to an absence of control of the crystalline surface.

3. Absolute measurements of ionization efficiency

In most recent work on SI, the absolute value of β is not determined. The experimental quantity is a number proportional to β, where the proportionality constant is presumably not dependent on any parameters of the experiment (i.e. temperature, atom flux, ion flux, residual pressure, etc.). Such measurements will be referred to as relative ionization efficiency experiments. All of the work done thus far by this group has been measurement of relative ionization efficiencies. Measurements of this type can only be used to study the exponential dependence of β on 1/T and do not provide any

information on the nature of the coefficient $A = (g_+/g_o)$.

E. Objectives of This Investigation

Because of the strength of a theory based on equilibrium thermodynamics and its reasonable agreement with experiment for the alkali atom on tungsten systems there has been little question made of its applicability to the more complicated systems. As has been stated earlier, there are good reasons to doubt the use of such a theory in an experiment such as this one in which atomic beams are employed under conditions of low ionization efficiency. It was therefore felt that a careful examination of the phenomenon was necessary to determine if the theory was as generally applicable as has been thus far assumed. In making an investigation of this type it is imperative to make every effort to establish a clean and simple surface since these are the assumptions of the theory. For this reason, the experiments should be performed under ultra-high vacuum conditions. Efforts must be taken to detect the adsorption of contaminants and to remove them as often as is necessary. Polycrystalline surfaces should be avoided and plane single crystal surfaces should be used.

Because there is no indication that the general form of the Saha Langmuir equation is wrong the data will be analyzed in terms of the general equation:

(21) $$\beta = A\, e^{-e/kT}.$$

If the experiment verifies the Saha Langmuir equation then $A = Q_+/Q_o$ and $E = V-\phi$ and if not departures from these constants can be considered. Because of the interest in establishing the applicability of the theory, atoms should be chosen for which there is a reasonable knowledge of the electronic structure. The electronic work function of the surface should also be established by an independent experiment. With these parameters of the SI process determined by independent means we are thus in a better position to evaluate the applicability of Equation 6 under the experimental conditions actually employed.

II. EXPERIMENTAL APPARATUS

A. Introduction

The apparatus used in this experiment consisted of a mass spectrometer and associated equipment as shown schematically in Figure 1. The atoms whose ionization was to be studied were ionized in the source (S) and formed into a beam that traveled through a glass mass tube (T) into the mass analyzing magnetic field (M). The ions of interest were focused through the mass tube (T) into the collection chamber (C). The collected ions constituted a small direct current which was amplified by a vibrating reed electrometer system. The magnitude of the ion current was displayed by a Brown strip chart recorder. The mass analyzing magnetic field was of the type developed by Kerwin (25,26,27) using inflection focusing to gain higher resolution and luminosity than the Nier type field for the same size magnet. The constructional details of the mass spectrometer and the associated vacuum system are discussed in Appendix A.

B. The Ion Source

The ion source consisted of the atom source, the ionization filament, the ion focusing and accelerating parts, and a shutter for interrupting the atomic beam. Figure 2 is a schematic diagram showing a side view of the ion source. The Knudsen cell, containing the rare earth sample (r), and heating

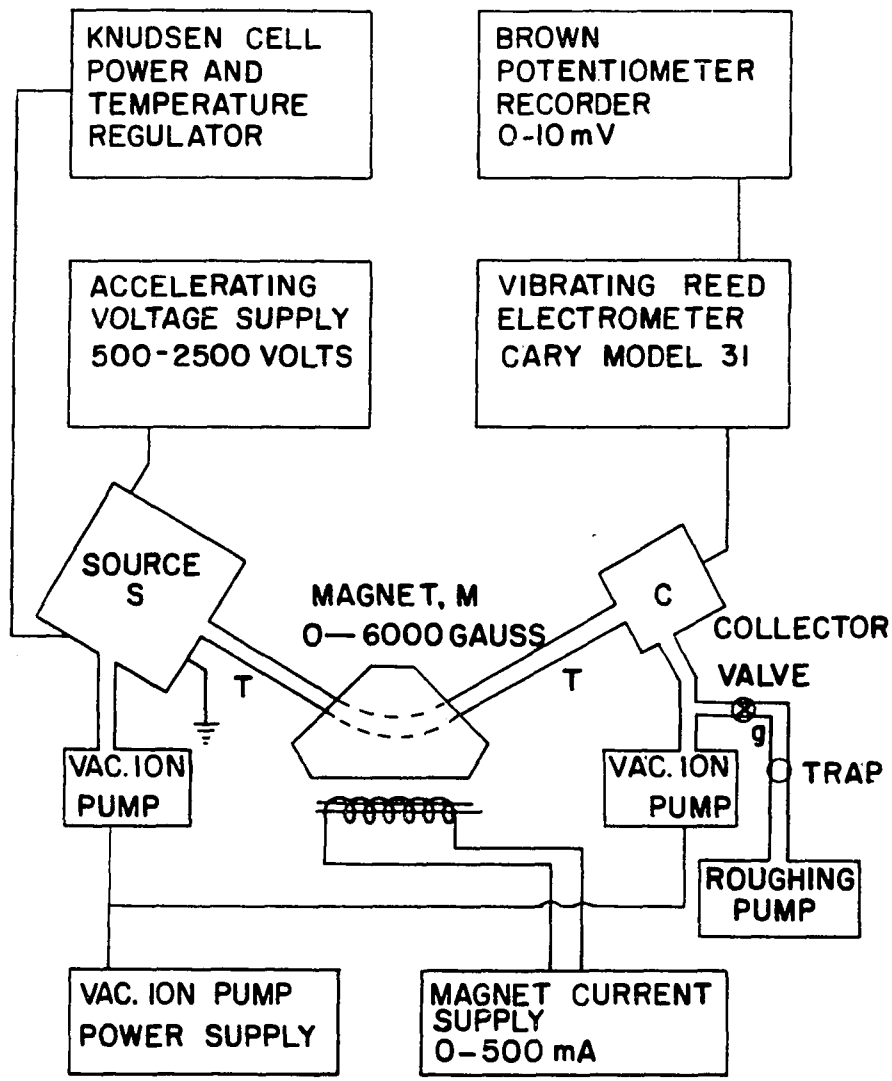

Figure 1. Block diagram of the mass spectrometer and its associated electronics

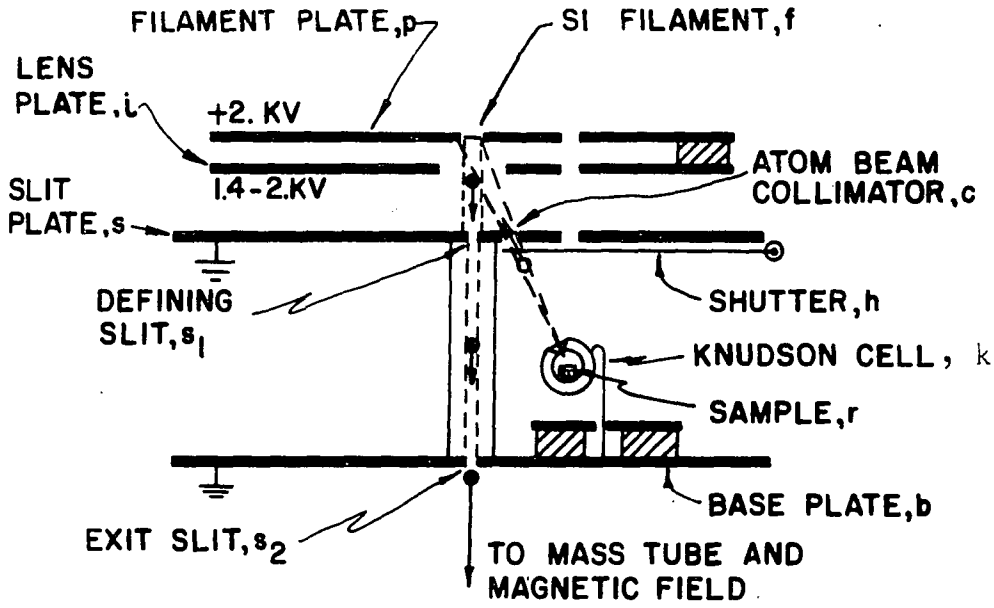

Figure 2. Cross sectional view of the ion source and ion optical system

and the potassium cell holes were 3 mils deep. The filaments were mounted on vycor insulating blocks which were drilled for mounting with an ultrasonic drill. The cell was supported by two wires which were connected to the cell base plate and thus grounded.

2. Filament assembly

The filament was mounted as shown in Figure 4. The ends of the filament were bent to curl around the 0.018 inch tungsten mounting wires. The mounting wires were spread far enough apart to produce a slight tension on the filament so as to eliminate the tendency to sag while hot. (Usually after running the filament, it was found that the filament had been spot welded to the mounting wires.) The filament was made from 0.001 inch x 0.040 inch tungsten ribbon cut into about 3/4 inch lengths. In the preliminary investigations no special preparation was given to this material but in the final work the filaments were strain annealed to insure a single crystal face normal to the surface of the ribbon. The mounting wires were secured to two stainless steel blocks by a set screw, and one of the stainless blocks sat on a vycor insulating block which had been drilled for mounting with an ultrasonic drill. The other stainless block was attached to a third stainless steel block which was identical in shape with the vycor block to preserve the symmetry of the filament mounting.

3. Ion optics

After the ions are formed at the surface of the filament, they are drawn through the lens plate, l, of Figure 1 for focusing and are collimated by the slits s_1, and s_2. The ions are drawn by 2,000 volts applied to the filament plate, p, relative to the ground potential of slit plate, s. The lens plate, l, could be biased from 1100 to 2000 volts above ground for focusing the beam. The filament plate was mounted to the slit plate by two vycor blocks that had been drilled to pass stainless steel screws. The lens plate was mounted to the filament plate by one vycor block which had also been ultrasonically drilled. After passing through slit s_1, the ions pass through a field-free region and are then collimated by slit s_2. A field-free region between the slit and base plates was insured by a rectangular cylinder of tantalum also mounted to the base plate. Both slits were adjustable from 0.25 inch to 0.001 inch. The shutter, h, consisted of a tantalum rectangle mounted to an iron rod. This rod was coaxial with two copper solenoid which had been wound on quartz tubing and which were used to move the shutter.

4. Accessory apparatus

Introduction. Accessory apparatus for the ion source were used to power and regulate the heat to the cell, to power the filament, to accelerate the ions, and to focus the ions.

Effusion cell power. The cell was bombarded with a constant current of 500 volt electrons for the higher temperature work. A power supply was built for this function which regulated the emission current from the filaments by controlling the power to them and thus their temperature. (The circuit diagram is shown in Appendix B.) For the low temperature work the cell was heated by thermal radiation from the heaters. In this case the temperature of the cell was controlled by the output of a thermocouple. The signal from the thermocouple was used to drive a servo amplifier which controlled the power to the heaters. This circuit was sensitive to slightly less than a microvolt change in the thermocouple voltage and the cell temperature was held stable to less than 0.2C°. (The circuit diagram is shown in Appendix B.)

Surface ionization filament power. The surface ionization filament was powered by either AC or DC power. Data was taken with DC through the filament but the filament was left on AC power at all times except when data points were being taken. The filament required from 2 to 8 amps with voltages up to 12 volts. The procedure of AC heating was followed to minimize "DC etch" (29).

Acceleration voltage power supply. The acceleration voltage was provided by a power supply which was manufactured by P R L Electronics of Rahway, New Jersey as model number PM-2K01. It was capable of providing from 500 to 2500 volts

at 10 milliamps.

Focusing voltage power supply. A voltage was applied to the lens plate by means of a voltage divider and three 300 volt minimax batteries. The voltage could be varied continually from 0 to 900 volts by a three position range switch and a potentiometer.

C. Auxiliary Equipment

Temperature measuring equipment. The Knudsen cell temperature was measured by a Pt-Pt + 13% Rh thermocouple in the lower temperature work. When the cell temperatures were in the incandescent region, a Leeds and Northrup optical pyrometer was used. The optical pyrometer was also used for measuring the filament temperature. A General Electric pyrometer lamp which had been calibrated by the National Bureau of Standards was used for calibrating the observer and optical pyrometer to a true temperature scale. Temperatures could be read with an accuracy of .3% (30).

Strain annealing equipment. The strain annealing equipment was an electron beam zone refiner manufactured by MRC manufacturing corporation. This zone refiner provided an excellent method of driving a high temperature gradient along the filament material at a slow rate. The model EBZ-93 electron beam zone refiner was operated in the region of its

minimum power output to heat a small portion of the filament to 2900° K and temperature gradients in the realm of 3000° K/cm. This hot spot was then driven down the filament at rates from 0.1 to 1 cm per minute.

III. EXPERIMENTAL PROCEDURE

A. Introduction

The primary effort of this experiment was to generate the absolute ionization efficiency β as a function of temperature for several atomic species on tungsten surfaces. Other parameters (beam flux and vacuum) of the system were varied to determine if β had dependences on other parameters than those predicted by theory. In performing such an experiment it is necessary to insure that sufficient controls are maintained on the surface and on the atom beam to insure data which can be reliably interpreted.

Surface conditions. The nature of the filament surface is dependent on two things, the first is the physical nature and shape of the crystalline surface on the atomic scale, and the second is the amount of contamination on the surface either due to the environment or the atomic beam being studied. The discussion of the attempts to control the surface conditions will be divided into those which were done before the filament was inserted in the mass spectrometer and those which were done during the course of the experiment.

Atomic beam. To insure that the atom beam flux is that calculated from the known vapor pressure data one must use high purity samples in clean cells. One must further insure that atoms of the source material that arrive at the filament

from places other than the effusion hole are eliminated from the measured current. Again, these controls are either done prior to insertion in the vacuum system or else done during the course of the experiment.

Surface environment. Ultra-high vacuum techniques are of course a necessity to satisfy the requirement of clean filament surfaces. However, because of the specialized nature of the technology of this field and the fact that the technology has little significance to the performance of the experiment (as long as the proper environment is maintained) we will discuss this area of control as a separate entity.

Specialized techniques. In this section techniques and shortcuts which have been used and found of value are summarized. This section is not intended to give further insight to the meaning of this experiment but is offered as an aid to future workers employing similar pieces of equipment.

B. Preparations for a Run

1. Preparation of the filament

The filament was prepared for use from raw tungsten material obtained from the H. Cross Company. The raw material was subjected to a strain annealing technique in an attempt to produce a single crystal filament. After x-ray analysis the filament was cleaned and installed in the vacuum system.

The strain annealing was performed on one-foot lengths of raw material in the apparatus described earlier. A spot

on the filament was heated to between 2800° K and 3000° K. This spot was then driven down the filament once or twice at a fairly slow rate. Optimum results were found to occur when the spot had an apparent brightness of 2350° K (about 3000° K when corrected for emissivity and window absorption) and the spot was moved at a rate of 5mm/min. Under these optimum conditions several inches of single crystal material could be obtained. Most of the filaments used in this study were annealed at about 2900° K. This annealing produced a filament made up of several long crystals oriented nearly in the same direction. A quantitative discussion of the results of this crystal growing can be found in the discussion of auxiliary surface studies on page 42. After the annealing was completed the SI filament was cut out of the ribbon. The filament was next studied by x-rays to determine its crystal orientation. Finally the filament was cleaned by ultrasonic agitation in acetone and installed in the ion source.

2. Preparation of the atom source

The preparation of the atom source for a given run can be discussed in two sections. We will first consider the preparation of the sample and secondly the cleaning and loading of the cell.

Sample preparation. The samples of rare earth metal used in this experiment (Er, Gd, and Yb) were provided by Physical and Inorganic Chemistry Group VIII of this laboratory. They were either in the form of arc melted buttons or chips of

vacuum distilled material and were of the highest purity available at this laboratory. Small pieces were cut from this material and were filed with clean files till all surfaces were visibly clean and shiny. The potassium sample was carved from a stick of potassium obtained from Mallinckrodt Chemical Works. The potassium was rinsed in trichloroethelene (to remove the mineral oil from packaging) and then placed in a beaker of benzene where it was scraped until all surfaces appeared shiny.

Cell loading. As soon as the sample was clean it was loaded into the cell as rapidly as possible. Prior to loading, the cell had been carefully cleaned ultrasonically. The cell was then installed in the atom source and aligned for insertion into the ion source. In the case of K a further precaution was employed to prevent oxidation of the sample while loading. A few drops of benzene were added to the cell (with one end installed) before adding the sample. Next the open end was sealed and the loading proceeded normally. When the mass spectrometer was first pumped down the benzene pumped out of the cell and was trapped in a liquid N_2 trap thereby leaving the K sample clean and in a nonoxidizing environment.

C. Operational Details of a Run

In this section we will first go through the operations of a run and then the steps taken to insure that the necessary surface and beam conditions had been met.

1. Procedure of a run

After the system had been pumped down and outgassed sufficiently for operation below 5×10^{-8} Torr a run could be initiated. The mass spectrometer current was continuously recorded on a Brown strip chart recorder. All other data were entered by hand on the strip chart as they were taken. A run was begun with the filament at about 2500° K. The filament temperature was entered on the strip chart adjacent to the recorded beam current. The shutter was closed, the filament was flashed and the shutter opened. The filament was set to a temperature about 100° higher and the process was repeated. This procedure continued until the filament was about 2900° K. The temperature was then increased about 50° and the process was continued decreasing the temperature in 100° intervals until the beam current was too small to be separated from the noise level. Finally the temperature was increased in several steps back to the starting temperature. Taking data in this cyclic pattern allowed one to check for shifts in experimental parameters presumably held constant (particularly cell temperature). The filament temperatures were read at least twice on the optical pyrometer as a check against eye fatigue.

Runs were repeated for several different beam fluxes.

2. Surface conditions

Two conditions were used to maintain reproducible surface conditions. In order to maintain a clean surface the filament was flashed to 2900° K immediately before a datum point was taken. If the beam current before and after flashing were identical the surface was considered clean. At lower filament temperatures the mass spectrometer current was observed to decay slowly after a flash. This was interpreted as an observation of filament contamination and therefore the current was extrapolated back to the instant the flash had been concluded.

The second condition necessary for repeatable results was the powering of the filament with AC as much as possible. The surface of filaments heated by DC current has been observed (29) to become etched when operated at high temperatures in vacuum systems. We, therefore, ran the filaments with AC power as much as possible to prevent this etching of the surface. After employing this technique the data was found to be much more reproducible. It was necessary to take data on the filament heated with DC because of the 120 cps fluctuation in filament temperature that could be observed when heated with AC.

3. Atomic beam conditions

Because of the dependence of the calculation of absolute ionization efficiency on the atom beam flux, extra precautions must be taken to insure that the experimental atom flux is that calculated. In addition to the cleanliness and purity conditions of the sample discussed earlier, the mass spectrum was checked for peaks other than those being investigated. Potassium peaks were the only impurity peaks ever found and these undoubtedly originated from the manufacture of the tungsten filament since they decayed away after the first few days of operation. Rare earth oxide and fluoride ions were particularly sought because these ions have been observed by Werning (15) and Reynolds (16) in similar experiments.

The shutter was used to eliminate the effect of sample material re-evaporating from other parts of the source onto the filament. This effect was never large but a small background current was observed at the higher filament temperatures, particularly for the high vapor pressure materials.

D. Vacuum Technique

1. Preparation and loading

The source was made of stainless steel with vycor used as an insulating material and tantalum sheet used for shielding purposes. Electrical connections were made with OFHC copper wire. Before the source was assembled all parts were cleaned and triple rinsed first in trichloroethelene and subsequently

in acetone. The parts were then ultrasonically agitated in fresh acetone, rinsed, and allowed to air dry. The ion source was assembled using only cleaned tools to handle the parts. The ion source was installed in the source vacuum chamber. The chamber was closed using a copper shear gasket which had been cleaned by ultrasonic agitation.

2. Pump down and initial outgassing

The system was first pumped down to 0.1 Torr with the roughing pump (see Figure 1). The trap was refrigerated with liquid nitrogen and the pressure dropped to below 0.002 Torr within an hour. The Vacion pumps were turned on and they generally began pumping within 15 minutes. When the Vacion pumps had lowered the pressure below 2×10^{-5} Torr the valve (g) could be closed and the pumps would pump the system down to the low 10^{-6} Torr range in a half hour. When the system reached the 10^{-6} Torr range the Bayard Alpert guage was turned on and outgassed. Next the SI filament was turned on for outgassing. When the vacuum could be maintained below 5×10^{-6} Torr with the filament at 2500° K, the atom source was turned on and outgassed until it could be left at its operating temperature without affecting the pressure. At the conclusion of the above outgassing procedures all power to the source, S, was turned off and preparations were begun to initiate the bakeout of the vacuum system. With the power off the pressure was usually below 2×10^{-7} Torr.

peak could be found and if it responded reasonably to closing of the shutter, to change in cell temperature (T_c), and to change in the SI filament temperature, no further time was spent before initiating bakeout. After bakeout at 400° C the large kovar to glass seal developed small leaks. If was found that Torrseal (a product of Varian Associates) was a very effective patching material whose vapor pressure did not interfere with vacuums down to 1×10^{-9} Torr or lower. It was also found that when only minor changes were made in the ion source, bakeout to 250° C was adequate for this work, and at this temperature the Torrseal, although charred black, still did not leak.

IV. AUXILIARY STUDIES

A. Introduction

Surface ionization is a process that is very sensitive to surface conditions and for this reason every effort must be made to know the nature of the experimental surface. In this section we discuss our efforts to study the physical nature of the surface. The tools employed in this investigation were the x-ray camera, the microscope, and the SI process.

B. X-ray Studies

The four filaments used in this investigation were subjected to x-ray analysis to determine their crystal orientation and whether they were single crystals. The four filaments were designated W6, W7, W8, and W9. Filaments W6 and W9 were used in the supplementary studies of SI, and W7 was used in the potassium calibration runs. Filament W8 was used for all of the data tabulated as final results.

The x-ray instrument used was standard Norelco equipment which employed 35 KV electrons to bombard a Cu target. The resultant x-rays were collimated into a beam about 1 mm in diameter and directed onto the filament surface. The SI filament was mounted in the camera sample holder by imbedding the filament in modeling clay. A high precision mechanical technique was used to insure that the filament was normal to the x-ray beam.

Figure 5 is a stereographic projection of the Laue pattern for filament W9. The direction of the filament axis and the surface normal are indicated. Two angles are defined in Figure 5 to locate the surface normal relative to the (112) direction. The (112) surface is the simplest crystal plane whose normal is in the vicinity of the surface normals of our filaments. We will, therefore, consider that basically we have a (112) surface for which small allowances can be made when the surface normal is not parallel to the (112) direction.

Figure 6 and Figure 7 are the Laue patterns for filament W8 before and after use in the experiment. We see that a shift in orientation has occurred somewhere during the experiment. It is concluded that this shift most likely occurred during the initial outgassing since there is such good consistency from run to run. If the shift did not occur before the first run we might conclude that the shift was not large enough to produce a measurable difference in the SI efficiency. Another possibility is that the shift occurred between the Yb and Er runs, since there is a larger discontinuity in ϕ-V from element to element (see Equations 25, 26, and 27) than expected from the change in V. This possibility seems to be unlikely since the filament had been at elevated temperatures for the majority of two months during the Gd and Yb experiments; one would expect that the change would take place gradually. However, if the change were abrupt and at some random time, the week between the last Yb data and the first Er data is a

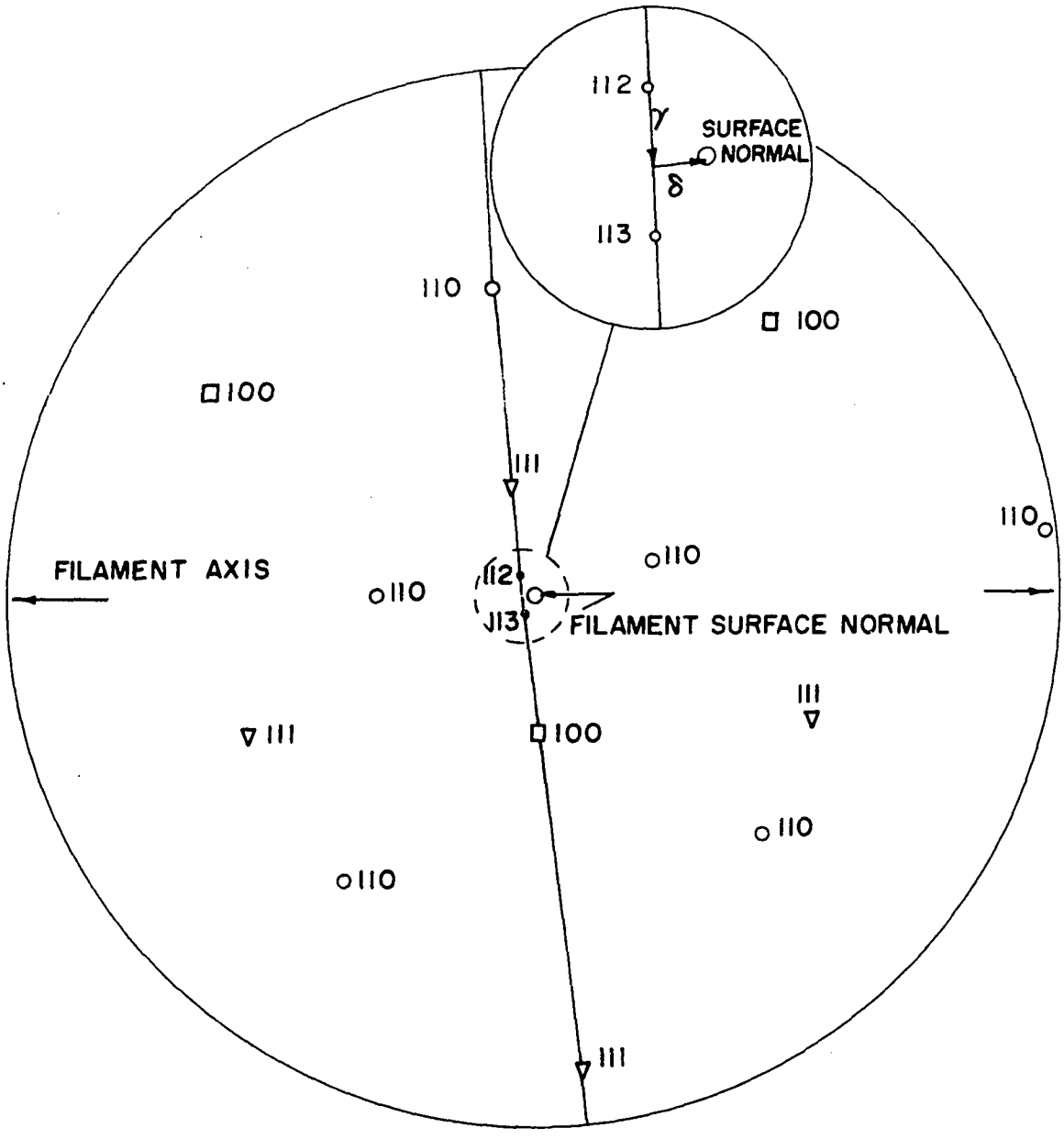

Figure 5. Stereographic plot of W9 showing crystal orientation relative to tungsten filament. The angles γ and δ are defined.

Figure 6. Back reflection Laue pattern of W8 before use in mass spectrometer

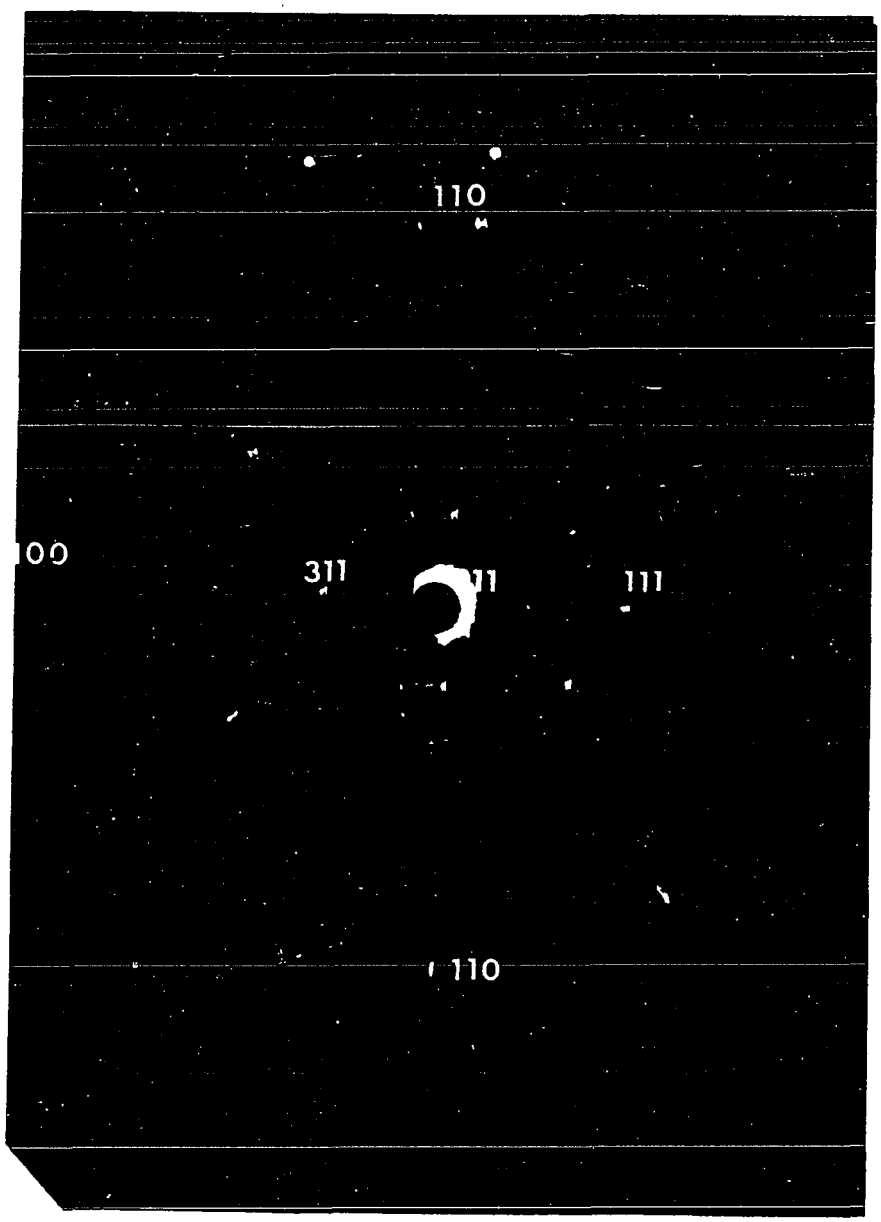
110
00
311
111
110

Figure 7. Back reflection Laue pattern of W8 after use in mass spectrometer

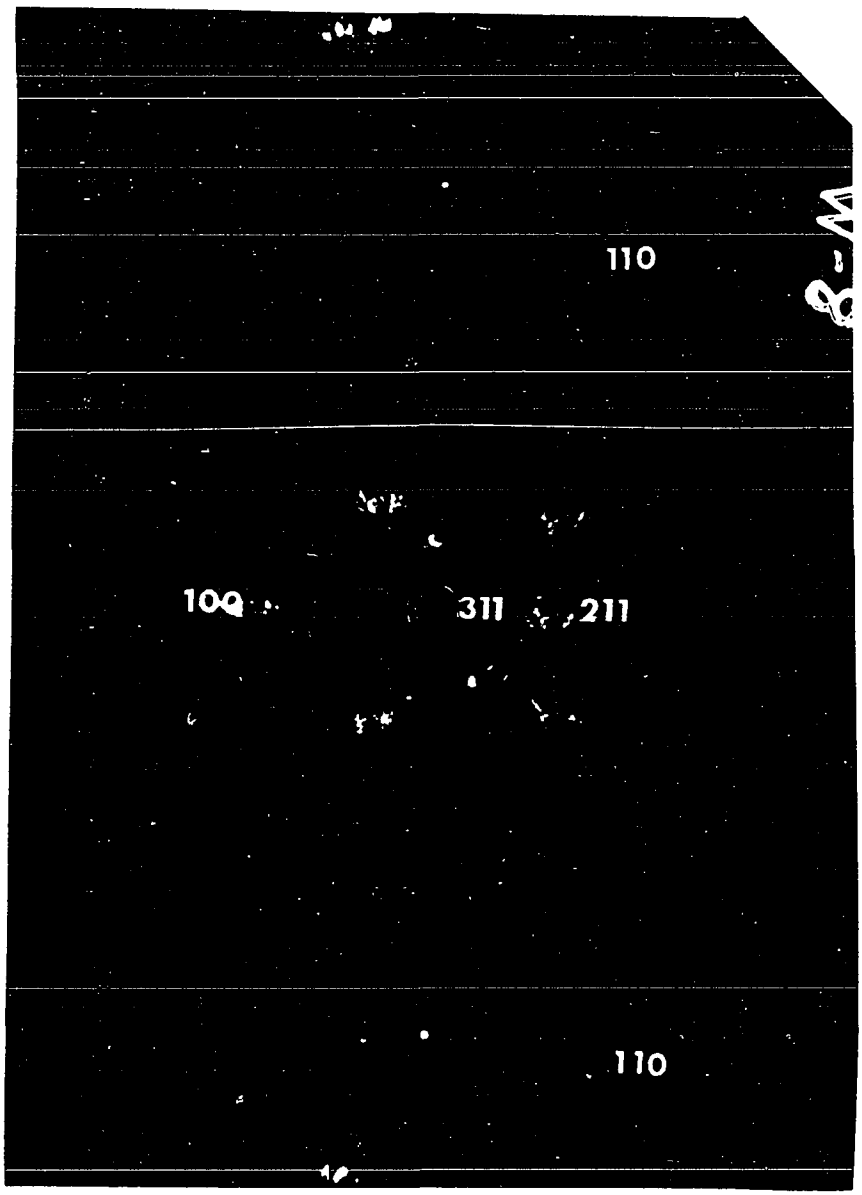
110
100
311
211
110

Table 1. Summary of the x-ray analysis

Filament	γ	δ	Total number of crystals	Maximum deviation of crystals from	
				γ	δ
W-6	8.0°	0.6°	6	3.4°	1.0°
W-7	11.0°	4.4°	3	1.0°	1.0°
W-8	15.0°	2.0°	3	3.5°	1.0°
W-9	6.4°	3.0°	1	--	--

small fraction of the total time spent with the filament hot. Table 1 is a summary of the x-ray analysis of the filaments used in this experiment.

Unfortunately the parameters necessary to produce filaments such as W9 were not discovered until this work was nearly completed. The filament (W8) used in this experiment had a very similar stereographic projection to that of W9 except that each of the directions were represented by several points instead of a single point.

C. Optical Studies

The filament was studied optically to determine as much as possible of the microscopic structure of the surface. A microscope capable of up to 500X magnification was used. Picutres were taken with a metallograph using 50X and 250X magnifications. Pictures of W8 are shown in Figure 8.

Figure 8. Microscopic views of W8 after use in the mass spectrometer

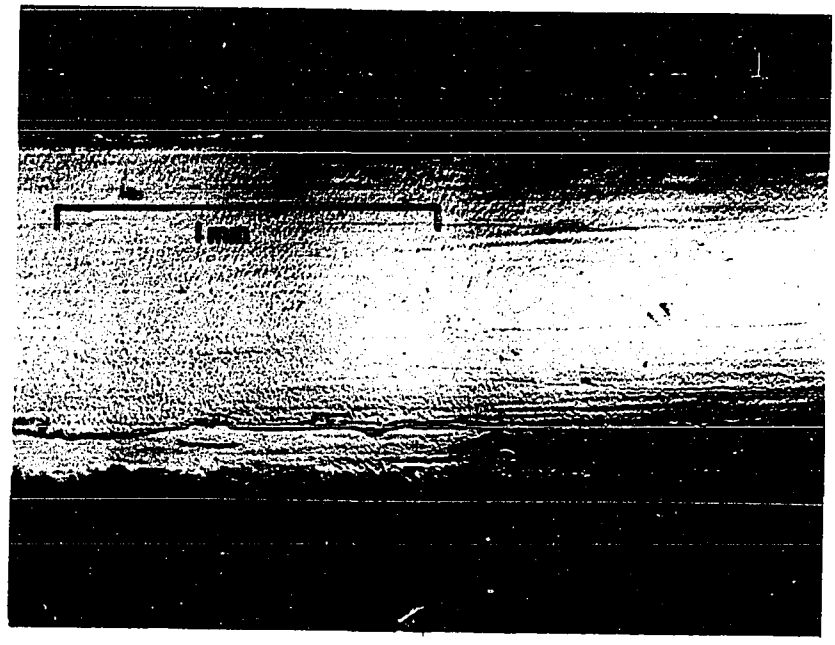

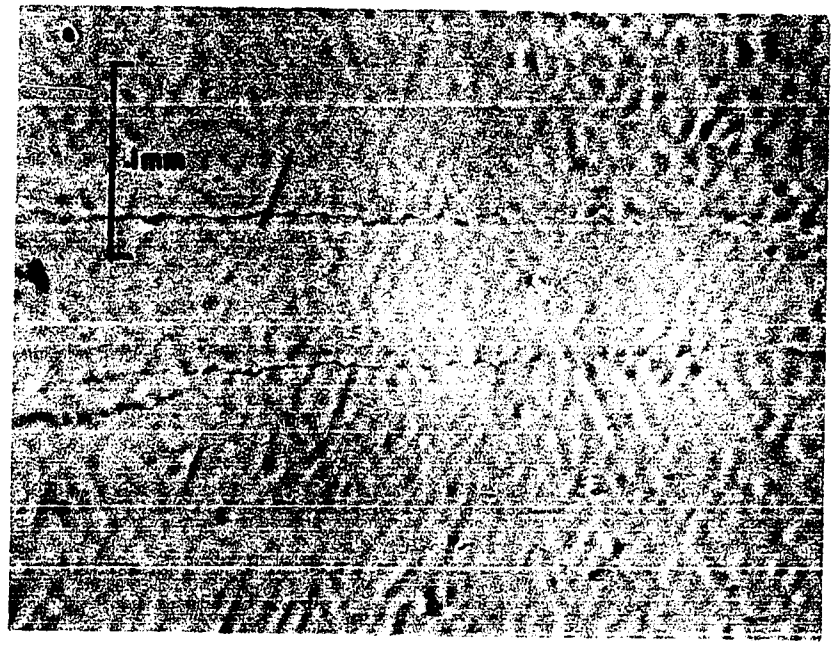

In the lower magnification we can see the overall characteristics of the surface. Along the edge of the filament one can see the grain boundaries separating the crystals which gave rise to the multipointed x-ray patterns. Note the dissimilarity in the nature of the surface across the grain boundaries. The region shown here includes the region which gave rise to the mass spectrometer ion current.

In the larger magnification we see that the surface is quite ripply, so that even though we have a single crystal, the surface is so rough that it cannot be considered a true (112) surface. Because of this, work function data reported in the literature could not be used. The fine lines which can be observed on the higher magnification are seemingly another type of crystal fault. They usually come to a dead end somewhere in the crystal and the nature of the surface is continuous across the crack. This type of crack may be an indication that the crystal was slightly twisted and the crack formed to relieve this strain. If so, this is another source of the fuzziness of the individual spots on the after x-ray of W8. The pictures of the filament presented in Figure 8 were taken after the filament was used in the experiment.

D. Auxiliary SI Studies

Two sets of SI experiments were performed in addition to the main experiments to be discussed later. These two studies provide information of an auxiliary nature to the experiment

and are therefore presented here despite the fact that the method of data analysis for the SI studies is presented in the following section. For each of the runs a value of E and A (as defined in Equation 21) is given to represent the run in the high temperature region. The discussions involving analysis and errors would be identical with that to be presented for the main core of the experiment and are therefore not presented with this section.

The first set of SI runs to be considered is the SI of Er from filament W6. This set of runs is significant in that it shows first of all that the slope of the SI data from W6 is nearly equivalent to that of W8. Because of this equivalence the validity of applying the results of the work function data to filament W8 is much greater. The second value of the runs is in showing the wide scatter of points when the filament is heated entirely by DC current. Figure 9 is a typical result of this set of runs. As will be seen later, this curve is also quite typical of the later Er SI runs. Below $10^4/T = 5.1\ ^\circ K^{-1}$ a "tail off" is noted. This "tail off" is attributed to the contamination of the surface by Er. Above this temperature the surface is assumed clean. Table 2 is a summary of the SI of Er on W6.

The second set of runs was performed with a Gd beam on filament W9 at the conclusion of the experiment. This set of runs was also taken with a twofold purpose. The primary reason for this set of runs was to see if improved vacuum

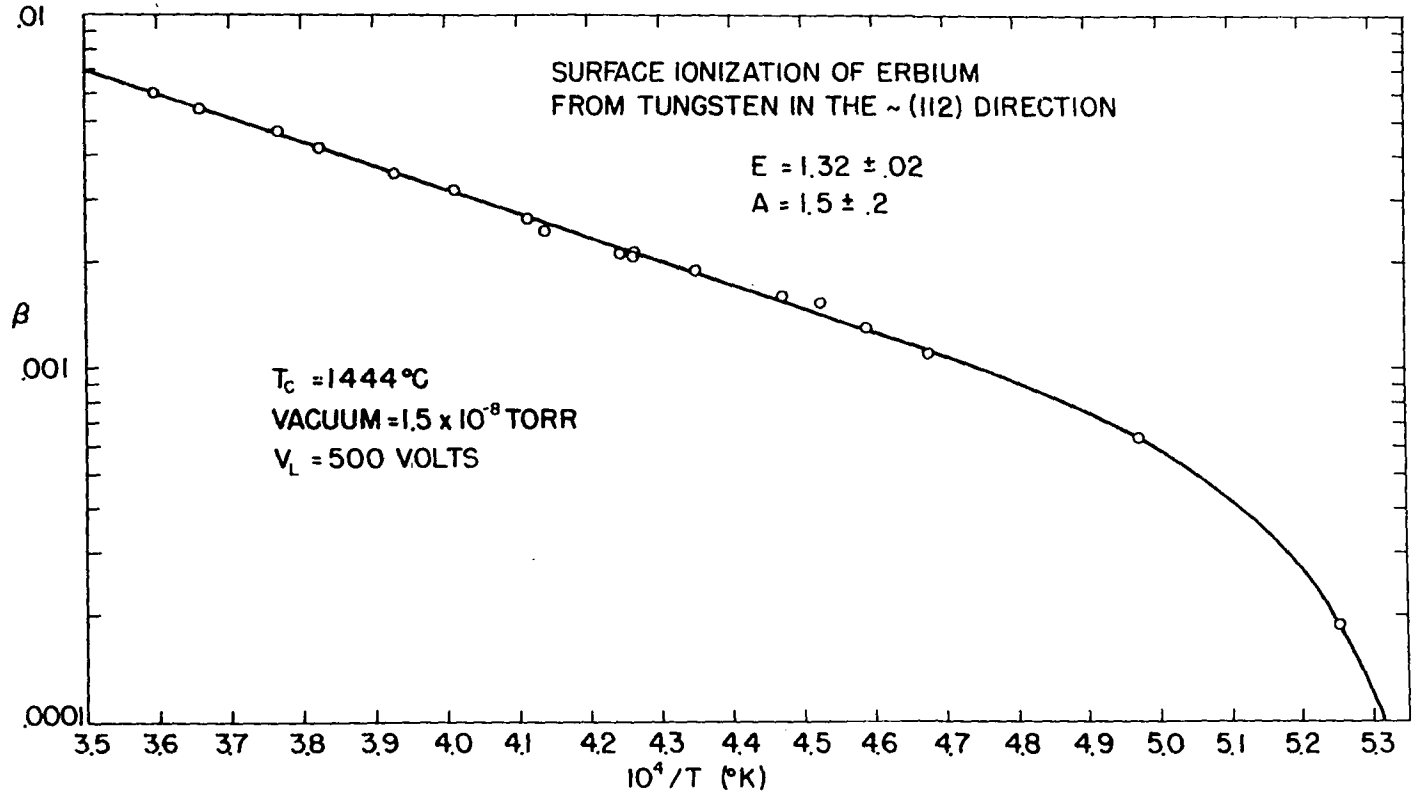

Figure 9. Ionization efficiency of erbium from tungsten

Table 2. The surface ionization of Er on filament W6

Run W6-Er3	E (eV)	σ_E (eV)	A	σ_A	Range of T (°K)	T_c (°K)	Vacuum 10^{-8} Torr Mean	Max.
1	1.35	.03	1.87	.26	1770-2849	1272	3.5	14
2	1.24	.04	1.59	.27	2178-2860	1228	4.3	15
3	1.31	.02	1.74	.18	1931-2901	1320	2.5	19
4	1.64	.03	5.30	.57	2298-3035	1285	3.4	34
5	2.40	.03	57.0	8.0	2248-3061	1326	2.9	15
6	1.44	.02	5.85	.47	2043-3070	1218	1.0	12
7	1.17	.04	1.70	.30	1881-2982	1159	0.4	2
8	1.22	.02	0.91	.07	1870-3270	1434	2.0	8

Average value of E	1.36 eV
Statistical scatter of mean of E	0.06 eV
Average value of A	2.35
Statistical scatter of mean of A	0.72

conditions (over those of Gd on W8) had any effect on the SI of Gd. A secondary purpose was to see what effect the more perfect crystal surface of W9 had on the SI process. The results of this set of runs is summarized in Table 3. These data were taken for fluxes to the filament from 3.7 to 9.0×10^{-5} atoms/sec A^2. The filament was flashed much more heavily than in the main experiments of Gd on W8. The vacuum was a factor of ten better than in the main experiment. This

Table 3. The surface ionization of Gd on filament W9

Run W9-Gd2	E (eV)	σ_E (eV)	A	σ_A	Range of T (°K)	T_c (°K)	Vacuum 10^{-8} Torr
1	1.37	0.15	16.0	11.0	2105-2861	1518	2.0
2	1.47	0.07	19.9	6.0	2098-2878	1566	2.0
3	1.47	0.06	17.5	4.6	2254-2851	1560	0.6
4	1.49	0.09	19.1	7.6	2216-2848	1540	0.7
5	1.36	0.13	12.5	7.1	2252-2863	1550	0.7
6	1.47	0.09	20.0	8.1	2182-2874	1526	0.8

Average value of E	1.46 eV
Standard deviation of the mean of E	0.02 eV
Average value of A	18.1
Statistical scatter of the mean of A	1.0
Error in A due to calibration	3.1
Standard deviation of the mean of A	3.2

experiment yields results that disagree with those obtained from earlier measurements, but it is felt that the discrepancy is due to the difference in the surfaces and not due to the vacuum environment. Filament W9 appeared microscopically smoother than did W8. The orientation of this filament is much closer to the (112) direction than W8 and preliminary work function measurements indicate that its thermionic work function is 0.18 eV higher than W8. For these reasons it is obvious that we cannot expect the data to be identical with the SI data on W8. Because there is still a large discrepancy

between the coefficient A for Gd and the other rare earths it is felt that vacuum is not the primary source of this discrepancy and therefore the SI data for Gd on filament W8 can be considered as clean surface data.

V. ELECTRONIC WORK FUNCTION STUDIES

A. Introduction

Because of the need to know the work function of the surface under investigation, it was felt that the best knowledge of the surface could be attained by performing a direct measurement of the thermionic (or Richardson) work function. The Richardson equation for thermionic emission is

$$J_o = I_o/A_o = AT^2 e^{-e\phi/kT}. \tag{4}$$

In this expression I_o is the saturation current with zero electric field, A_o is the emitting surface area, and A is the thermionic constant theoretically given by

$$A = (1-R)4\pi mek^2/h^3. \tag{22}$$

Schottky has corrected Equation 4 for the case of electric fields and thereby expresses the saturation current for an electric field F at the emitter surface as

$$I = I_o \exp[e(F/4\pi\varepsilon_o)^{1/2}/kT], \tag{23}$$

where e is the electronic charge, ε_o is the permittivity of free space, and all units are expressed in the MKS system. A thorough discussion of the theoretical and experimental problems of thermionic emission are presented by Nottingham (31).

The usual approach in the experimental determination of

ϕ is to measure the emitted current at constant temperature as a function of the voltage applied between the emitting surface and a collector. At voltages large enough to eliminate space charge one observes the saturation current. If the natural logarithm of the saturation current is plotted as a function of $V^{1/2}$, a straight line is found. If this line is extrapolated to V = 0, the current obtained will be I_o. These measurements are then repeated for other filament temperatures to determine the experimental dependence of I_o on T. If the emission follows Equation 4, a plot of $\ln(I_o/T^2)$ vs. 1/T gives a straight line whose slope is $-\phi/k$.

B. Apparatus and Procedure

The work function of filament W6 was measured in the mass spectrometer so that SI experiments could be run alternately with work function experiments. Referring to Figure 2 we see that if we apply negative voltages to the filament plate, p, the SI filament, f, becomes the cathode of a simple diode for which the slit plate, s, is the anode. During this experiment the lens plate, l, was removed. Figure 10 is a schematic diagram of the circuit used in this measurement. The power supply was used either as an AC or a DC source. When the AC voltages were used the signal outputs were applied to the x and y axes of an oscilloscope. For each temperature, a current versus applied voltage curve was generated on the CRT face and photographed with a polaroid camera. An X-Y recorder

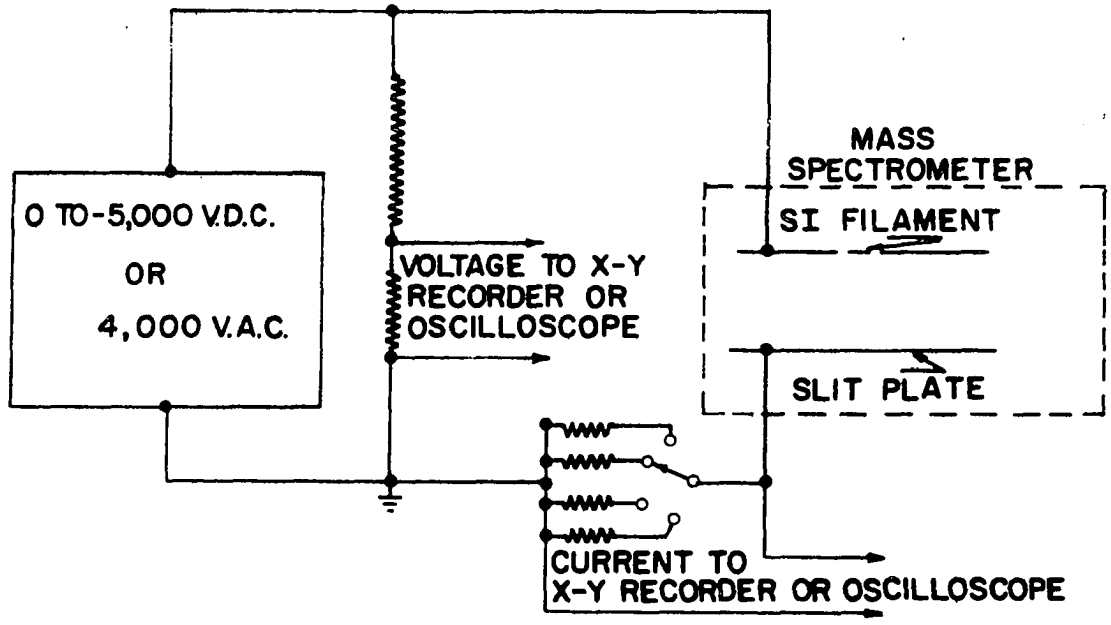

Figure 10. Schematic diagram of the circuit used for the thermionic emission experiment

was used with the DC voltages so that as the voltage was slowly varied a current versus voltage curve was recorded. These two types of gear were used to insure that the rate at which the voltage was varied did not affect the results of the experiment. The vacuum during these measurements was in the 10^{-9} Torr range. The filament was flashed (as in the SI experiments) to 2900°K just before a data curve was taken. Electric fields at the surface were varied up to 2.8×10^{5} volts/m.

C. Results

1. Introduction

In a discussion of the results of the thermionic measurements it is of value to recall the nature of the surface used. Filament W6 was one of the more polycrystalline filaments used. The orientation of the surface normals was closer to that of the (113) direction. Microscopically the filament was very similar in appearance to W8.

2. Work function results

Typical oscilloscope traces can be found in Figure 11. Although many wiggles are apparent in these pictures which have linear coordinates, when the data are converted to a ln I versus $V^{1/2}$ plot the wiggles are less apparent and the extrapolation to zero field is much easier. Figure 12 is the Schottky plot for the same curves displayed in Figure 11 plus

Figure 11. Oscilloscope traces of current versus voltage for thermionic emission (run 3-W6) from the (112) direction of a SI filament

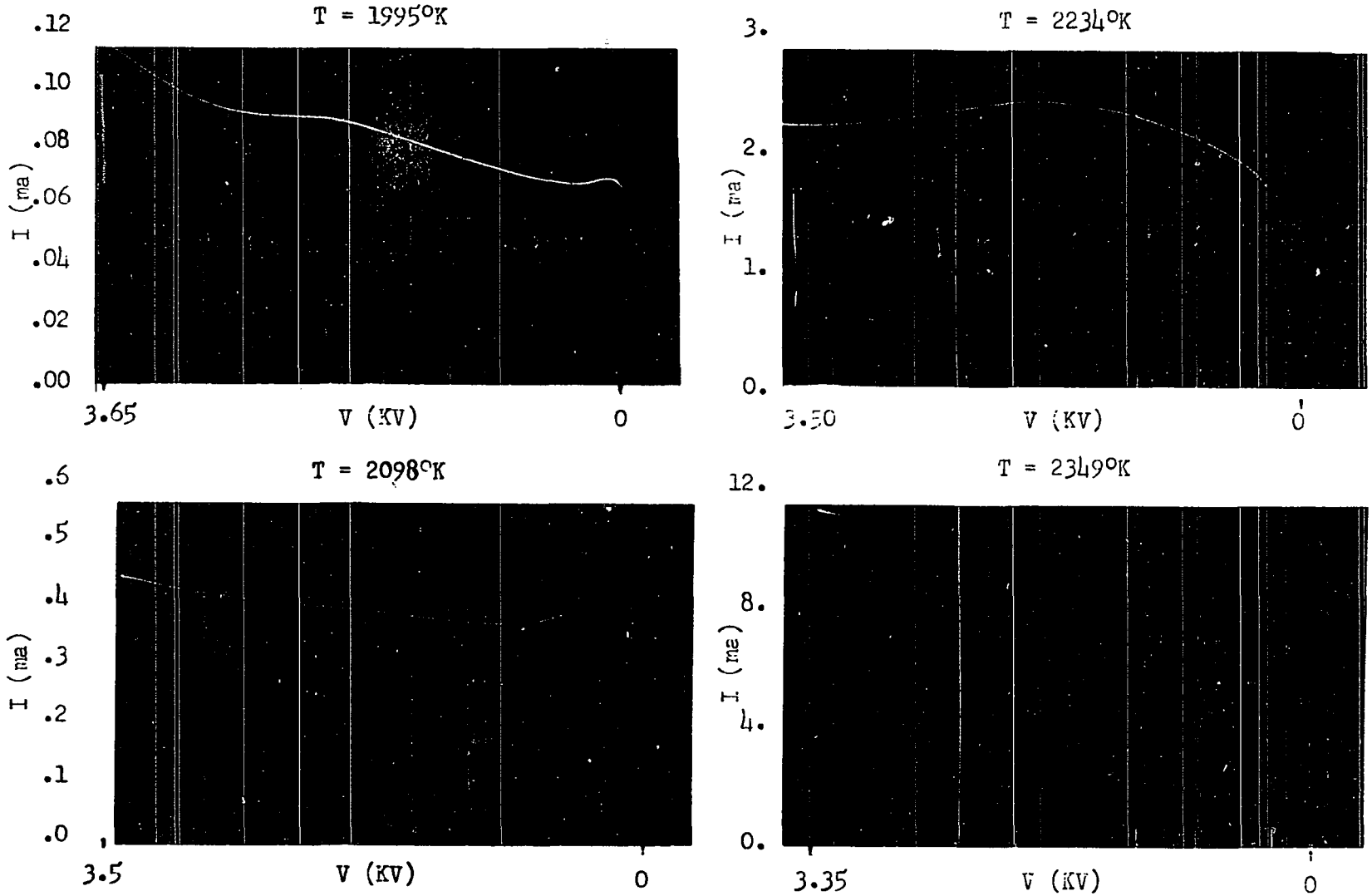
T = 1995°K
.12
.10
.08
.06
.04
.02
.00
I (ma)
3.65
V (KV)
0
T = 2234°K
3.
2.
1.
0.
I (ma)
3.50
V (KV)
0
T = 2098°K
.6
.5
.4
.3
.2
.1
.0
I (ma)
3.5
V (KV)
0
T = 2349°K
12.
8.
4.
0.
I (ma)
3.35
V (KV)
0

Figure 12. Schottky Plot--thermionic emission from tungsten in the ~ (112) direction

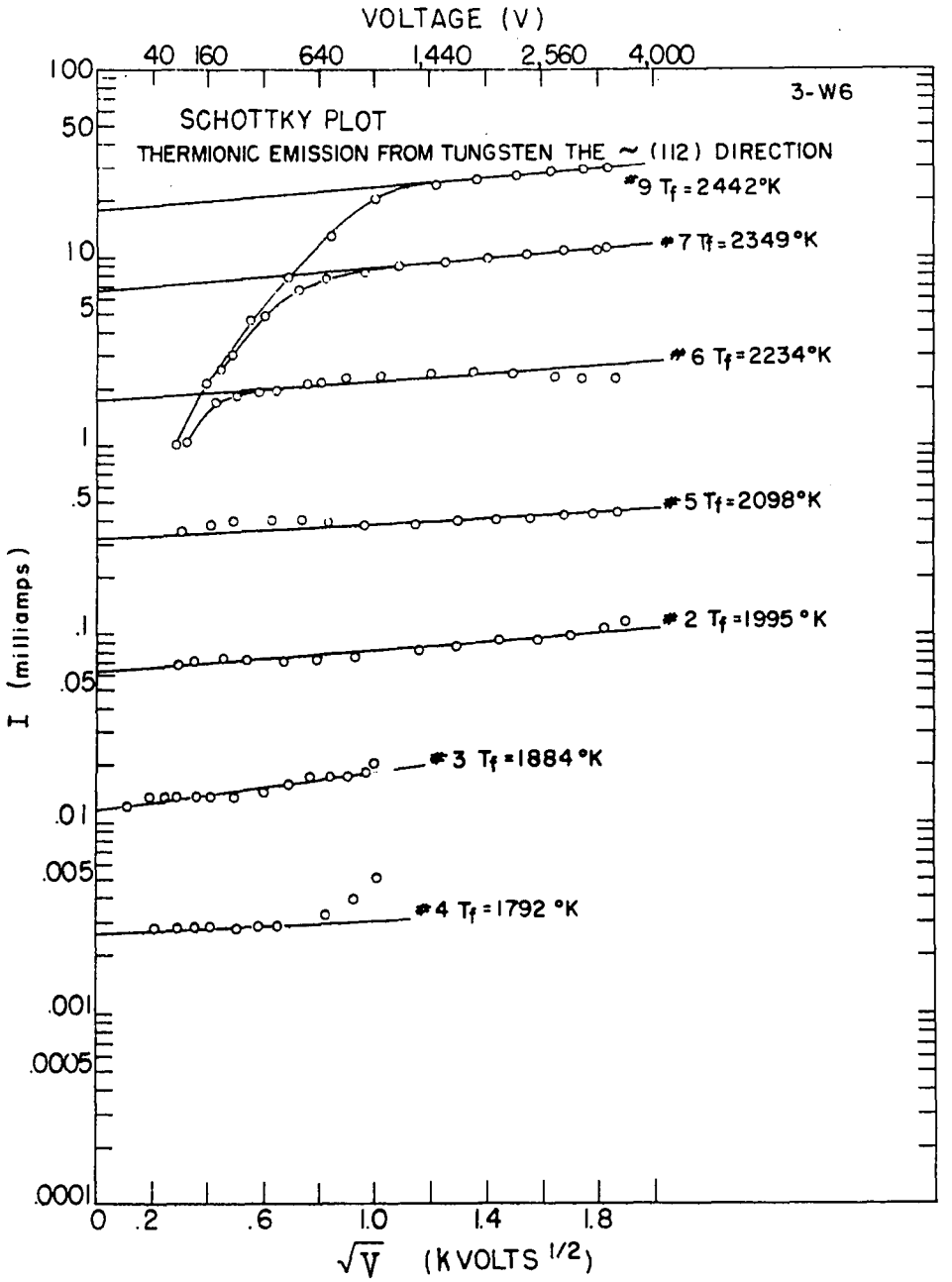
VOLTAGE (V)
40 160 640 1,440 2,560 4,000
3-W6
SCHOTTKY PLOT
THERMIONIC EMISSION FROM TUNGSTEN THE ~ (112) DIRECTION
#9 Tf = 2442°K
#7 Tf = 2349°K
#6 Tf = 2234°K
#5 Tf = 2098°K
#2 Tf = 1995 °K
#3 Tf = 1884 °K
#4 Tf = 1792 °K
I (milliamps)
100
50
10
5
1
.5
.1
.05
.01
.005
.001
.0005
.0001
0 .2 .6 1.0 1.4 1.8
√V (KVOLTS 1/2)

Table 4. Summary of the work function measurements of the W surface

Run	ϕ (eV)	σ_ϕ (eV)	Statistical weight	Taken before SI W6-Er3 run	Vacuum 10^{-8} Torr	Temp. range T(°K)
1-W6	4.90	0.11	0.06	3	1.0	1762-2279
3-W6	4.82	0.03	0.67	3	0.5	1792-2442
4-W6	4.52	0.11	0.00	6	0.6	1837-2445
5-W6	4.73	0.19	0.02	6	0.6	1893-2474
6-W6	4.92	0.06	0.24	7	0.4	1694-2316
	Weighted mean of ϕ					4.85 eV
	Statistical scatter of the mean of ϕ					0.03 eV
	Experimental uncertainty in the mean of ϕ					0.01 eV
	Standard deviation in the mean of ϕ					0.03 eV

the other curves taken for run 3-W6. Figure 13 is the Richardson plot for run 3-W6. Table 4 is a summary of the thermionic work function runs. Since the work function runs were taken intermittently with the SI runs previously discussed, their correlation with the SI runs is also tabulated in Table 4. Run 4 was taken without flashing to demonstrate the necessity of flashing and is assigned a statistical weight of 0. Run 6 was taken using the DC voltage technique and the others were taken using the AC voltage technique. Because there is no apparent difference in the shape of the curves taken by the two methods, raw data from the DC technique are not displayed. It can also be concluded that the wiggles in

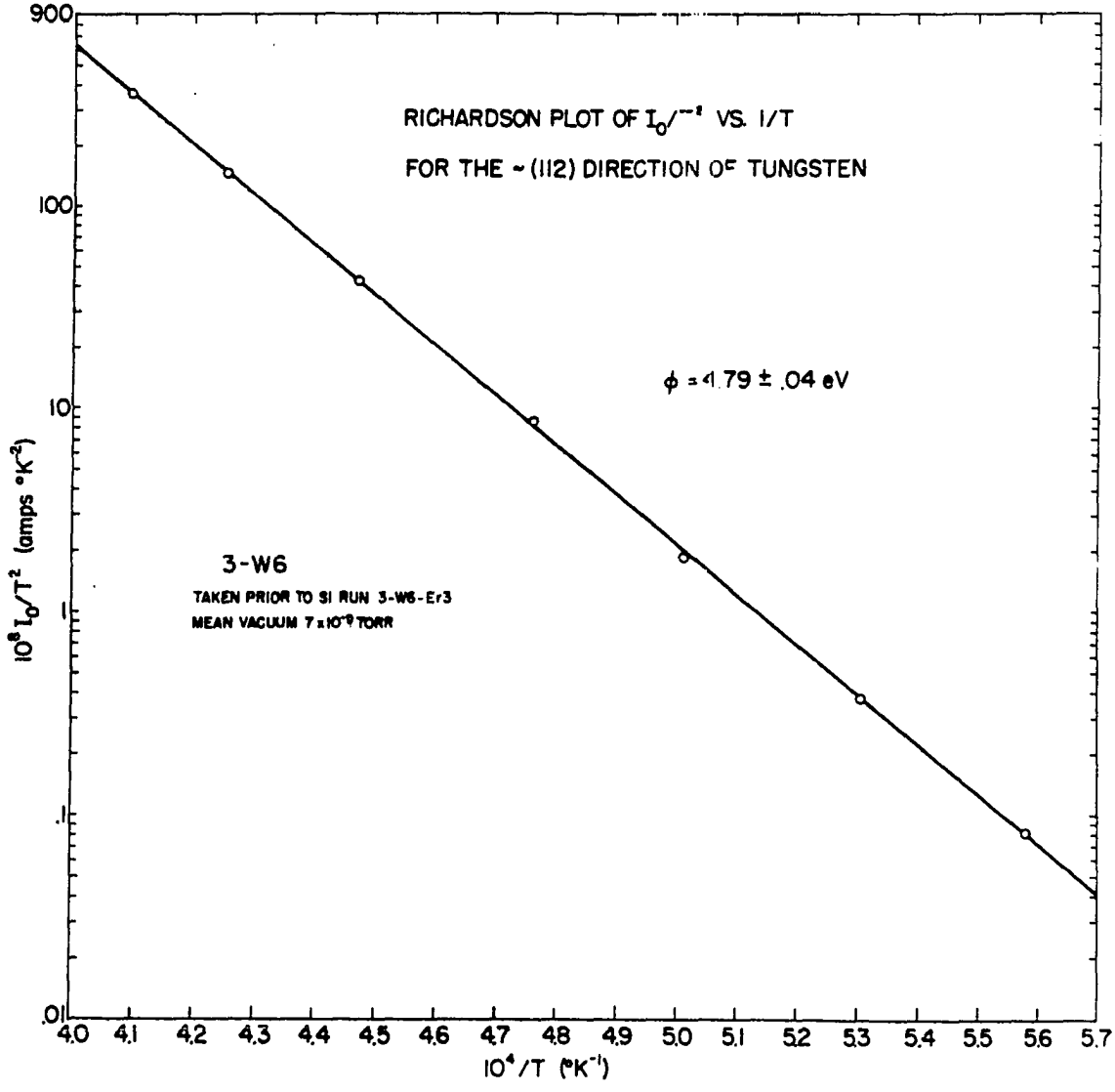

Figure 13. Typical Richardson plot of thermionic emission from the (112) direction of tungsten filament W8

the curves of Figure 11 are not due to the rapid changes in voltage of the AC technique since the curves were unchanged in appearance when the voltage was changed slowly in the DC method. The correlation of the thermionically measured work function with the SI work function was also observed in this experiment. The fluctuation in work function from run to run was within the limits of error for that run and thus no significant change in ϕ could be seen. The sequence of SI runs is correlated with the sequence of thermionic runs in Table 4. If one considers just the mean value of ϕ obtained for each run, the change in its magnitude is in the same direction as the change in ϕ-V would predict and the magnitude of the change is reasonable. It would thus seem that the value measured here is a good measure of the thermionic work function of our tungsten surface. Since we are unable to determine the exact nature of the microstructure of the surface, we cannot be certain that our data is identical with that of a pure (112) surface. Because of the limited data on thermionic emission from a single crystal surface the necessary restrictions on surface field and filament temperature to insure a meaningful measurement of ϕ have not been established. This writer is not aware of any other observations of the lump which appears (on the I vs. V curves) just as the emission current becomes saturated. Perhaps this is characteristic of data from single crystal faces.

D. Discussion

Nottingham (31) points out for polycrystalline tungsten emitters that surface fields of 40 KV/cm or greater are necessary (for surface temperatures up to 1800°K) to overcome the effects of patch fields. In our experiment we were not able to achieve such high surface fields. Because we were using the mass spectrometer source for the measurement, voltages above 4KV were associated with leakage currents and breakdown. According to Nottingham at these fields one should not be out of the space charge limited region of the ln I vs. $F^{1/2}$ plot. However, our data indicated that we were well into the saturation region of the curve. This is to be expected in the case of higher work function surfaces than the one treated by Nottingham in reference (31). If one takes the Schottky plot of Nottingham and extrapolates the 3-40 KV/cm portion of the curve to zero field one gets a work function that is 0.035 eV higher than the work function obtained from his higher field data. Thus we see that the effect of patch fields is small compared to the experimental errors in this work; our lower field data can be used reliably in the determination of the work function of our surface. The value of ϕ = 4.85 eV is in good agreement with the values reported by other workers for this direction of a tungsten single crystal. Table 5 is a listing of some of the other values reported for this surface and the method used to determine it. The value

Table 5. Reported values of the work function from the (112) surface

Ø (eV)	Method	Reference
5.25	Thermionic emission Surface ionization	Hughes, Levinstein, and Kaplan (32)
4.69	Thermionic emission	Nichols (33)
4.65	Thermionic emission	Smith (34)
4.9 ± 0.2	Field emission	Smirnov and Shuppe (35)
4.65 - 4.88	Field emission	Müller (36)
4.73	Field emission	Houston (37, Table III)

reported by Hughes et al. (32) is the thermionic work function from an etched tungsten single crystal. Although they made their measurement in the (112) direction, they feel that their surface was grooved with (110) surfaces making up the sides of the grooves. They use these grooves to explain the high value of Ø that they report. It is also quite possible that we have such a microstructure on the surface which might explain why our value of Ø is higher than other thermionic values. It is also possible that edge effects caused a lowering of the apparent work function in the other thermionic experiments since these used cylindrical emitters.

E. Conclusions

We conclude that the thermionically measured work function is the best appraisal of the work function of this surface. We have no evidence that a microstructure smaller than that seen in Figure 8 exists. It is therefore believed that the surface employed in this experiment should display the characteristics of a (112) surface most closely. The work function of this surface is $\phi = 4.85 \pm 0.03$ eV and is characteristic of a (112) surface.

VI. ANALYSIS OF THE DATA

In this section we will discuss the techniques used to analyze the SI data. Analysis of the work function data required the same type of corrections as are presented here and involved a similar analysis; a separate treatment of the analysis of the work function data will be omitted.

The surface ionization data were analyzed from the point of view that they should be predictable from the Saha-Langmuir equation. In other words the high temperature SI data were fit to an equation of the form:

$$\ln\beta = \ln A - E/T. \tag{24}$$

The Saha-Langmuir equation is valid then if $A = g_+/g_o$, and $-E = (\phi - V)/k$ by comparison of Equation 24 to 6.

At the conclusion of a set of runs all the raw data were recorded on the strip chart records of beam current versus time. The data were copied from this chart onto the data forms shown in Appendix C. These data forms provided colums for the recording of the data as various corrections were applied. For each setting of the filament temperature there was a current reading (designated "upper" in the table) and a background reading (designated "lower"). The actual ion current, I, was then recorded in the column designated upper-lower as the difference in the upper and lower readings.

The observed temperatures were corrected first for window

absorption and calibration errors. The window absorption corrections were taken from a table compiled in this laboratory from experimental observation. The calibration corrections were taken from data of the experimenter's observed temperature of the NBS filament as compared to the calibration of the filament. This procedure insured that individual differences in the reading of a pyrometer were calibrated for each experimenter. These "brightness" temperatures in °C were then converted to absolute temperatures and corrected for emissivity. The emissivity corrections were calculated from the data given in the International Critical Tables (38). Thus the absolute temperature T of the filament was determined. A graph of ln I vs. 1/T was then made so that the region of clean surface data could be found. The clean surface region of the curve is that portion of the graph which is linear. (This data also provided a check on the consistency of the data during a run.)

The current values, I, could be converted to ionization efficiencies, β, by the technique described in Appendix D. The values of β and T for the high temperature (clean surface) range were then fit, using a least squares program on the IBM 7074 computer, to a straight line of slope E/k and intercept A at $1/T = 0$. The computer also calculated the standard deviation in A and E due to the statistical scatter of the data for each run. A final weighted mean value of E and A was calculated for the entire set of runs on a given material

using a weight for each run proportional to the square of the reciprocal of the standard deviation of that run for E or A respectively. Finally the standard deviations of the means of E and A were calculated.

VII. EXPERIMENTAL RESULTS

A. Introduction

The results of the surface ionization studies are presented and examined in terms of their agreement with the Saha-Langmuir equation. The results of the potassium experiments are presented first because their purpose is only in calibration of the mass spectrometer. The data for the surface ionization of the rare earths will be interpreted as absolute ionization efficiencies using the results of the potassium experiment to establish the transmission constant of the mass spectrometer. Data is presented for the SI of erbium, gadolinium, and ytterbium from the ~(112) direction of a tungsten crystal. A critique of the experiment pointing out the uncertainties experienced in the different phases of the experiment is presented. Following the critique is a comparison of the theory with the experimental results. In the comparison we will demonstrate the points at which the theory shows the greatest agreement and disagreement. Finally we will present a discussion of possible explanations for our results and reasons for the discrepancies demonstrated earlier.

B. Surface Ionization Results

1. Potassium

Five runs were taken to determine the relative ionization efficiency of potassium. Knudsen cell temperatures, Tc, ranged

from 380°K to 450°K which corresponded to fluxes at the surface from 4.8×10^{-6} to 1.8×10^{-4} atoms/sec A^2. (All atom fluxes in this discussion will be expressed as atoms per second per square Angstrom unit since this dimension gives one a better feeling of the coverage per unit lattice spacing that is occurring during the experiment.) A summary of the five runs is given in Table 6 and a plot of one of the runs is shown in Figure 14.

Table 6. Summary of the surface ionization of potassium on tungsten

Run W7-K2	Range of filament temperature T_f (°K)	T_c (°K)	Atom flux (atoms/sec A^2)	$10^3 B$	Vacuum 10^{-7} Torr
1	1439-2459	380.7	4.75×10^{-6}	5.73	2.0
2	1727-1926	410.8	3.29×10^{-5}	4.73	2.5
4	1643-2386	410.0	3.14×10^{-5}	4.35	2.0
5	1456-2016	438.0	1.53×10^{-4}	3.03	1.5
6	2313-2716	440.8	1.77×10^{-4}	5.61	2.0 - 30
	Average value of B				B =0.0047
	Standard deviation of the mean value of B				σ_B=0.0008

While the data could be fit to the data of Datz and Taylor (13) very well in the range of 1400°K to 1800°K it is seen that there is a slight falling off of the curve at higher temperatures. This phenomenon was not explained, but it is felt that the error it could produce could not be greater than

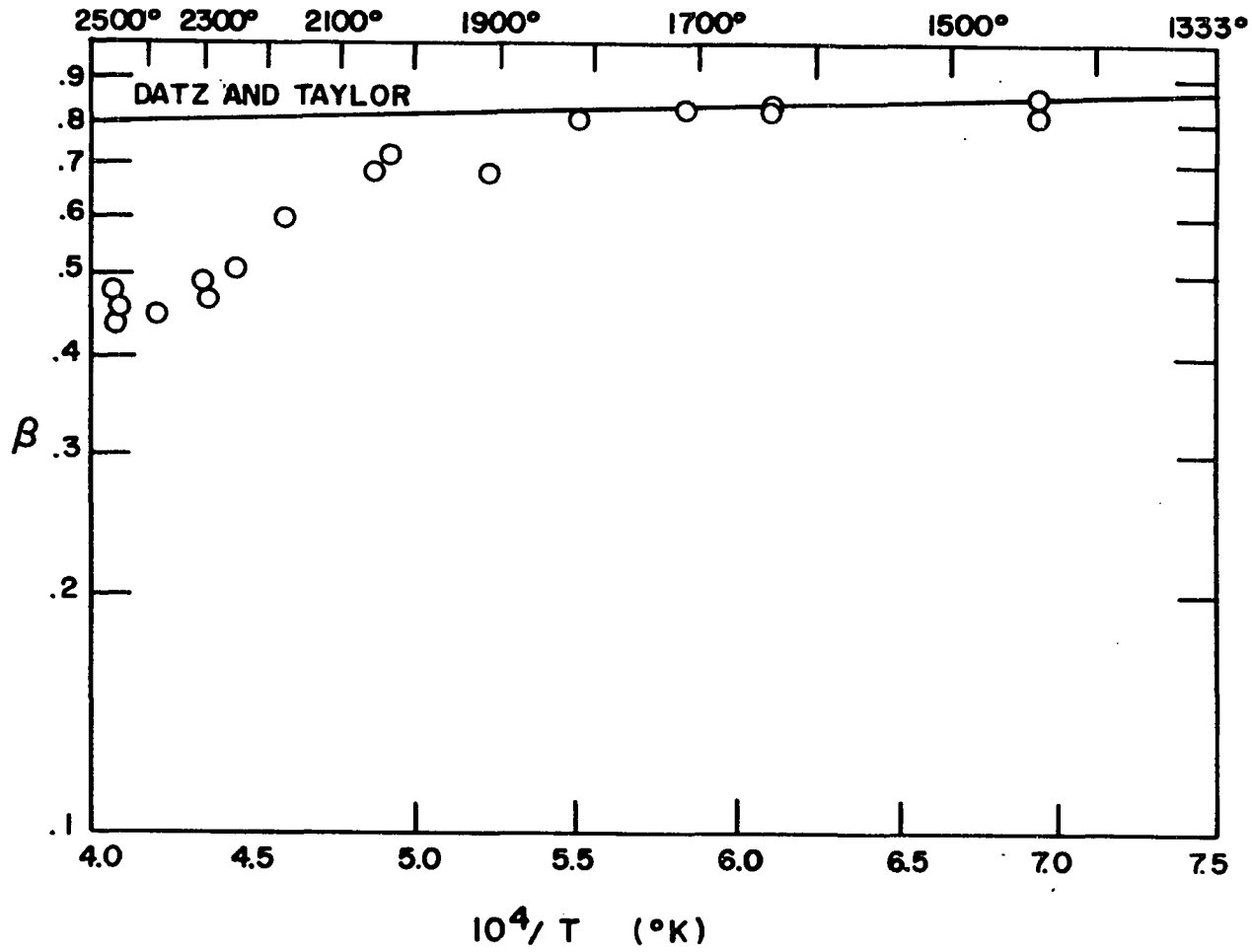

Figure 14. Surface ionization of potassium on tungsten. The value of β is adjusted to fit the data of Datz and Taylor on the low temperature end.

20 per cent. It is quite possible that a small amount of oxygen contamination was present up to 1800°K but not above this temperature. In this case the transmission coefficient B (see Appendix D) would be smaller than is calculated here.

We have by this measurement established the transmission coefficient of the mass spectrometer. It is B = 0.0047 $\pm$ 0.0008.

2. Erbium

The surface ionization of erbium on tungsten filament W8 was studied in a set of nine runs. The cell temperatures varied from 1296 to 1449°K which corresponded to fluxes at the filament from 1.1 to 26 x 10^{-5} atoms/sec A^2. The results of this investigation are tabulated in Table 7. Included in Table 7 are the coefficients A and E in the equation $\beta = A \exp(-E/kT)$ and other conditions that were observed during the run. Figure 15 is a ln β vs. 1/T plot for one of these runs. It should be noted that the "tail off" can be seen to begin at about 2080°K which corresponds to a kT of 0.18 eV. We therefore express the clean surface ionization efficiency of erbium from the (112) direction of a tungsten crystal as

$$\beta = (2.1 \pm 0.4)\, e^{-(1.38 \pm 0.02)/kT}. \tag{25}$$

3. Gadolinium

The surface ionization of gadolinium was studied in a series of eight runs on filament W8. The residual vacuum in this set of runs was not quite as good as for the other

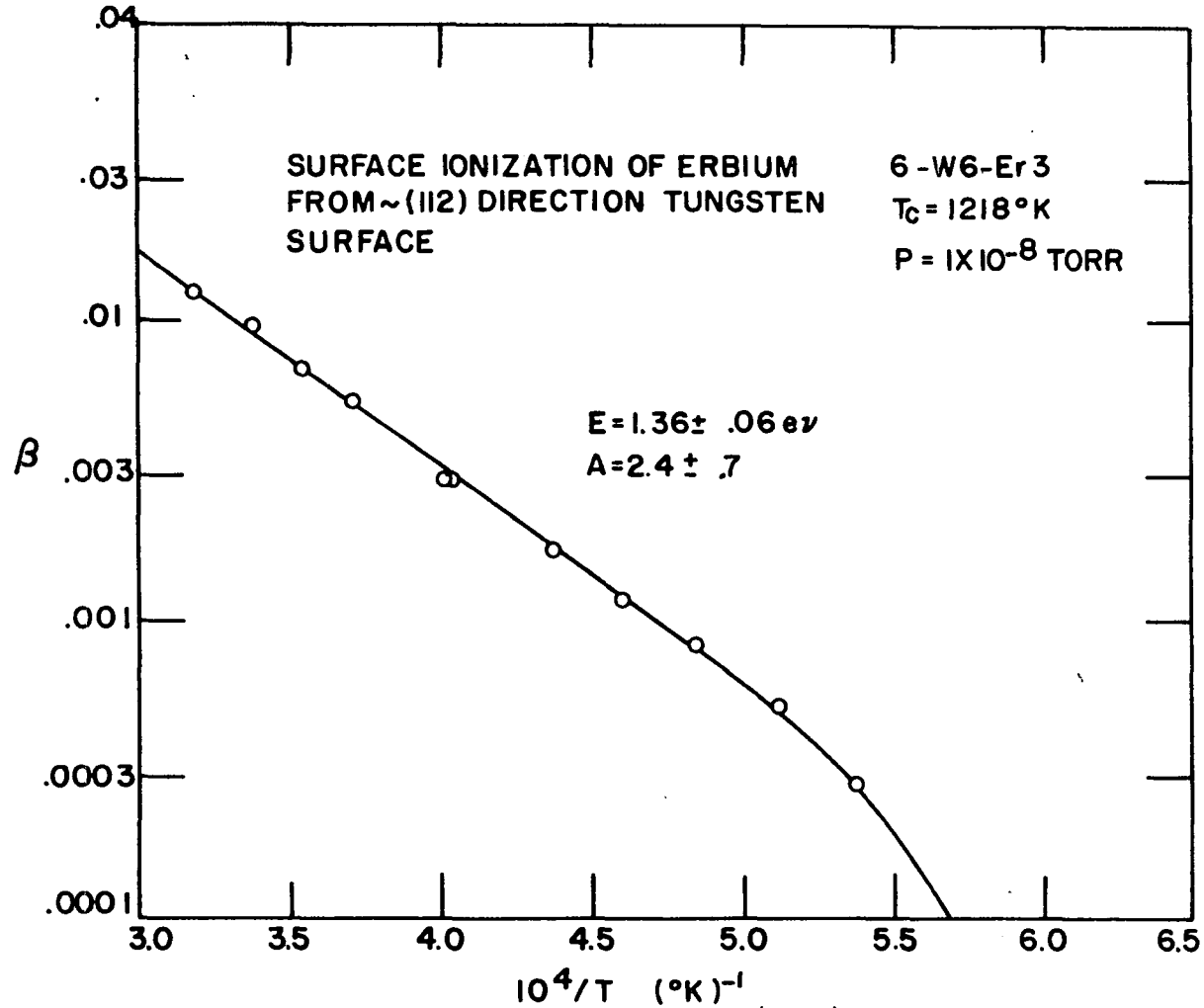

Figure 15. The surface ionization of Er from the ~ (112) direction of a tungsten crystal

Table 7. Summary of W8-Er4 data

Run W8-Er4	E (eV)	σ_E	A	σ_A	Range of T (°K)	T_c (°K)	Vacuum 10^{-8} Torr
1	1.45	0.03	3.2	0.5	2113-2829	1386	2.0
2	1.40	0.05	2.5	0.5	2135-2840	1419	2.0
3	1.43	0.01	2.9	0.2	1969-2835	1421	3.0
4	1.32	0.02	1.5	0.2	1904-2780	1444	1.5
5	1.32	0.02	1.5	0.1	2049-2874	1449	2.0
6	1.34	0.02	1.6	0.2	2134-2940	1400	1.0
7	1.35	0.03	1.7	0.3	2124-2926	1387	1.5
8	1.27	0.05	2.0	0.5	2414-2906	1303	1.5
9	1.40	0.02	2.6	0.2	2339-2913	1423	2.0

Average value of E	1.38 eV
Standard deviation of the mean of E	0.02 eV
Average value of A	2.12
Statistical scatter of the mean of A	0.23
Error in A due to calibration	0.36
Standard deviation of the mean of A	0.43

experiments, but it was well within the fluctuations of vacuum in the preliminary runs on Erbium for which no effect due to poor vacuum could be attributed. Furthermore, no fluctuation in β was evidenced that could be correlated with the factor of ten improvement in vacuum during the eight runs. The runs provide data for atom fluxes to the filament from 2 to 11 x 10^{-5} atoms/sec A^2. The results of these runs are shown in Table 8.

Table 8. Summary of the W8-Gd1 data

Run W8-Gd1	E (eV)	σ_E (eV)	A	σ_A	Range of T (°K)	T_c (°K)	Vacuum 10^{-8} Torr
1	1.61[a]	0.11	6[a]	3	2161-2831	1533	50
2	1.86	0.02	38	3	2128-2826	1522	50
3	1.88	0.03	29	4	2130-2881	1612	20
4	2.01	0.05	60	13	2089-2981	1616	16
5	1.81[a]	0.06	8[a]	3	2161-2821	1572	20
6	2.07	0.09	90	35	2119-2822	1582	7
7	1.85	0.06	30	8	2161-2821	1595	5
8	2.00	0.10	67	30	2114-2522	1582	4

Average value of E (omit runs 1 and 5)	1.88 eV
Standard deviation of the mean of E	0.02 eV
Average value of A (omit runs 1 and 5)	37.6
Statistical scatter of the mean of A	4.0
Error in A due to calibration	6.1
Standard deviation of the mean of A	7.3

[a]Omit from final analysis.

Figure 16 shows a graph of a typical gadolinium run.

At the conclusion of the sets of W8 runs, it was observed that runs 1 and 5 were significantly different than the other eight runs. It was realized that these two runs were the first runs taken after the system had been open to air. It is therefore probable that these filaments, even after being flashed, were not clean until a run had been made. The first

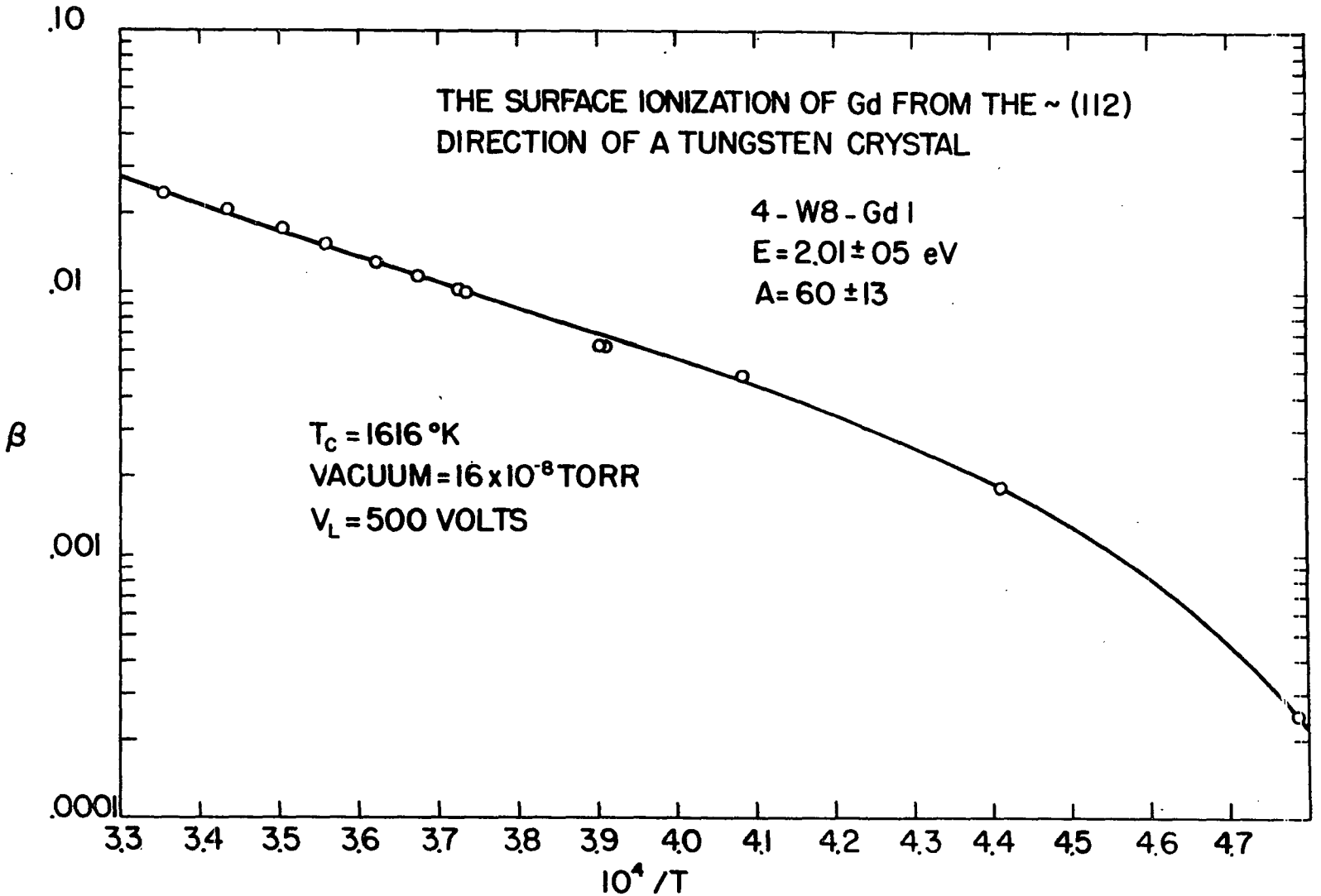

Figure 16. The surface ionization of Gd from the ~ (112) direction of a tungsten crystal

runs, therefore, served as a cleaning mechanism by leaving the filament at elevated temperatures for a length of time in the order of 15 minutes. It is therefore felt that the best value of the ionization efficiency of gadolinium from tungsten is given by

$$\beta = (38 \pm 7)\, e^{-(1.88 \pm 0.02)/kT} \tag{26}$$

In the low temperature range Gd was observed to break away from the straight line at higher temperatures than any of the other rare earths. This may be an indication that the binding energy of Gd to W surfaces is greater. In Figure 16 one can see that the "tail off" sets in at about 2300°K which corresponds to a kT of 0.205 eV.

4. Ytterbium

Eleven runs were made on ytterbium using atom fluxes from 3 to 50 x 10^{-5} atoms/sec A^2 and vacuum pressures in the 10^{-9} Torr range. All the data were taken on filament W8. Table 9 is a summary of the ytterbium runs. After the first two runs a spot was observed on the viewing port window due to the atoms from the Knudsen cell. Since the spot appeared at the point where light from the filament passed to go to the optical pyrometer, a systematic time dependent error in filament temperature of up to 70° was introduced. For this reason the data from these first two runs is not included. All subsequent temperatures were taken with the pyrometer

Table 9. Summary of the ytterbium data

Run W8-Ybl	E (eV)	σ_E (eV)	A	σ_A	Range of T (°K)	T_c (°K)	Vacuum 10^{-9} Torr
3	1.88	0.02	8.4	0.8	2109-2888	671	5
4	1.86	0.006	8.7	0.3	1563-2800	671	4
5	2.17[a]	0.03	44.0[a]	0.6	2008-2939	651	2
6	1.96	0.07	15.0	15.0	2187-2879	649	4
7	2.17[a]	0.04	34.0[a]	7.0	2181-2905	630	2
8	2.03	0.09	9.3	3.7	2139-2908	626	3
9	1.87	0.03	6.6	0.9	2239-2905	628	2
10	1.87	0.03	6.3	1.0	2205-2916	614	2
11	1.87	0.06	5.3	1.7	1935-2722	616	3

Average value of E (omit 5 and 7)	1.84 eV
Standard deviation of the mean of E	0.01 eV
Average value of A (omit 5 and 7)	8.47
Statistical scatter of A	0.38
Error in A due to calibration	1.44
Standard deviation of the mean of A	1.5

[a]Data omitted from final averages.

positioned such that no interference could be caused by subsequent plating out of the atom beam. The only wide discrepancies in this set of runs occur for runs 5 and 7. These runs were the first taken after the system had been dormant for 24 hours or more. Furthermore, the only runs that were taken after such a dormant period were 5, 7, and 11. During

the dormant time the filament was left around 2500°K and the cell temperature turned down to about 500°K. During run 11 the filament was flashed very frequently to 2900°K and this procedure was evidently adequate for cleaning the surface. In runs 5 and 7 the filament was flashed only a few times. We therefore consider the ionization efficiency of ytterbium from the (112) direction of a tungsten crystal to be

$$\beta = (8.5 \pm 1.5)\, e^{-(1.84 \pm 0.01)/kT}. \tag{27}$$

Figure 17 is a graph of a Yb run. A low temperature "tail off" was never found for the Yb runs and data were taken down to 1563°K.

C. Discussion of the Experiment

1. Introduction

The possible difficulties in this experiment are best discussed by considering them to occur in three different areas. The calibration of the experiment from the potassium ionization data is the first area discussed. The nature of the tungsten surface in the absence of contamination is next studied, and finally an examination of the vacuum conditions as related to surface contamination.

2. Calibration

The use of the potassium data as a calibration of the mass spectrometer has several inherent difficulties. We are

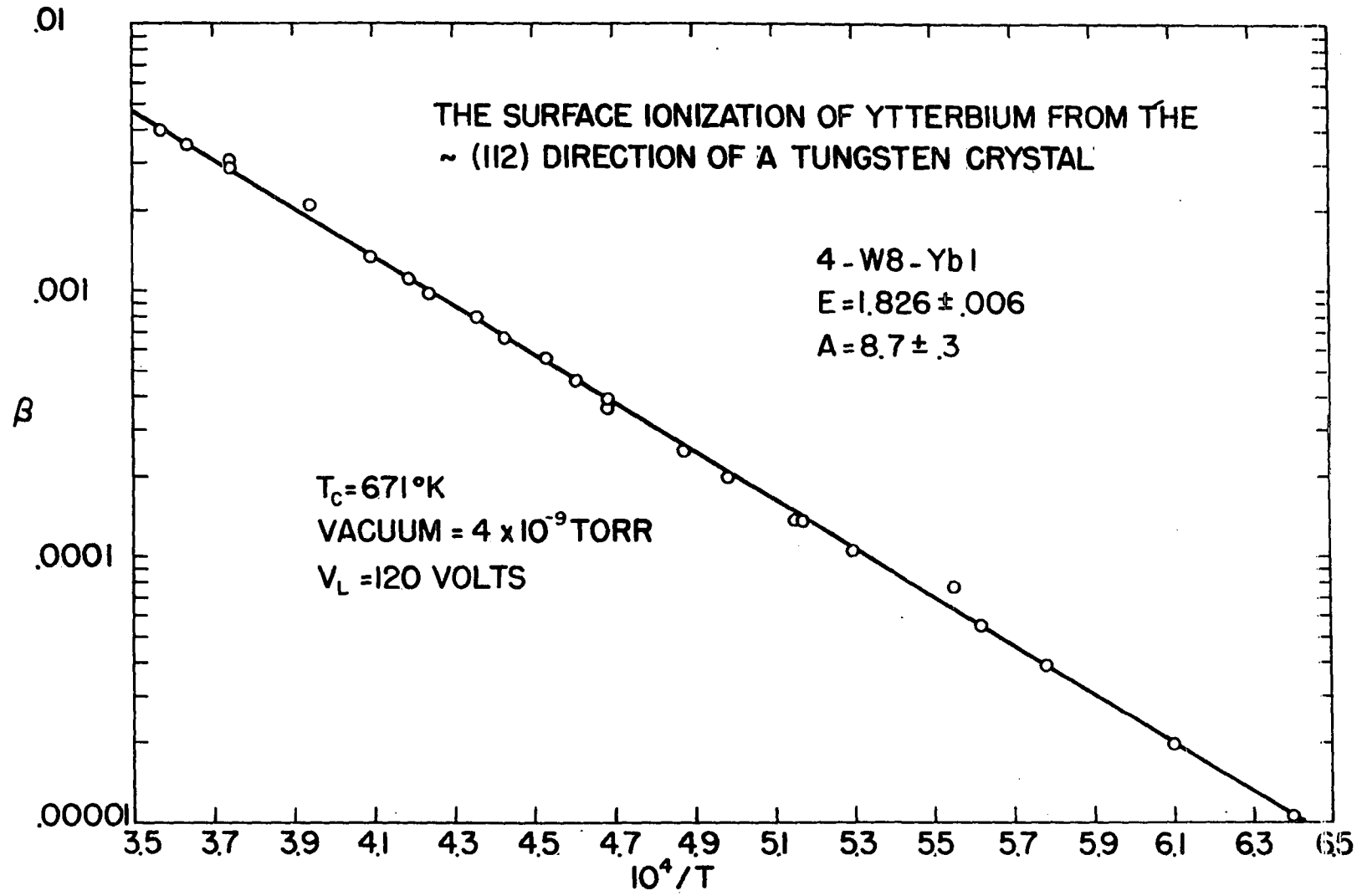

Figure 17. The surface ionization of Yb from the ~ (112) direction of a tungsten crystal

confident that the potassium data in the temperature range from 1400 to 1900°K does adequately describe surface ionization from a clean tungsten surface. However, we were unable to reproduce the potassium data over the entire range, so we must explain the basis of this presumption. Another problem in calibration is the difficulty of determining the proper setting of lens plate voltage such that the transmission of ions from the filament through the slits is not mass dependent. The curves of ion current versus lens plate voltage (see Appendix D) are reproducible to 3 per cent but vary significantly from material to material. For example v(450) for potassium is 0.24 and for erbium it is 0.11. It is assumed that the trajectory of the ions is independent of whether the lens plate voltage is set for maximum beam current or set for maximum transmission. After the ions leave the slit they also pass through the magnetic field whose transmission could also be mass dependent. The dispersion of the ion beam is certainly mass dependent so that the difference in peak heights for different masses will depend on slit width if the slit is narrower than the widths of either peak.

The effect of errors in calibration due to any of the above causes of course acts only as a constant for all of the rare earth data and thus can only cause a shift in all of the intercepts of the rare earth data (except for a minor shift due to the small differences of mass in the rare earths). The

ionization of potassium yielded a fractional error of 0.15 in the mean of six runs. The fluctuations and errors in reading of cell temperature (σ_{T_c} = 1°K) could contribute a fractional error of 0.03. If the work function of the surface were changing from 4.3 to 5.4 eV, the fractional error in the transmission coefficient would be 0.27. If, as is observed in the preliminary studies of erbium, the standard deviation of the surface work function changes is 0.29 eV, then the fractional error in the transmission coefficient will be 0.15, which is in good agreement with the observed standard deviation of the mean. The accuracy of the applicability of the potassium vapor pressure data to our experiment has not been determined but should be within 0.20 of the value used.

3. Surface conditions

If we assume our surface to be clean (we will consider contamination in the next section), the problem of determining its work function is manyfold. The best approach is, of course, an independent measurement which we have made; but because of the sensitivity of the emission current to low work function regions and the sensitivity of SI to high work function regions, one cannot expect the two to be identical for nonuniform surfaces. By x-ray analysis one can determine the orientation of the surface and then use the values of work function quoted in the literature. The reliability of this approach taken by itself is even more doubtful than the

first. The microscopic nature of the surfaces whose work function is used is rarely reported and how these surfaces compare to those of interest on the atomic level is never known. We therefore use the work function measurement as the best measurement of our surface's work function and also consider the values reported in the literature as a check on the validity of our observed work function. Although the precision of our measured work function is 0.03 eV, we would not be surprised to find that the experimental error involved is more like 0.2 eV, since the technique of measurement does not follow the electric field conditions required by past experience. Because of the use of the same filament for all of the runs and the consistent results obtained during each run, it is felt that there is little change in the surface work function during the course of the three runs.

4. Vacuum conditions and surface contamination

To maintain that the vacuum was good enough to insure clean surfaces is a most difficult assertion to make with perfect confidence. We can state that our vacuum was in the range of 2 to 50 x 10^{-9} Torr. This is equal to or less than the pressure ranges reported by any other work in surface ionization known to this writer. The vacuum is not as good as that reported in other areas such as field emission. Our emitting surface temperature was, however, much higher than the temperatures of a field emitter and should therefore not

require such a good vacuum to maintain a clean surface. There is no significant trend apparent when one looks at the results as a function of vacuum. Another check on the cleanliness of the surface is provided by the flashing technique. By flashing the filament to 2900°K during a run one could watch to insure that the current before and after flashing was the same. Changes in beam current were never noted before and after a flash when the filament was above 2500°K. If the filament temperature was between 2000 and 2500°K, and if a difference was observed, there was a long period (greater than 15 minutes) before the filament would return to its preflash ion emission rate. Below 2000°K the contamination of the surface due to the beam generally became appreciable and the decay (or buildup) after flashing could be observed to have time constants in the order of a minute. Again, one cannot be certain that the impingent atoms do not affect the work function of the surface at temperatures greater than the "tail off". However, with considering the extremely low atom fluxes used and considering the lack of correlation between atom flux to the filament and the fluctuations in A and E (see Appendix C), it would again seem that this effect is most unlikely. To demonstrate the correlation of vacuum with the values of E and A, Appendix C shows these quantities plotted as a function of residual vacuum for Er, Gd, and Yb respectively. It should be noted that, in general, the vacuum improves in time and that the observed trends may therefore be evidence of filament

aging or some other time dependent process. It is also true that the vacuum is dependent on cell temperature and thus the values of E and A might be manifesting a variation with atom flux. Appendix C also shows a plot of E and A vs. flux to the filament. The possible trends noted on the figures in Appendix C are not considered large enough relative to the limits of error of the experiment to make a valid correction to the numbers presented here.

D. Comparison with Theory

1. Introduction

In order adequately to compare the results of the surface ionization studies to the theory, we must first establish the parameters to be used in the theoretical equations. Table 10 presents the electronic properties of atoms and ions. The value of Q_+/Q_o was calculated from the energy levels listed in the lower half of Table 10. Unfortunately the levels of neutral erbium were not available to this author so that the assumption $E_+^j = E_o^j$ was necessary to calculate the value of Q_+/Q_o at 2500°K. A sample calculation of Q_+/Q_o for gadolinium is presented in Appendix E. In all discussions we shall assume that the work function of filament W8 is 4.85 $\pm$ 0.03 eV as was determined by the thermionic emission experiment.

A summary of the results of the surface ionization studies is given in Table 11.

Table 10. Electronic properties of atoms and singly charged ions used in this experiment

Atom	Ground State Term Symbols		g_+/g_o	Q_+/Q_o (at 2500°K)	V (eV)	Ref.
	Atoms	Ions				
Potassium	$^2S_{1/2}$	$^1S_0$	0.50	0.50	4.34	(39)
Gadolinium	$^9D_2$	$^{10}D_{5/2}$	1.20	1.06	6.16	(40, 41)
Erbium	$^3H_6$	$^4H_{13/2}$	1.08^+	1.08^-	6.08	(40, 42)
Ytterbium	$^1S_0$	$^2S_{1/2}$	2.00	2.00	6.22	(40)

Gadolinium and erbium have low lying energy levels which are listed below.

Gd^o		Gd^+		Er^+	
Term	E_o^j (eV)	Term	E_+^j (eV)	Term	E_+^j (eV)
$^9D_6$	.213	$^{10}D_{13/2}$	.240	$^4H_{9/2}$	.892
$^9D_5$	.124	$^{10}D_{11/2}$	.144	$^4H_{11/2}$	.886
$^9D_4$	.0661	$^{10}D_{9/2}$	.0785	$^2F_{7/2}$	.670
$^9D_3$	.0266	$^{10}D_{7/2}$	.0324	$^4F_{9/2}$	.636
				$^2H_{11/2}$	.0546

Table 11. Summary of the surface ionization of the rare earths on filament W8

Material	E (eV)	A	$(V-\emptyset)_{theo}$[a] (eV)	A_{theo}[a] S-L	Dob.
Erbium	1.38±.02	2.1±0.4	1.24±.05	1.08	2.00
Gadolinium	1.88±.02	38.0±7.0	1.32±.04	1.06	2.15
Ytterbium	1.84±.01	8.5±1.4	1.38±.04	2.00	2.00

[a]The subscript "theo" means that these coefficients were calculated from the definitions given in Saha-Langmuir or Dobretsov's derivation of ionization efficiency.

The results of the experiment are compared to the theoretical predictions of the Saha-Langmuir theory.

2. Correction to the data

Two corrections should be applied to the slopes as represented by E. These corrections are the Schottky correction for the electric field present and a correction for the temperature dependence of the coefficient A. For the electric field F, at the filament surface we calculate $F = 1.31 \times 10^5$ volts/m which gives a Schottky correction to E of 0.014 eV. For Gd the temperature dependence of A produces an error in E of -0.008 eV and we see that these two nearly insignificant corrections almost cancel each other out. Without knowing the excitation levels of neutral Er we cannot estimate the error in the slope since the assumption of $E_+^j = E_o^j$ renders

the correction negligible.

If the work function of the surface is temperature dependent, we can write $\phi = \phi_o + (d\phi/dT)T$ for a first order approximation. We define ϕ_o as the work function at T = 0. Very little has been reported on the temperature dependence of work function from single crystal surfaces. A letter by Van Oostrom (43) indicates that $(d\phi/dT)$ for the (116) surface is 5.7×10^{-5} eV/°K measured at room temperature. He also indicates that $(d\phi dT)$ for the (111) surface is a factor of ten less. The effect of this first order temperature dependence of ϕ is just a multiplicative factor which appears as part of A. Algebraically we have Equation 6 as

$$\alpha = (g_+/g_o)e^{e(\phi_o+(d\phi/dT)T-V)/kT}.$$

This equation can be simplified to the form

$$\alpha = (g_+/g_o)e^{e(d\phi/dT)/k}\ e^{e(\phi_o-V)/kT}. \tag{28}$$

If we define A_ϕ as

$$A_\phi = e^{e(d\phi/dT)/k},$$

then Equation 28 can be written as

$$\alpha = A_\phi(g_+/g_o)e^{e(\phi_o-V)/kT}. \tag{28}$$

The value of A_ϕ for the (116) surface is calculated to be 1.94 and the value of A_ϕ for the (111) surface is 1.07. One would not be surprised to find the coefficient A_ϕ in the range

$1 < A_{\phi} < 4$ for other surfaces. Van Oostrom indicates that the (116) value of the temperature coefficient is about equal to the average temperature coefficient for a tungsten surface. This is not surprising since it is expected that the average temperature coefficient of the surface will be heavily weighted to low work function planes like the (116). It is also quite possible that the higher work function planes such as those used in this experiment have a higher temperature coefficient than that reported for the (116) direction. Hutson (44) reports a temperature coefficient of -8.3×10^{-5} eV/°K in the (112) direction. This negative coefficient would make $A_{\phi} < 1$.

3. Interpretations

In order to get a better feeling for the difference between the Saha-Langmuir theory and our results we have tabulated the parameters necessary to correct the theory to agree with our results. We define A* and ΔE in the equation

$$\alpha = A' A^* e^{e(\phi_o - V - \Delta E)/kT}, \tag{29}$$

where A′ can be interpreted as the ratio predicted by Saha-Langmuir or that predicted by our interpretation of Dobretsov. Table 12 presents this comparison. The results are in closest agreement with the theory if A* = 1 and $\Delta E = 0$.

Erbium. For erbium it can be seen that the theory is in reasonable agreement with the experiment. The ΔE could be the result of using a ϕ that is not true for the surface. The

Table 12. The constants A* and ΔE required to fit the experimental results to theory

Element	ΔE (eV)	A* Saha-Langmuir	A* Dobretsov
Erbium	.14 ± .05	1.9 ± 0.4	0.9 ± 0.2
Gadolinium	.56 ± .04	35.0 ± 6.0	17.0 ± 3.0
Ytterbium	.46 ± .04	4.3 ± 0.7	4.3 ± 0.7

effect noted earlier (see page 69) from using electric fields that are too small does yield a work function higher than the true work function of the surface and a shift of 0.14 eV lower is certainly in good agreement with other measurements of the (112) work function. The coefficient necessary to fit the Saha-Langmuir theory for erbium could be explained as the result of a temperature coefficient of work function while the Dobretsov result needs no explanation.

Gadolinium. For gadolinium the agreement is poor; it is very improbable that the work function could have been low enough to create this difference. Indeed it would require a work function lower than any (to the author's knowledge) thus far reported for a tungsten surface. The coefficient for gadolinium is also in strong disagreement with the theory. If the value of A* as given by Dobretsov is explained as a temperature coefficient of work function, it would require $(d\phi/dT) = 2.44 \times 10^{-4}$ eV/°K. This value is not only much

larger than is expected, but using it would require the Er and Yb coefficients to be in wide disagreement with the theory. If a theory can be constructed which has in it the concepts used by Dobretsov in the technique for determining the statistical weights of the states, perhaps the SI of Gd can be explained in terms of the number of electrons involved in the adsorption process and the degeneracy of the states while adsorbed on the surface.

Ytterbium. The results of the SI of ytterbium provide little confirmation of the established theories. Whereas the coefficient A* is small enough that arguments of temperature coefficient of the work function and reflection coefficients might be used to explain it, the exponent ΔE is similar to that of Gd in that it is too large to be explained in terms of the work function of the surface. We therefore see that in the process of SI for the rare earths on tungsten the Saha-Langmuir equation is unable to provide an adequate description.

E. Discussion

1. Introduction

The results of this experiment can give us a little insight into the nature of surface interactions with the adsorbed atoms and effects of the surface on the adatoms. We will consider first the effects of the surface on the electronic

structure of the adatoms and secondly the nature of the bonding mechanism for rare earths to tungsten.

2. Electronic structure

The ground state outer electronic structures of the rare earths in their solid or gaseous forms have been established. Moore reports (40) that in addition to the filled shells Gd has seven 4f electrons and one 5d electron, Er has twelve 4f electrons, and Yb has fourteen 4f electrons in the gaseous form. Trulson (45) reports the number of outer electrons in the solid state for Gd to be three, for Er to be three, and for Yb two. All the rare earths used here have two 6s electrons as their outer shell so we see that of our materials we would normally expect Gd to be trivalent ($5d^1 6s^2$), Er to be divalent ($6s^2$), and Yb also divalent ($6s^2$). However, in the light of the solid data it would appear that Er might become trivalent while adsorbed on the tungsten surface. If so, we would expect a larger coefficient for A′ as given by Dobretsov's theory (however, not great enough to be detected in an experiment of this kind). Another indication of the trivalent nature of Er would be from the binding forces. Since the "tail off" of SI sets in at fairly high energies for both Er and Gd but not for Yb, it would seem plausible to claim that they were both being adsorbed with a trivalent mechanism. It would also seem that the ultimate explanation of this experiment must rest, at least partially, upon the electronic

structure of the particular atoms and thus should provide a further probe to understanding electronic structures and the effect of surface forces upon them.

3. Bonding mechanisms

The "tail off" of the curve is explained as the onset of the adsorption of the rare earth on the filament. Other explanations infer the existence of molecular ion beams evaporating from the surface. These were never found in this experiment. The trend of the data is consistent with other investigations or rare earth bonding. Trulson (45) has summarized the results of this laboratory on the cohesive energy of the rare earths. In his work he found the cohesive energy of gadolinium to be 81 Kcals/mole as compared to 75 for erbium and 40 for ytterbium. The presence of three valence electrons in Gd must surely increase the energy of binding of Gd to a surface as compared to Yb. The fact that Er seems to be bound with an equivalent force to that of Gd is an indication that Er might be trivalent when bound to a tungsten surface.

If one looks at the model in Figure 18, the white ball represents a rare earth atom adsorbed on the surface. One can see that the rare earth atoms have many sites on the surface to which they can bond with at least four nearest neighbors. On the (113) surface there are sites that could have six nearest neighbors depending on the radius of the particular

Figure 18. Adsorption of rare earths on tungsten crystal surfaces. The pyramid is formed by the intersection of (a) four (113) planes and (b) four (112) planes.

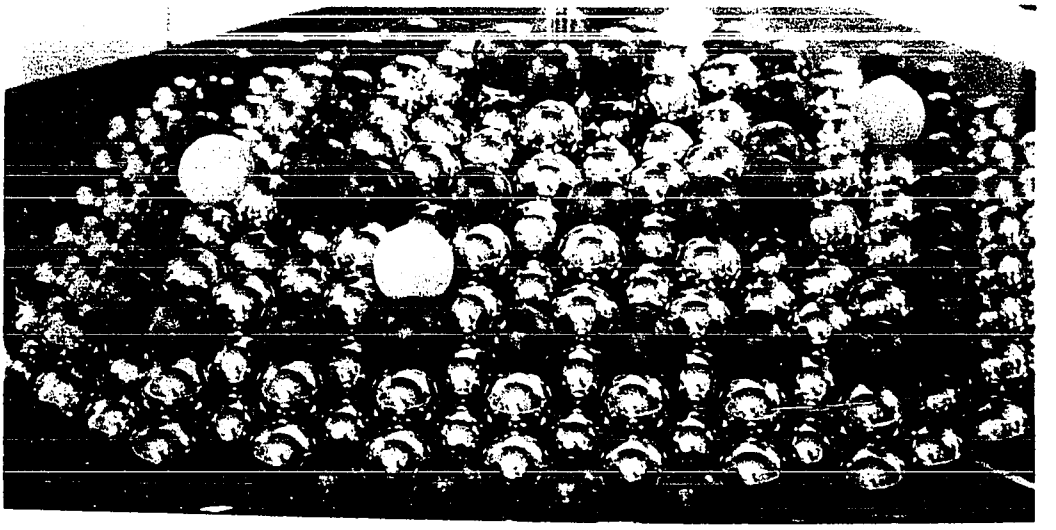

(a)

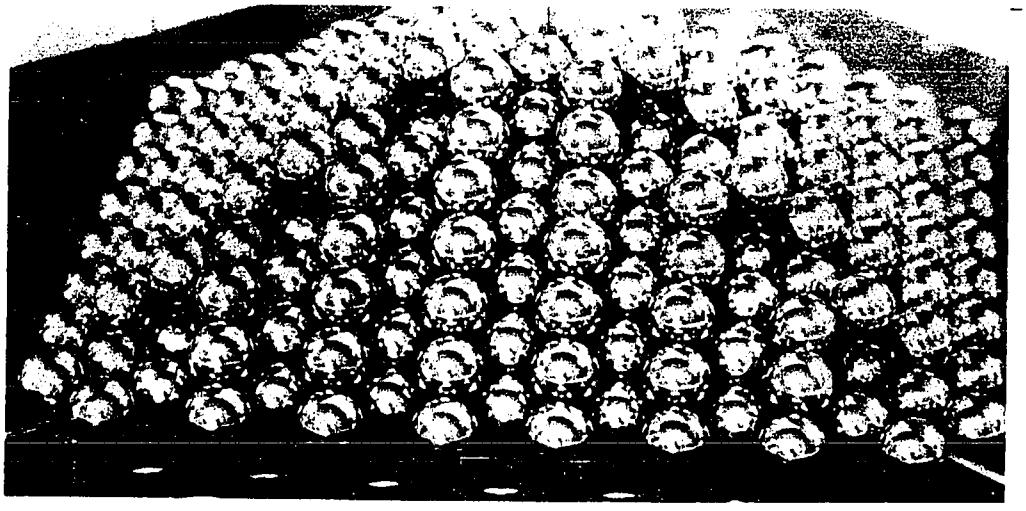

(b)

rare earth in the hard sphere approximation. Because of the possible trivalent surface bonding and the availability of very stable sites for adsorption, it is not surprising to have the "tail off" appearing at high temperatures (compared to the "tail offs" observed for other materials) for Er and Gd, and therefore implying large desorption energies.

4. Discussion of the electronic data

The ionization potentials as reported by Moore (40) were determined spectroscopically for Gd and Yb. The value given for Er was determined by a surface ionization technique described by Zandberg and Ionov (2). The technique was one of comparing the ionization efficiency of In to that of Er. Since the ionization potential of In is well known the slope of,

$$(30) \quad \ln (\beta_{Er}/\beta_{In}) = \ln (A_{Er}/A_{In}) + (V_{In}-V_{Er})/kT,$$

provides the energy difference and thus the ionization potential of Er. This technique does not rely entirely on the validity of Equation 2, but actually requires only that β can be described by the product of two functions, one which is dependent on the surface and the other which is $Q_+/Q_o \exp(-V/kT)$. Zandberg demonstrated that this is true for the case of a patchy surface if the emission from each patch of the surface can be described by Equation 6. However, if the results of this study are to be believed, it is not clear that this

separation of β is possible for the rare earths. Preliminary results of Mr. Peter Sivgals of this research group (Exp. Phys. Gr. V) indicate that the ionization potential of Er determined by electron bombardment is 6.13 $\pm$ 0.05 eV which does in fact agree quite well with the value of 6.08 $\pm$ 0.03 eV as reported by Ionov (46). It appears that the value given for erbium was good due to a fortunate choice of materials since our results indicate that of the materials studied Er follows the Saha-Langmuir equation most closely. The measurement of the ionization potentials of the rare earths by this group also indicate that the ionization potential of Gd is about 0.05 eV greater than that of Er which is in good agreement with the spectroscopic information on Gd. Thus it is felt that the ionization potentials of the rare earths studied are sufficiently well known that they could not cause any of the observed discrepancies. Because there are low lying excitation levels in both Er and Gd their effect on the results should also be mentioned. Their effect on the density of states coefficient is minor as can be seen in Table 10. It can also be seen that if the atoms were being taken from an excited state to the ionic ground state that our observed E should be less than V-$\emptyset$ rather than greater as is observed.

VIII. SUMMARY

In summary we can state that the absolute ionization efficiency of gadolinium, erbium, and ytterbium from the (112) direction of a clean tungsten surface has been measured. The results of these measurements are best expressed in terms of the experimental equations:

(31) Erbium $\beta = (2.1 \pm 0.4)\ e^{-(1.38 \pm .02\ eV)/kT}$,

(32) Gadolinium $\beta = (38.0 \pm 7.0)\ e^{-(1.88 \pm 0.02\ eV)/kT}$,

and

(33) Ytterbium $\beta = (8.5 \pm 1.5)\ e^{-(1.84 \pm 0.01\ eV)/kT}$.

Much effort has been directed toward insuring clean, stable, and single crystalline surfaces. The above equations represent data taken in an ultrahigh vacuum environment in which proper care has been taken to insure a clean surface at all times. The Richardson work function of the surface is 4.85 $\pm$ 0.03 eV; the (112) direction is normal to the surface. It is evident that the Saha-Langmuir equation does not apply to these observations and that further theoretical studies must be made to describe the surface ionization of rare earths from tungsten.

IX. LITERATURE CITED

1. Good, R. H. and Müller, Erwin W. Field emission. In Flugge, S., ed. Handbuch der Physik. Vol. 21. pp. 218-230. Berlin, Germany, Springer Verlag. 1956.

2. Zandberg, E. Ya. and Ionov, N. I. Surface ionization. Soviet Physics-Uspekhi 67: 255. 1959.

3. Langmuir, Irving and Kingdon, K. H. Thermionic effects caused by vapors of alkali metals. Royal Society (London) Proceedings Series A 107: 61. 1924.

4. Fox, Harold Gene. Ionization of some rare earth atoms at metallic surfaces. Unpublished M.S. thesis. Ames, Iowa, Library Iowa State University of Science and Technology. 1959.

5. Copley, M. J. and Phipps, T. E. Surface ionization of potassium on tungsten. Physical Review 48: 960. 1935.

6. Becker, J. A. Thermionic and adsorption characteristics of cesium on tungsten and oxidized tungsten. Physics Review 28: 341. 1926.

7. Langmuir, Irving. Thermionic effects caused by alkali vapors in vacuum tubes. Science 57: 58. 1923.

8. Kaminsky, M. Atomic and ionic impact phenomena. [To be published in Ergebnisse der Exacten Naturwissenschaften circa 1964].

9. Dobretsov, L. N. Electronen-und ionenemission. Berlin, Germany, VEB-Verlag Technik. 1954.

10. Romanov, A. M. and Starodubtsev, S. V. Adsorption and ionization of sodium on hot tungsten. Soviet Physics-Technical Physics 2: 652. 1957.

11. Zemal, J. Surface ionization phenomena on polycrystalline tungsten. Journal of Chemical Physics 28: 410. 1958.

12. Szhenov, Yu. K. On the mechanism of surface ionization of atoms of the alkali earth metals. Soviet Physics JETP. 10: 239. 1960.

13. Datz, Sheldon and Taylor, Ellison H. Ionization on platinum and tungsten surfaces. I. The alkali metals. Journal of Chemical Physics 25: 389. 1956.

14. Datz, Sheldon and Taylor, Ellison H. Ionization on platinum and tungsten surfaces. II. The potassium halides. Journal of Chemical Physics 25: 395. 1956.

15. Werning, Joseph R. Thermal ionization at hot metal surfaces. U. S. Atomic Energy Commission Report UCRL 8455 [University of California, Berkeley, Radiation Laboratory] 1958.

16. Reynolds, F. L. Ionization on tungsten single-crystal surfaces. Journal of Chemical Physics 39: 1107. 1963.

17. Ramsey, N. F. Molecular beams. Clarendon Press, Oxford. 1956.

18. Inghram, Mark G. and Hayden, Richard J. A handbook on mass spectroscopy. National Academy of Sciences-National Research Council Publication 311. 1954.

19. Mueller, Donald D. The theory of surface ionization and its application to ion propulsion. U. S. Atomic Energy Commission Report AD 268,695. [Armed Services Technical Information Agency, Dayton, Ohio.] 1961.

20. Cayless, M. A. Thermionic generation of electricity. British Journal of Applied Physics 12: 437. 1961.

21. Saha, Megh Nad. Ionization in the solar chromosphere. Philosophical Magazine Series 6, 40: 472. 1920.

22. Landau, L. D. and Lifshitz, E. M. Statistical physics. Reading, Massachusetts, Addison Wesley. 1958.

23. Johnson, Robert G., Hudson, Donald E., Caldwell, Wallace C., Spedding, Frank H., and Savage, William R. Mass spectrometric study of phase changes in aluminum, praseodymium, and neodymium. Journal of Chemical Physics 25: 917. 1956.

24. Johnson, Robert G., Hudson, D. E. and Spedding, F. H. Mass spectrometric determination of latent heats of metals. U. S. Atomic Energy Commission Report ISC-293 [Ames Laboratory, Ames, Iowa]. 1952.

25. Kerwin, Larkin. Improved magnetic focussing of charged particles. Review of Scientific Instruments 2: 36. 1949.

26. Kerwin, Larkin. A new type mass spectrometer. Review of Scientific Instruments 21: 96. 1950.

27. Kerwin, Larkin. Note on the resolving power of mass spectrometers. Canadian Journal of Physics 30: 503. 1952.

28. Caulfield, Henry John. Cohesion in the intermetallic series Mg_2Si, Mg_2Ge, Mg_2Sn, and Mg_2Pb. Unpublished Ph.D. thesis. Ames, Iowa, Library, Iowa State University of Science and Technology. 1962.

29. Romanov, A. M. and Starodubtsev, S. V. Role of surface nonuniformity in the adsorption and ionization of sodium and lithium on tungsten. U. S. Atomic Energy Commission Report AEC-tr-5668. [Technical Information Service Extension, AEC] 1956.

30. Kostkowski, H. J. and Lee, R. D. Theory and methods of optical pyrometry. National Bureau of Standards Monograph 41. 1962.

31. Nottingham, Wayne B. Thermionic emission. In Flugge, S., ed. Handbuch der Physik. Vol. 21. pp. 1-175. Berlin, Germany, Springer-Verlag. 1956.

32. Hughes, F. L., Levinstein, H. and Kaplan, R. Surface properties of etched tungsten single crystals. Physical Review 113: 1023. 1959.

33. Nichols, M. H. The thermionic constants of tungsten as a function of crystallographic direction. Physical Review 57: 297. 1940.

34. Smith, George F. Thermionic surface properties of tungsten crystals. Physics Review 94: 295. 1954.

35. Smirnov, B. G. and Shuppe, G. N. O rabote vykhoda elektronovu nekotorykh granei monokristalla vol'frama. Zhurnal Tekhnicheskoi Fiziki 22: 973. 1952.

36. Müller, Erwin W. Work function of tungsten crystal planes measured by the field emission microscope. Journal of Applied Physics 26: 732. 1955.

37. Dyke, W. P. and Dolan, W. W. Field emission. Advances in Electronics and Electron Physics 8: 89. 1956.

38. Coblenz, W. W. Thermal radiation from selected sources of radiation. In Forsythe, W. E , ed. International Critical Tables. Vol. 5. pp. 242-244. New York, New York, McGraw-Hill Book Co., Inc. 1929.

39. Herzberg, Gerhard. Atomic spectra and atomic structure. 2nd ed. New York, New York, Dover Publications. 1944.

40. Moore, Charlotte E. The atomic spectra of the rare earths: their presence in the sun. Applied Optics 2: 665. 1963.

41. Russel, Henry Norris. The arc and spark spectra of gadolinium. Journal of the Optical Society 40: 550. 1950.

42. Judd, B. R. and Marquet, L. C. Energy levels of Er II. Journal of the Optical Society 52: 504. 1962.

43. Van Oostrom, A. Temperature dependence of the work function of single crystal planes of tungsten in the range 78°-293°K. Physics Letters 4: 34. 1963.

44. Hutson, Andrew R. Thermionic emission from single crystal W. Physical Review 98: 889. 1955.

45. Trulson, O. Conrad. Cohesive energies of europium, gadolinium, holmium, and erbium. Journal of Chemical Physics 35: 1018. 1961.

46. Ionov, N. I. and Mittsev, M. A. Atomic first ionization potentials determined by the method of surface ionization. Soviet Physics JETP 13: 518. 1961.

47. Hultgren, Ralph, Orr, Raymond L., Anderson, Phillip D., and Kelley, Kenneth K. Thermodynamic properties of metals and alloys. New York, New York, John Wiley and Sons, Inc. 1963.

48. Haberman, C. E. Vapor pressures of the rare earth metals. Unpublished Ph.D. thesis. Ames, Iowa, Library, Iowa State University of Science and Technology. 1963.

X. ACKNOWLEDGMENTS

The author wishes to thank Dr. D. E. Hudson for his suggestion of this problem and for his continued guidance as the work developed. Without his efforts this research could not have been completed.

Dr. R. H. Good and Dr. R. S. Hansen generously helped in the interpretation of the theory of surface ionization. Dr. V. A. Fassel, Dr. D. Peterson, and Dr. H. J. Svec were generous in their respective consultations on spectroscopy of the rare earths, on tungsten crystal growing, and on mass spectrometer instrumentation.

Indispensible help was provided by the group of Dr. G. C. Danielson in the use of the crystal growing apparatus, by the group of Dr. J. F. Smith in the use of the x-ray equipment, and by the group of Dr. D. R. Fitzwater in the programming and use of the computer.

Special acknowledgment is accorded to Dr. F. H. Spedding, Dr. A. H. Daane, and Dr. C. E. Habermann who provided the rare earth samples used. Dr. Habermann also kindly provided rare earth vapor pressure data prior to its publication in his doctoral dissertation.

Thanks are given to the following present and former members of Experimental Physics Group V: Mr. P. Sivgals for his provision of information on the ionization potentials of the rare earths; Mr. R. M. Morgan for his assistance in taking

and analyzing data; Dr. H. J. Caulfield for his help in the design and initial construction of the mass spectrometer; and Mr. H. G. Fox for his guidance in the initial orientation of the writer to this project. The following research helpers have assisted in data analysis and instrumentation: Mr. M. B. Van Roekel, Mr. H. A. Ryder, Mr. A. Kirby, Mr. D. O. Nassen, and Mr. M. L. Wonio.

The efforts of the shops of the Ames Laboratory and especially of Mr. Gary Wells are greatly appreciated.

Finally, thanks must be given to my wife, Mrs. M. L. Dresser, who has not only aided in the analysis of much of this data, but whose interest and concern have made the completion of this project possible.

XI. APPENDIX A: THE HIGH VACUUM MASS SPECTROMETER

A. Introduction

A necessary requirement for the accomplishment of the SI experiment was a mass spectrometer which could be operated in the ultrahigh vacuum range. Since commercial mass spectrometers are not designed for this type of operation, it was necessary to construct our mass spectrometer in this laboratory. Considerations necessary in the design were first of all a mass spectrometer of sufficient resolution to be usable in the mass range of the rare earths and secondly that the system must be easily bakeable if the high vacuum conditions are to be met. In this discussion we will, therefore, first consider the system as a mass spectrometer and secondly as an ultrahigh vacuum system. Figure 19 is a photograph of the completed equipment during use. On the left is the mass spectrometer. The source chamber can be identified on the front by the large circular flange which was used as a vacuum seal. The Cary electrometer preamplifier head can be seen on the far end where it connects to the collector. The right coil of the magnet can be seen on the right of the mass spectrometer frame and the hydraulic jack for raising and lowering the magnet is visible in the base of the frame. The optical pyrometer is found in front of the mass spectrometer on its rigid isolated mount. The left relay rack contains the magnet and vacuum power supplies. The right relay rack contains the other power

Figure 19. The ultra-high vacuum mass spectrometer after completion

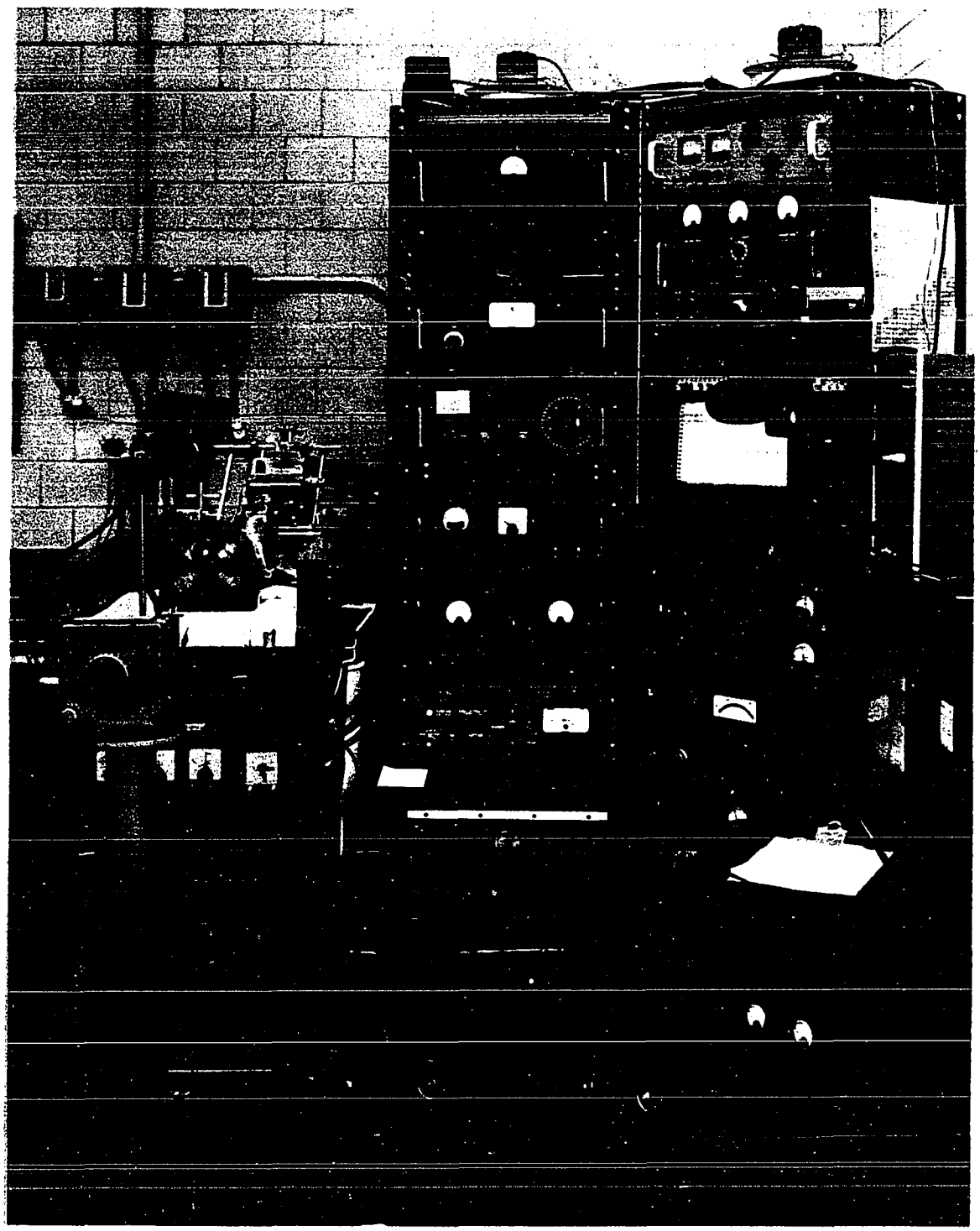

supplies and recording gear necessary for the experiments.

B. The Mass Spectrometer

Introduction. Referring back to Figure 1, we will break this discussion down into four parts. The source, S, the magnet, M, the collector system, C, and the accessory apparatus. Since the source has been carefully described earlier from a physical point of view in this discussion we will only present the dimensions, material, and design of the source.

Ion source. A dimensioned drawing of the source can be found in Figure 20. All the plates were made of stainless steel. The defining slit was made of two stainless knife edges and the exit slit was made of two pieces of Ta sheet. All electrical insulation was made from vycor blocks. The atom source heat and electrostatic shield was a box made from Ta sheet also.

Magnet. The mass analyzer is used to refer to the magnetic field. Because of the requirements of the high vacuum system for bakeout, some special considerations were required in the mounting of the magnet. The magnetic field was designed to deflect the tuned ion beam through an angle of 60° for an angle of 30° incidence to the magnetic field.

In most mass spectrometers the magnet need never be removed from the mass tube so that great efforts are not required to make the magnet's position easily reproducible.

Ion Source Dimensions

	Length (Cm)	Width (Cm)	Dia. (Cm)
Filament Slot	1.91	.318	
Lens Plate Slot	1.91	.635	
Slit S_1	1.27	.043	
Slit S_2	1.59	.051	
Viewing Hole V	—	—	.28
Collimator C	—	—	.28

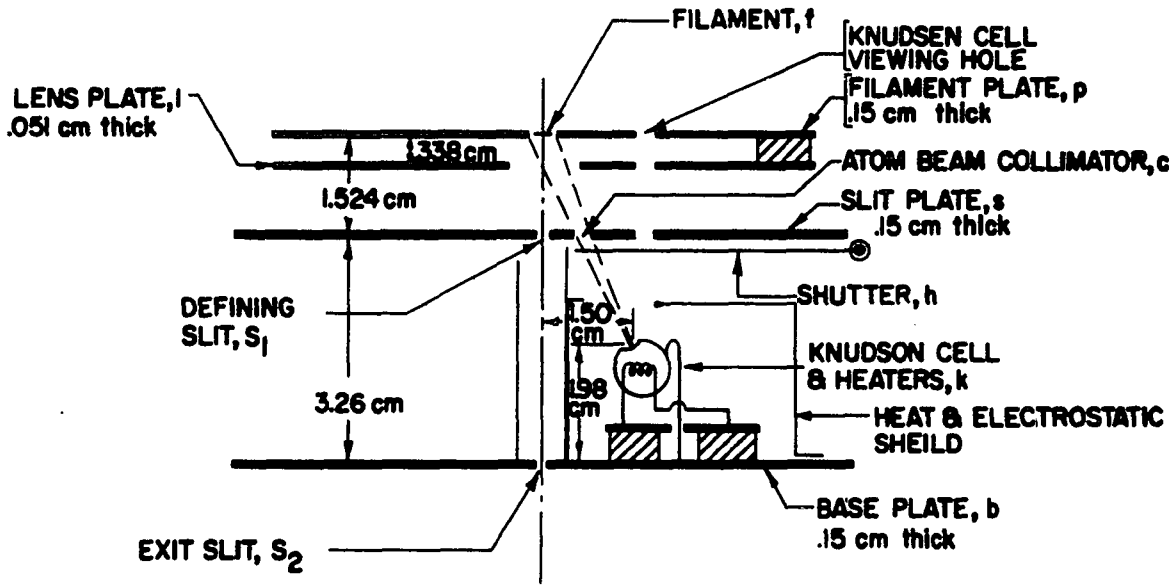

Figure 20. Cross sectional view of the ion source and ion optical system

However, when vacuum requirements necessitate a vacuum bake-out, one must either remove the magnet from the mass tube, heat the magnet pole pieces along with the mass tube, or devise very thin ovens to heat just the mass tube while in the gap. The first approach seemed the simplest and was therefore implemented. Past efforts in this direction have been to mount the magnet very rigidly to an adjustable base and by using very strong guide rods hope to reproduce the position accurately. Our method (see Figure 21) was to mount the magnet to an easily movable platform by four heavy-duty springs and a hydraulic jack. A set of guide plates (Figure 22) was then made so that as the magnet was raised by the hydraulic jack into position the guide plates, which were rigidly mounted relative to the mass tube, could position the magnet pole pieces in a repeatable position each time the magnet was raised. The guide plates were given two linear degrees of freedom and one rotational degree of freedom. The value of this type of approach is that the location of the magnet is determined by a device very close to the magnet gap and the positioning of the magnet is not done by a device that must also carry the weight of the magnet. This means the positioning device need not be so rigid.

The magnetic field was produced by pole pieces shaped as in (M) of Figure 1. The beam entered and left the magnetic field through faces that are at 90° to each other. The beam

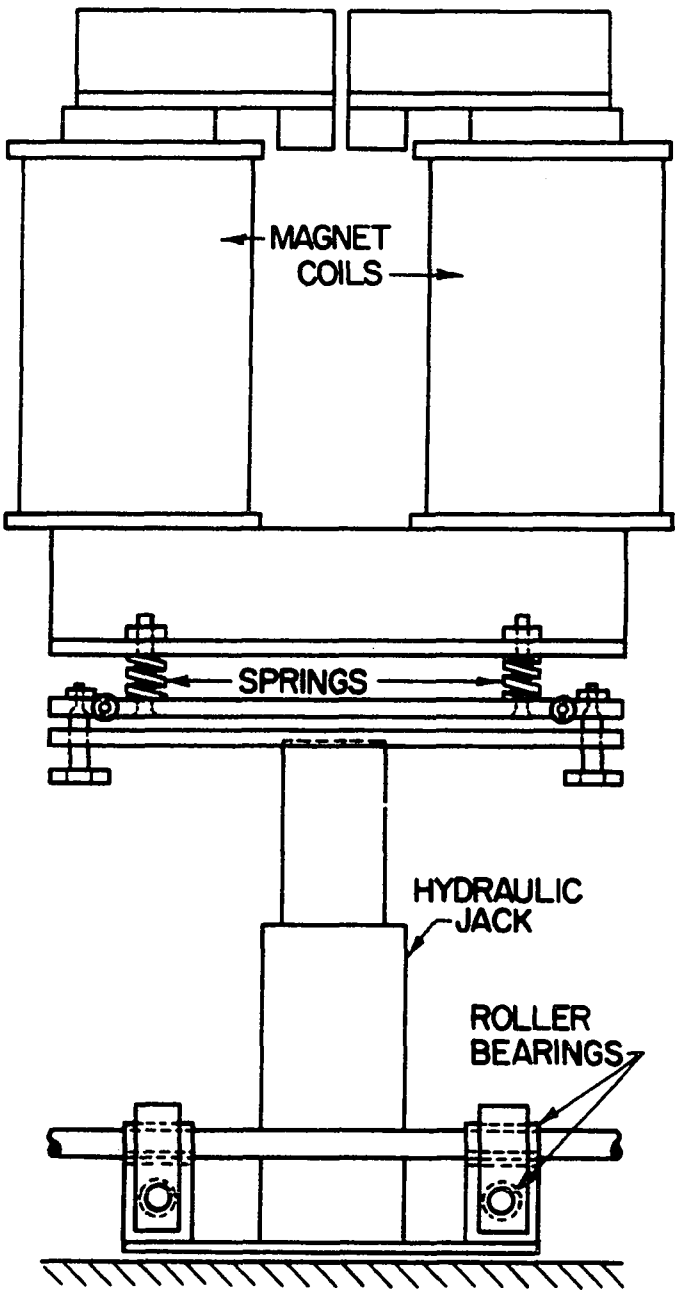

Figure 21. The magnet support

Figure 22. The magnet guide plates

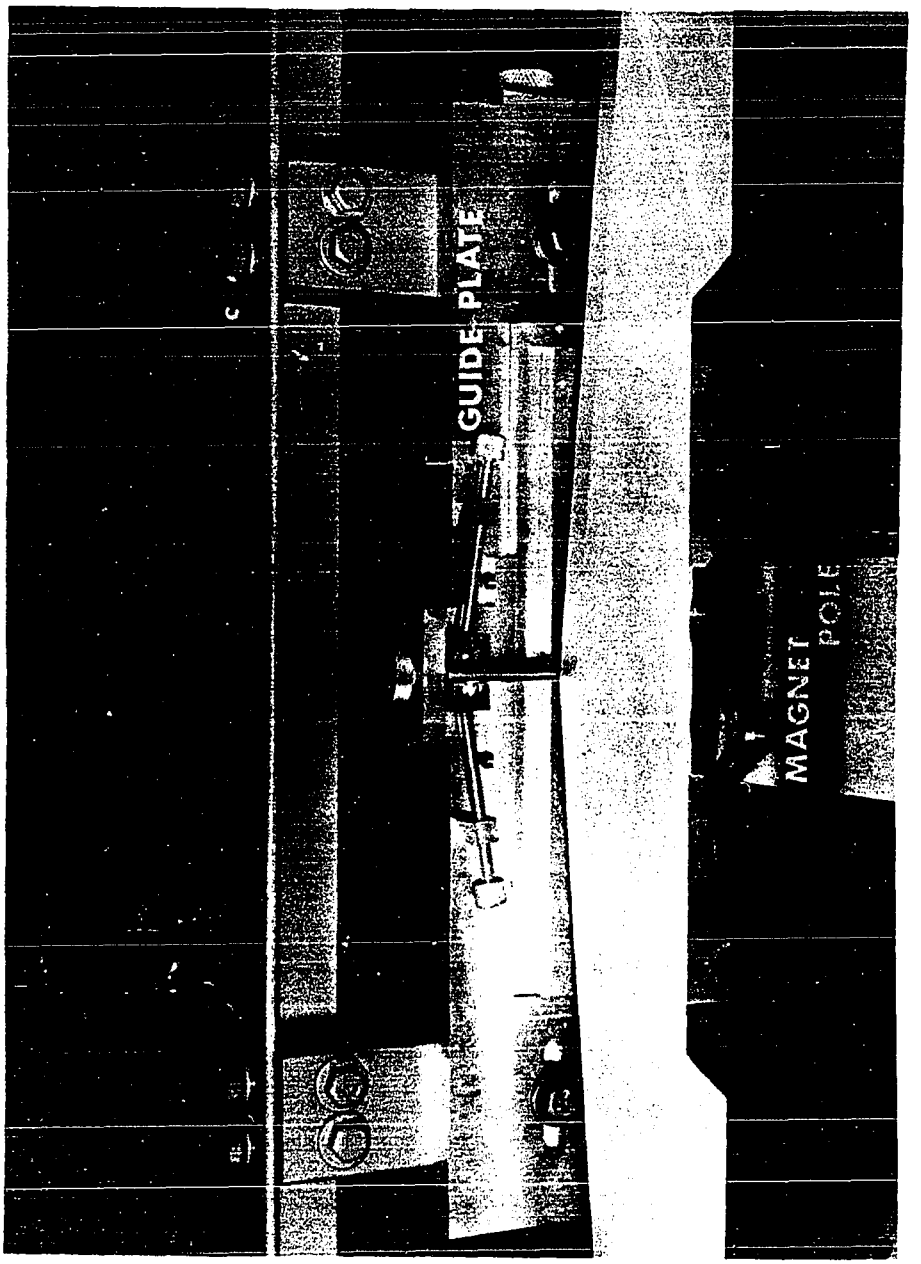
GUIDE PLATE
MAGNET POLE

had an angle of incidence of 30° to one face and an angle of excidence of 30° to the other face when focused on the collector. The beam was therefore bent through an angle of 60° when properly focused on the collector. While in the magnetic field the focused beam had a radius of curvature of 22.8 cm. The gap width between the pole pieces was 1.4 cm. The theory of inflection focusing has been discussed thoroughly by Kerwin (25,26,27). Kerwin has calculated the ideal field shape by finding the field shape that will take all the particles from a given source and focus them at some other point. He further required that the magnetic field should be symmetric about the midpoint of the two focal points. This ideal field can be best approximated by a straight line at two points. The first point is the case where the ion enters the magnetic field with no angle of incidence, and the second point is the one where the ion enters at the inflection point of the magnetic field outline. It is then shown by Kerwin that the second (or inflection) case provides a greater resolution for the same size magnet pole face than the first (or normal) focusing case.

Collector system. The collector system consisted of one slit plate and a Faraday cage collector. The physical arrangement can be seen in Figure 23. The collector slit was adjustable but set between 15 and 20 mils for all the work described herein. The Faraday cage collector was a tantalum

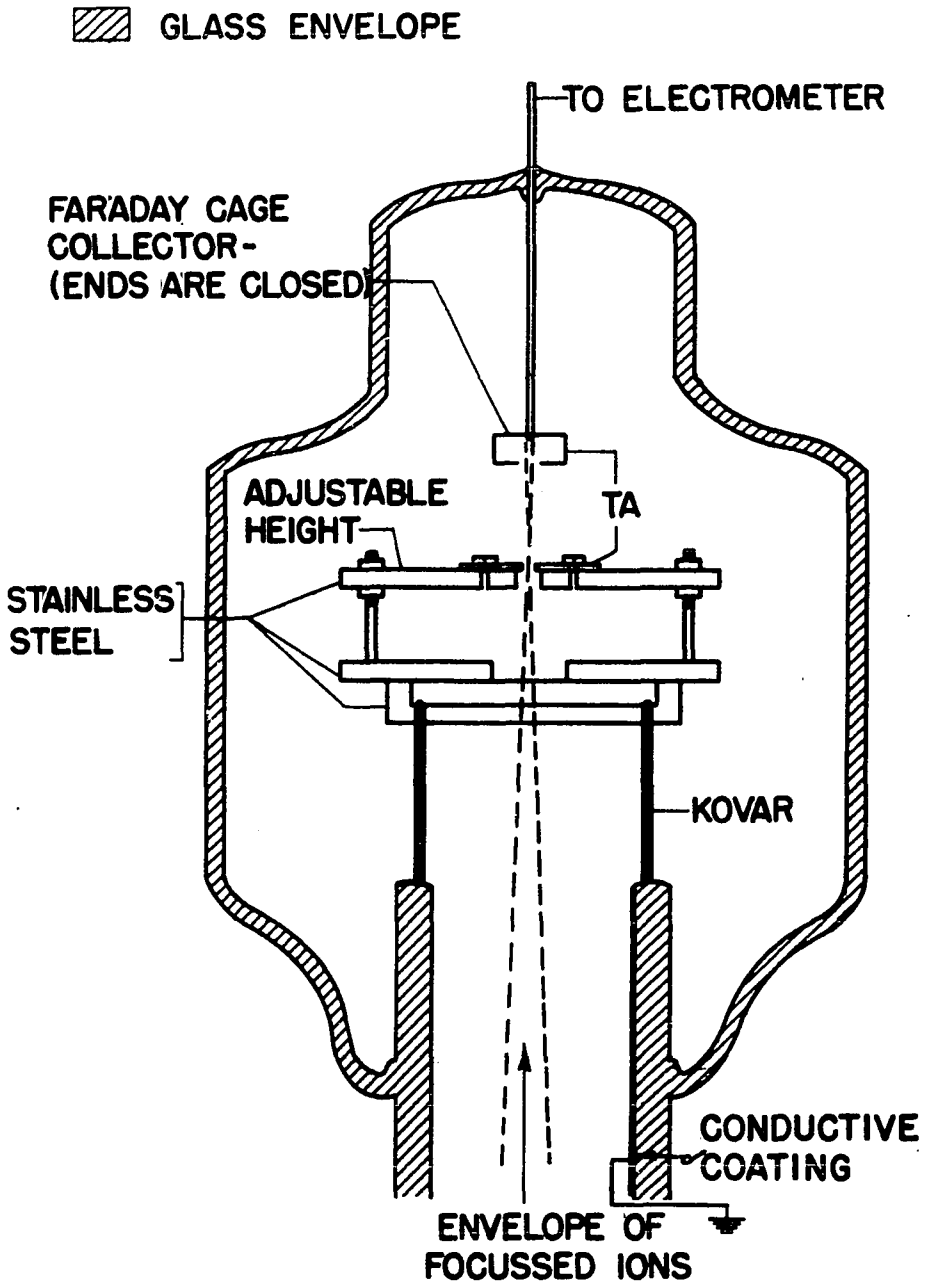

Figure 23. The ion collector

box about 3/4" x 1/2" x 3/16" and the ions entered the box through an opening about 0.04" x 3/4" in the front face.

Accessory apparatus. The magnet power supply was designed and built by the Instrumentation Group of Ames Laboratory. The power supply could deliver up to 500 mA to a 500 ohm load and was regulated for constant current to 0.025 per cent in an 8-hour period. The power supply operated by sensing the voltage across a 3.15 ohm resistor in series with the output. This signal was then compared to a standard reference voltage and the difference was then fed into a chopper amplifier whose output controlled the grid of a tube in series with the output of the power supply. The grid was controlled by the amplifier such as to null the input to the amplifier. The reference voltage was continuously variable to permit scanning to find the desired ion beam.

In the preliminary investigations, a Brown vibrating reed electrometer was used to measure the ion beam current and in all subsequent investigations an Applied Physics Corporation Cary Model 31 vibrating reed electrometer was used.

C. The Vacuum System

The vacuum system consisted of electronic pumps, initial pump down gear, the ultrahigh vacuum enclosure, and ovens for baking out the system. The vacuum system was pumped to as low as 5×10^{-10} Torr but most data were taken in the 5×10^{-8} to 5×10^{-9} Torr range.

The pumps. Two Varian Associates 5-liter per second Vacion pumps were used to maintain the high vacuum environment. The initial pump down to 2 microns was achieved with a Welch rotary vacuum pump in series with a liquid nitrogen trap.

The envelope. The envelope was predominantly glass with some kovar and stainless steel surfaces. In terms of Figure 1, the envelope can be discussed in four parts: the source chamber (S), the mass tube(T), the collection chamber (C), and the roughing section (g).

The source chamber was constructed from a 5.5" kovar to pyrex graded glass seal and a 4" Ultek viewing port. The viewing port was attached to the male half of a six inch Ultek copper shear seal. The large kovar seal was heliarced to the female half of the copper shear seal and the glass end of the kovar shear was tapered down to a ring seal with the mass tube. The Ultek copper shear gasket provided easy access to the source for changing samples, filaments, etc. Seven electrical pass throughs were provided by removing the inside of a NRC 507 ion gauge and then extending the wires to a useable length by spot welding on 60 mil nickel wire. The gauge enclosure was then resealed together and attached to the side of the source chamber. Two other pass throughs were provided by press sealing 40 mil tungsten wire to uranium glass and then attaching to the source chamber wall.

The mass tube was made from 1-1/4" medium wall pyrex

tubing. The section of the mass tube that passes between the magnet poles was flattened by a graphite mold while in an oven at 800°C. To mold the tube, the tube was bent to the proper curvature and placed in the mold. The mold was then placed in the oven and brought up to temperature. A pressure of 0.75 PSI of argon was used on the inside of the tube to prevent the tube from caving in on itself during heating. Thin wafers of graphite were placed inside of the tube so that if the tube caved in, the opposite walls would not stick together and prevent raising them back to the wall of the mold. Argon was used to prevent the oxidation of these graphite wafers. When the oven was hot enough, the two halves of the graphite mold slid together on steel pegs. The mold was then allowed to cool down slowly, the graphite wafers were removed and side tubes installed and annealed. The tube was then painted with DuPont conductive paint No. 4760 and heated to 550°C to bake out the organic carrier. The mass tube was then installed in the mass spectrometer. The extreme ends of the mass tube were graded to kovar seals. These seals were heliarced to stainless steel rings which were used for mounting the source and collector parts. The source and collector envelopes were connected to the mass tube by ring seals just below the graded seals. The collector envelope had one pass through for the beam current made with a tungsten to uranium glass button seal.

The bakeout apparatus. The bakeout apparatus consisted of an oven built in three sections and a temperature controller which regulated the temperature of each section of the oven to ± 15°C for the range from room temperature to 420°C. The ovens were all open on the bottom and the floor of the mass spectrometer envelope mount was covered with fire brick to form the floor of the ovens for the source and collector. The mass tube oven floor had to be installed after the magnet had been withdrawn from the mass tube section. Three Assembly Products, Incorporated, meter relays were used in conjunction with chromel alumel thermocouples as the oven temperature controller.

D. Summary

The construction of the high vacuum mass spectrometer has been discussed. It was of particular value for this experiment because, first of all, the Kerwin analyzing field provides greater transmission and less dispersion than the normal type of analyzing field (such as the Nier type). Secondly, the elemination of a multiplier collector means that the effect of mass on collector efficiency is grossly reduced. For the absolute measurement of ionization efficiency, the assumptions of mass independence of the mass spectrometer is necessary when using potassium as a calibrating substance

for studying the rare earths. As a vacuum system the equipment was observed as low as 5×10^{-10} Torr and could be operated in the 10^{-9} Torr range for the major portion of most experiments.

XII. APPENDIX B: ATOM SOURCE POWER SUPPLIES

This appendix shows the schematic diagrams for the circuits used to control the cell temperature for low or high vapor pressure materials. The operation and use of these circuits is discussed in II-B-4-b.

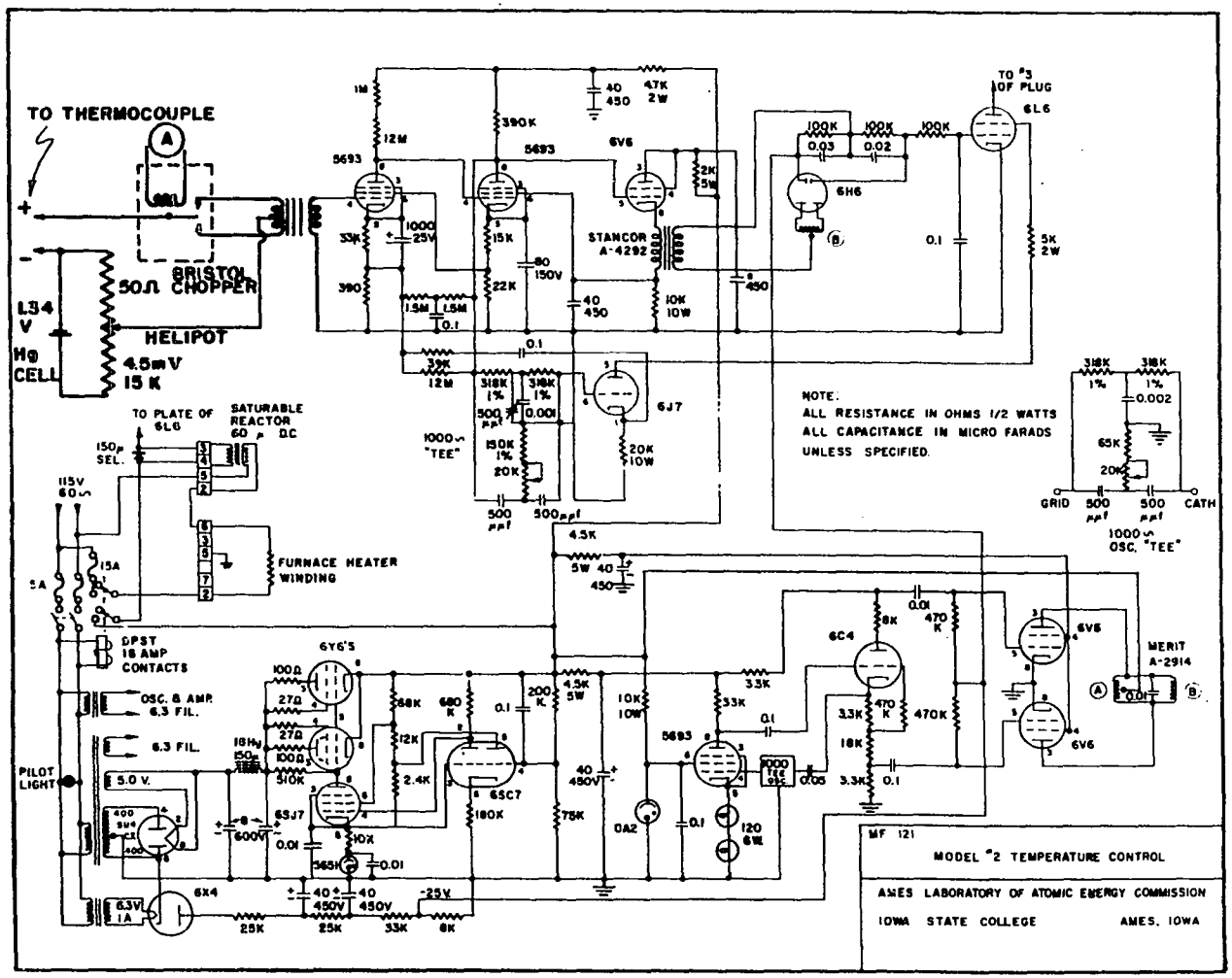

Figure 24. Schematic of circuit used for low cell temperatures

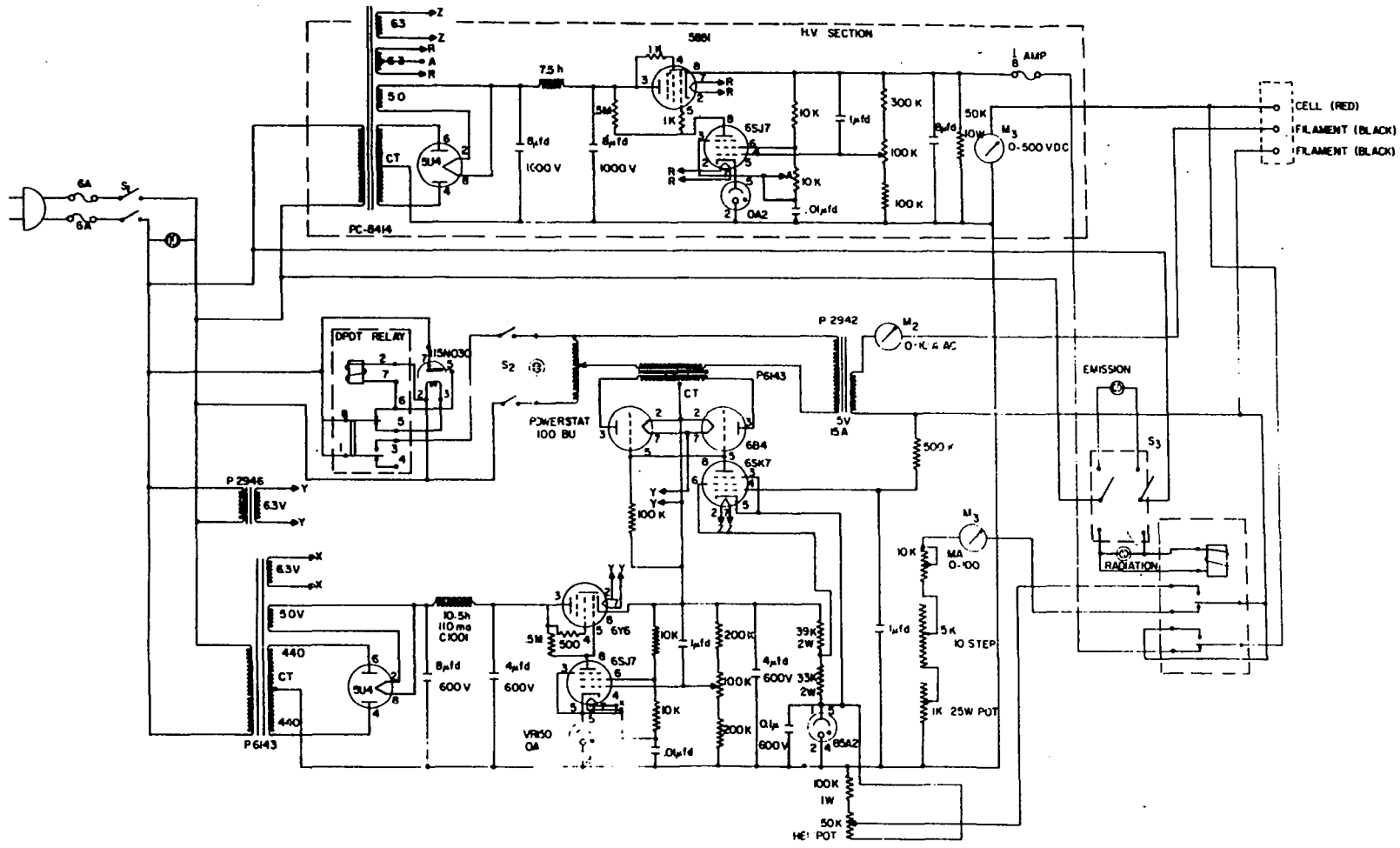

Figure 25. Schematic of circuit used for high cell temperatures

XIII. APPENDIX C: DATA FORMS

In this appendix a typical data form is displayed (Table 13) as well as the data (Table 14) used in the plotting of the typical graphs of the result section. Graphs showing the correlation of E and A with vacuum and atom flux are presented next.

Table 13. A typical data form

EXPERIMENTAL PHYSICS GROUP V

Sample Erbium Run 4-W8-Er4 Isotope 166 Date 3 Nov 63

Orifice Diameter 21.8 mils. Pressure 1.5×10^{-8} Torr

Cell Temperature 1149°C 1444°K Experimentalist Dresser

Lens Voltage 500 $\beta/I = 2.26 \times 10^{11}$ Time 4:23 p.m. (at point 8)

EXPERIMENTAL DATA

	ION CURRENT			FILAMENT TEMPERATURE				
Point no.	Upper reading 10^{-15} amps	Lower reading amps	Upper-lower	Obs. T °C	Corr T °C	True T °K	$10^4/T$ $°K^{-1}$	$\beta \times 10^4$
1	10.02	.66	9.36	1862	1882	2356	4.244	21.15
2	9.81	.66	9.15	1854	1874	2346	4.263	20.68
3	12.33	.66	11.67	1923	1945	2431	4.114	26.37
4	16.35	.63	15.72	2014	2038	2545	3.929	35.50
5	21.24	.63	20.61	2101	2127	2654	3.768	46.57
6	27.27	.63	26.64	2198	2227	2780	3.597	60.20
7	24.63	.63	24.00	2162	2189	2731	3.662	54.24
8	19.20	.63	18.57	2068	2094	2614	3.862	41.96
9	14.70	.63	14.07	1972	1995	2492	4.013	31.79
10	11.40	.63	10.77	1911	1932	2416	4.139	24.34
11	9.00	.63	8.37	1834	1854	2298	4.352	18.92
12	7.45	.72	6.73	1760	1773	2209	4.527	15.20
13	7.78	.72	7.06	1770	1783	2236	4.472	15.95
14	6.43	.69	5.74	1719	1735	2179	4.589	12.97
15	5.53	.69	4.84	1680	1701	2138	4.677	10.90
16	3.49	.69	2.80	1575	1594	2011	4.973	6.32
17	1.52	.69	0.83	1485	1502	1904	5.252	1.87
18	10.20	.69	9.51	1852	1872	2344	4.266	21.49

Table 14. Compilation of the data used in the typical curve plots

Erbium 6-W6-Er3		Erbium 4-W8-Er4		Gadolinium 4-W8-Gd1		Ytterbium 4-W8-Yb1	
β	T	β	T	β	T	β	T
.00190	2066	.00212	2356	.00628	2556	.00131	2410
.00117	1958	.00207	2346	.00634	2562	.00095	2329
.00273	2174	.00264	2431	.01004	2676	.00108	2356
.00400	2281	.00355	2545	.01034	2684	.00078	2268
.00674	2471	.00466	2654	.01158	2721	.00065	2230
.01226	2692	.00602	2780	.01297	2761	.00055	2179
.01603	2820	.00542	2731	.01333	2762	.00045	2146
.02158	2956	.00420	2614	.01531	2810	.00039	2109
.02862	3139	.00318	2492	.01764	2853	.00036	2110
.00677	2496	.00243	2416	.02383	2981	.00025	2030
		.00189	2298	.02066	2910	.00020	1986
		.00152	2209	.00485	2449	.00014	1922
		.00160	2236			.00013	1914
		.00130	2179			.00010	1870
		.00109	2138			.00008	1819
		.00215	2344			.00005	1766
						.00004	1718
						.00002	1631
						.00001	1554
						.00344	2709
						.00390	2759
						.00282	2635
E	1.44 ± .02		1.32 ± .02		2.01 ± .05		1.826 ± .006
A	5.85 ± .47		1.51 ± .15		60.0 ± 13.0		8.69 ± .31

Figure 26. Correlation of A and E with vacuum

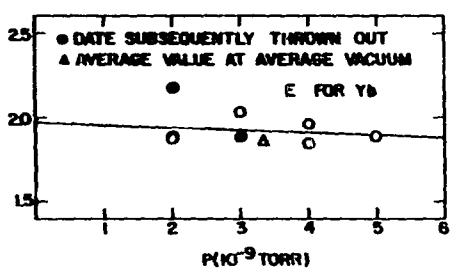
● DATE SUBSEQUENTLY THROWN OUT
Δ AVERAGE VALUE AT AVERAGE VACUUM
E FOR Yb
P(10⁻⁹ TORR)

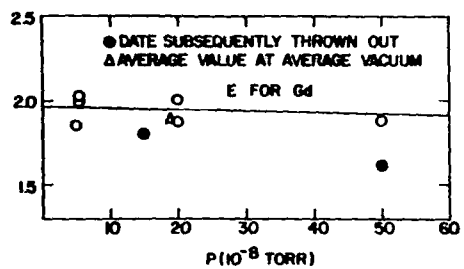
● DATE SUBSEQUENTLY THROWN OUT
Δ AVERAGE VALUE AT AVERAGE VACUUM
E FOR Gd
P(10⁻⁸ TORR)

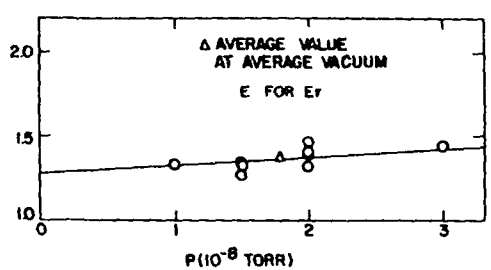
Δ AVERAGE VALUE
AT AVERAGE VACUUM
E FOR Er
P(10⁻⁸ TORR)

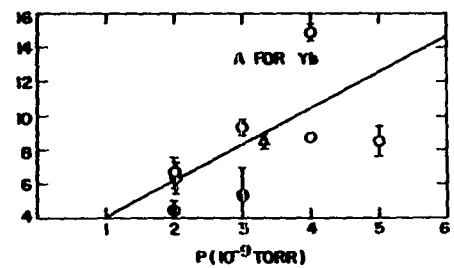
A FOR Yb
P(10⁻⁹ TORR)

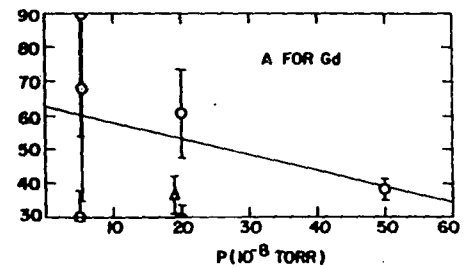
A FOR Gd
P(10⁻⁸ TORR)

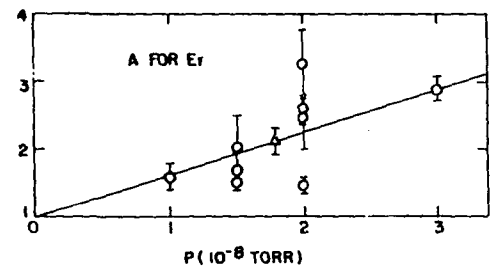
A FOR Er
P(10⁻⁸ TORR)

Figure 27. Effect of atom flux on A and E

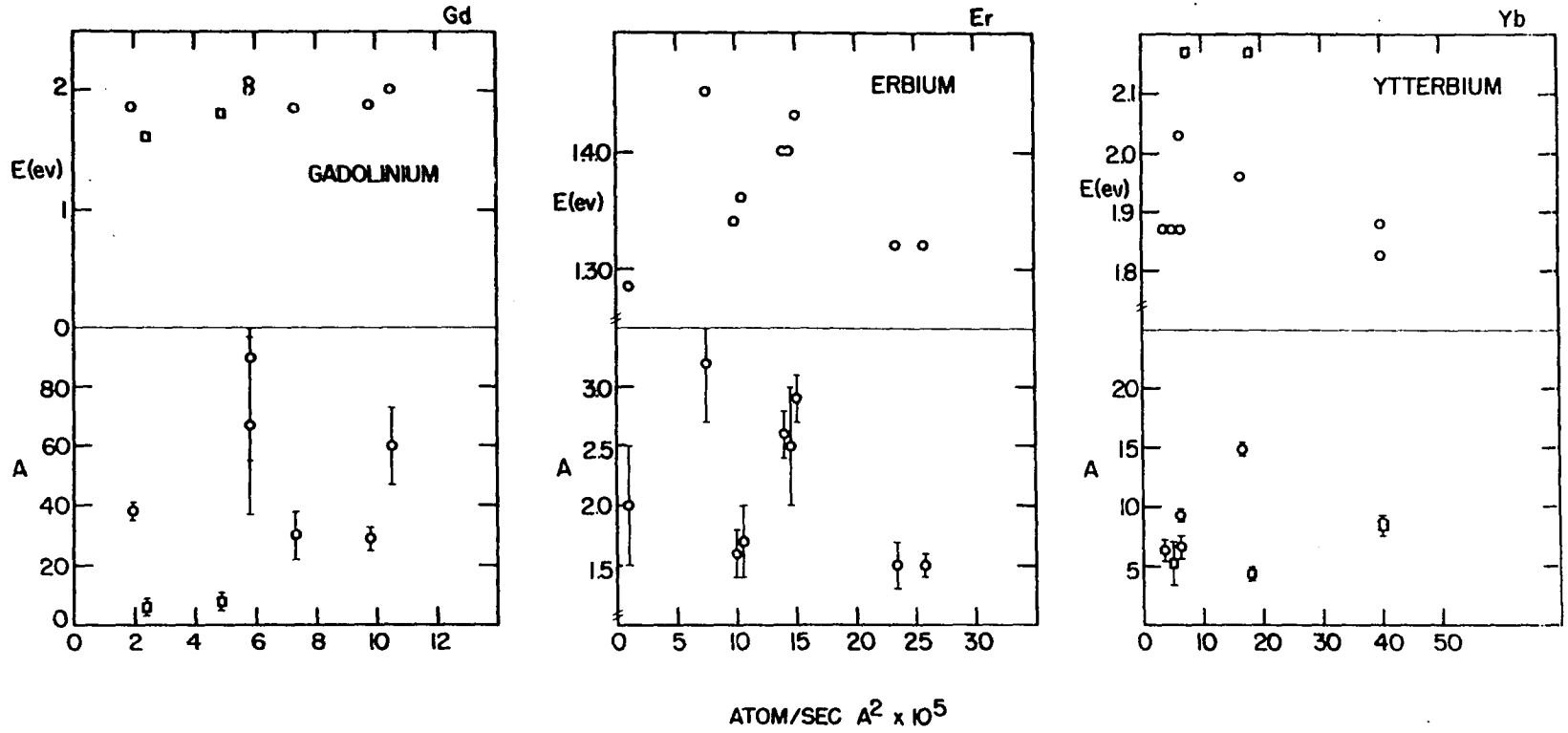
Gd
GADOLINIUM
E(ev)
A
Er
ERBIUM
E(ev)
A
Yb
YTTERBIUM
E(ev)
A
ATOM/SEC A² x 10⁵

XIV. APPENDIX D: ABSOLUTE CALIBRATION

The absolute calibration of the experiment was accomplished by using a sample of potassium whose ionization efficiency from a tungsten surface has been well established. The vapor pressure of potassium as a function of temperature has also been reported so that one can calculate the flux of atoms effusing from the atom source. From geometrical considerations we can therefore calculate the number of atoms that arrive at the filament. If we know how many atoms arrive at the filament and the ionization efficiency, we can calculate the number of ions leaving the filament. The transmission coefficient of the mass spectrometer is then the ratio of the number of ions per second (of a given isotope) arriving at the collector to the number of ions per second leaving the filament. We must make the reasonable assumption that the transmission coefficient is a constant for all masses for this particular source geometry. Using this assumption, we can calculate the number of ions leaving the surface of our filament. Furthermore, if we know the vapor pressure of the new atom source sample, we can calculate the number of atoms arriving at the filament per second and thus we have determined β absolutely as the ratio of the ions leaving the filament per second to the atoms arriving at the filament per second.

If one considers the Knudsen effusion out of a cell at temperature T_c, one can find from kinetic theory that the

number of atoms per second per unit solid angle is given by

$$n_k = a\ P \cos \chi/(2\pi^3\ m\ kT_c)^{1/2}, \tag{34}$$

where a is the orifice area, P is the pressure, χ is the angle between the beam and the normal to the effusion hole (for this work $\chi = 0$), and m is the atomic mass. All units are in the cgs system. If one then collimates this beam so that a region A of the filament (see Figure 28) is bombarded by atoms from the cell the number of atoms that arrive at the filament is given by

$$n = r^2 P\ A \cos \theta/R^2(2\pi\ m\ kT_c)^{1/2}, \tag{35}$$

where θ is the angle the beam makes with the normal to the filament, r is the radius of the orifice, and R is the distance from the effusion hole to the filament. The quantity A can be found from simple geometrical considerations to be given by

$$A = \frac{\pi d^2}{4} - \frac{d^2}{4}\left[2 \cos^{-1}(w/d) - \sin(2\cos^{-1} w/d)\right], \tag{36}$$

where d is the diameter of the beam when it strikes the filament of width w ($w < d$). One can also obtain d from geometrical considerations:

$$d = d_c X_f/X_c, \tag{37}$$

where d_c is the diameter of the last collimator and X_f and X_c are the distance from the effusion hole to the filament and collimator respectively. Thus we can write

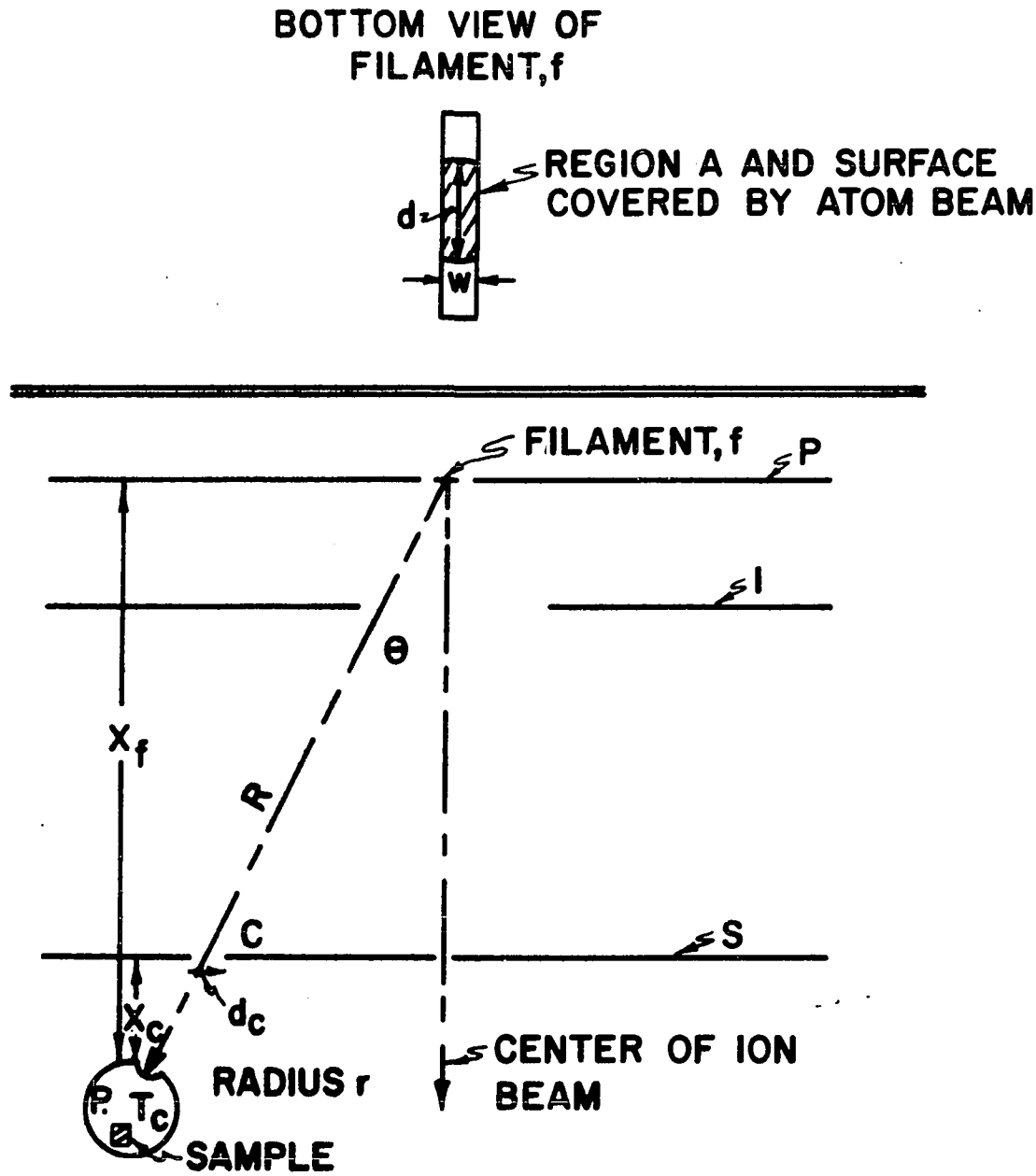

Figure 28. Schematic of source geometry with definitions of quantities used to calculate the atom flux to the filament

(38) $$n = C_s C_g \, P/T_c^{1/2},$$

where C_s is a constant dependent on the sample and orifice, and C_g is a constant dependent only on the source geometry. We can also include in C_g all the conversion factors necessary to convert the experimentally measured numbers to the cgs units required in Equation 35. C_g is then given by

(39) $$C_g = A \cos\theta (1.035 \times 10^{15})/R^2(2\pi k)^{1/2},$$

and C_s by

(40) $$C_s = r^2/m^{1/2}.$$

For the source geometry as given in Appendix A, we calculate

$$C_g = 2.01 \times 10^{20} \ (\text{sec}^{-1}\text{deg}^{1/2}\text{AMU}^{1/2} \ \text{mm of Hg}^{-1} \ \text{cm}^{-2}).$$

When we calculate Equation 38 we use P expressed in mm of Hg and we calculate C_s using r in cm and M in AMU.

P is given in Table 15 for the materials discussed in this dissertation.

The ionization efficiency of potassium is well known so that the number of ions (n_+) coming from the filament is just βn. We define a number B, the transmission coefficient of the mass spectrometer, to be the fraction of these ions that arrive at the collector. We can then determine B from the expression

(41) $$B = I_m/e \ f \ \beta \ n,$$

where I_m is the mass spectrometer current, e is the electronic

Table 15. Vapor pressure constants for $\log P = A - B/T_c$ (P in mm of Hg)

Material	A	B (°K)	Reference
Potassium[a]	7.338	4,500.4	(47)
Gadolinium	8.517	19,600	(48)
Erbium	9.222	17,324	(48)
Ytterbium	7.295	7,696	(48)

[a]These constants were calculated to fit this simple equation over our narrow temperature range using the more general equation of reference (47).

charge, and f is the relative abundance of the isotope being studied. Since I_m is a function of the lens plate voltage, the lens plate voltage is set for maximum current and it is then assumed that B is a constant for all isotopes. Since we now know B we can determine β for the rare earths absolutely by calculating n and measuring I. If measurements of a rare earth are made with the lens plate voltage at other than the maximum it is easy to tabulate the fraction of maximum beam current that occurs for different lens plate voltages. We thus calculate for every I an appropriate β from

$$\beta = I/efBnv, \tag{42}$$

where v is the fraction of maximum beam current that occurs for a given lens plate voltage. Figures 29, 30, 31 and 32 are plots of v versus V_L for K, Gd, Er, and Yb respectively.

Figure 29. Fraction of peak current, v, versus lens plate voltage, V_L, for potassium

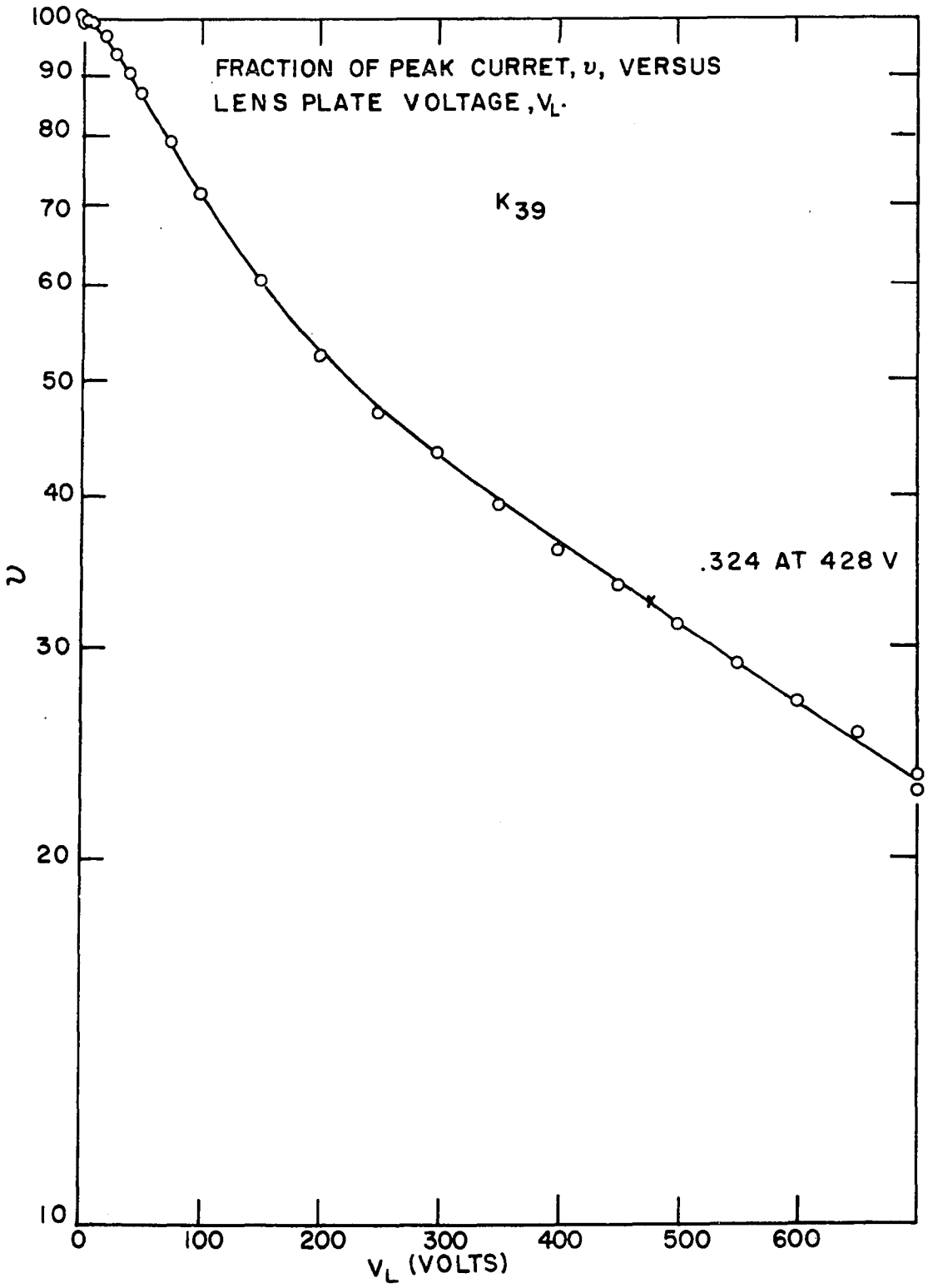
FRACTION OF PEAK CURRET, υ, VERSUS
LENS PLATE VOLTAGE, V_L.
K_{39}
.324 AT 428 V
υ
100
90
80
70
60
50
40
30
20
10
0
100
200
300
400
500
600
V_L (VOLTS)

Figure 30. Fraction of peak current, v, versus lens plate voltage, V_L, for gadolinium

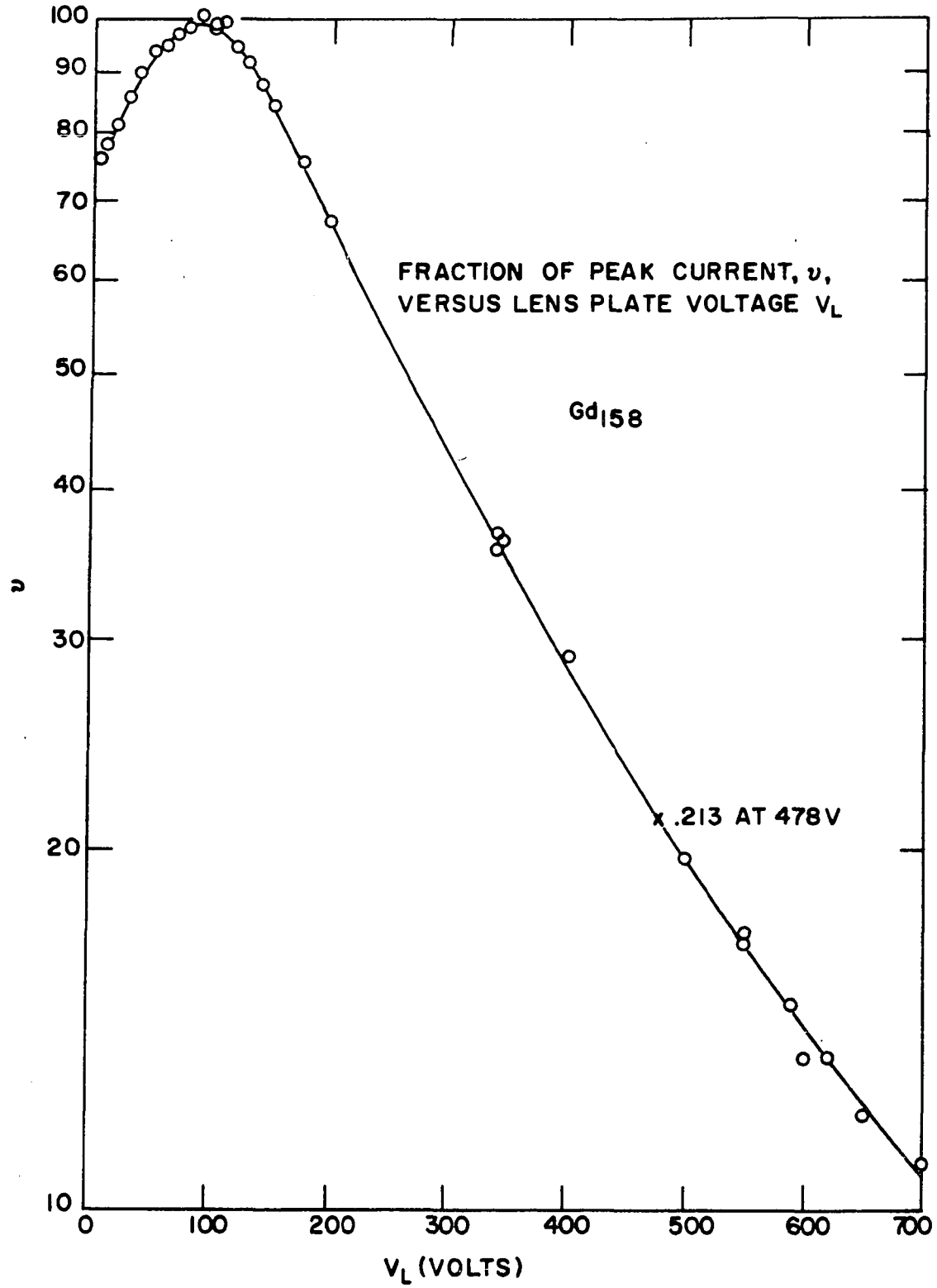
FRACTION OF PEAK CURRENT, υ,
VERSUS LENS PLATE VOLTAGE V_L
Gd_{158}
x .213 AT 478V
υ
100
90
80
70
60
50
40
30
20
10
0
100
200
300
400
500
600
700
V_L (VOLTS)

Figure 31. Fraction of peak current, v, versus lens plate voltage, V_L, for erbium

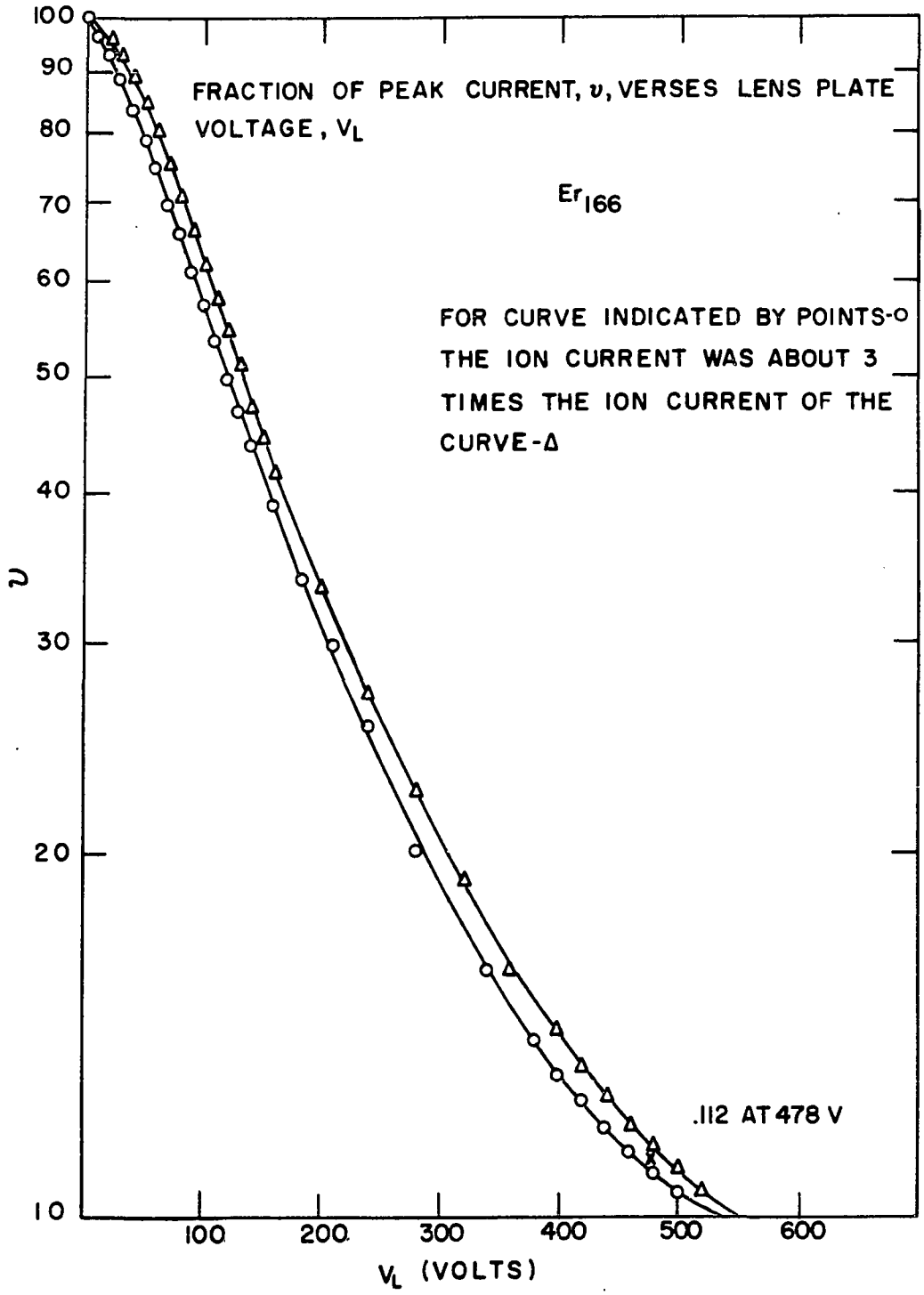
FRACTION OF PEAK CURRENT, υ, VERSES LENS PLATE VOLTAGE, V_L
Er_{166}
FOR CURVE INDICATED BY POINTS-o THE ION CURRENT WAS ABOUT 3 TIMES THE ION CURRENT OF THE CURVE-Δ
.112 AT 478 V
υ
100
90
80
70
60
50
40
30
20
10
100
200
300
400
500
600
V_L (VOLTS)

Figure 32. Fraction of peak current, v, versus lens plate voltage, V_L, for ytterbium

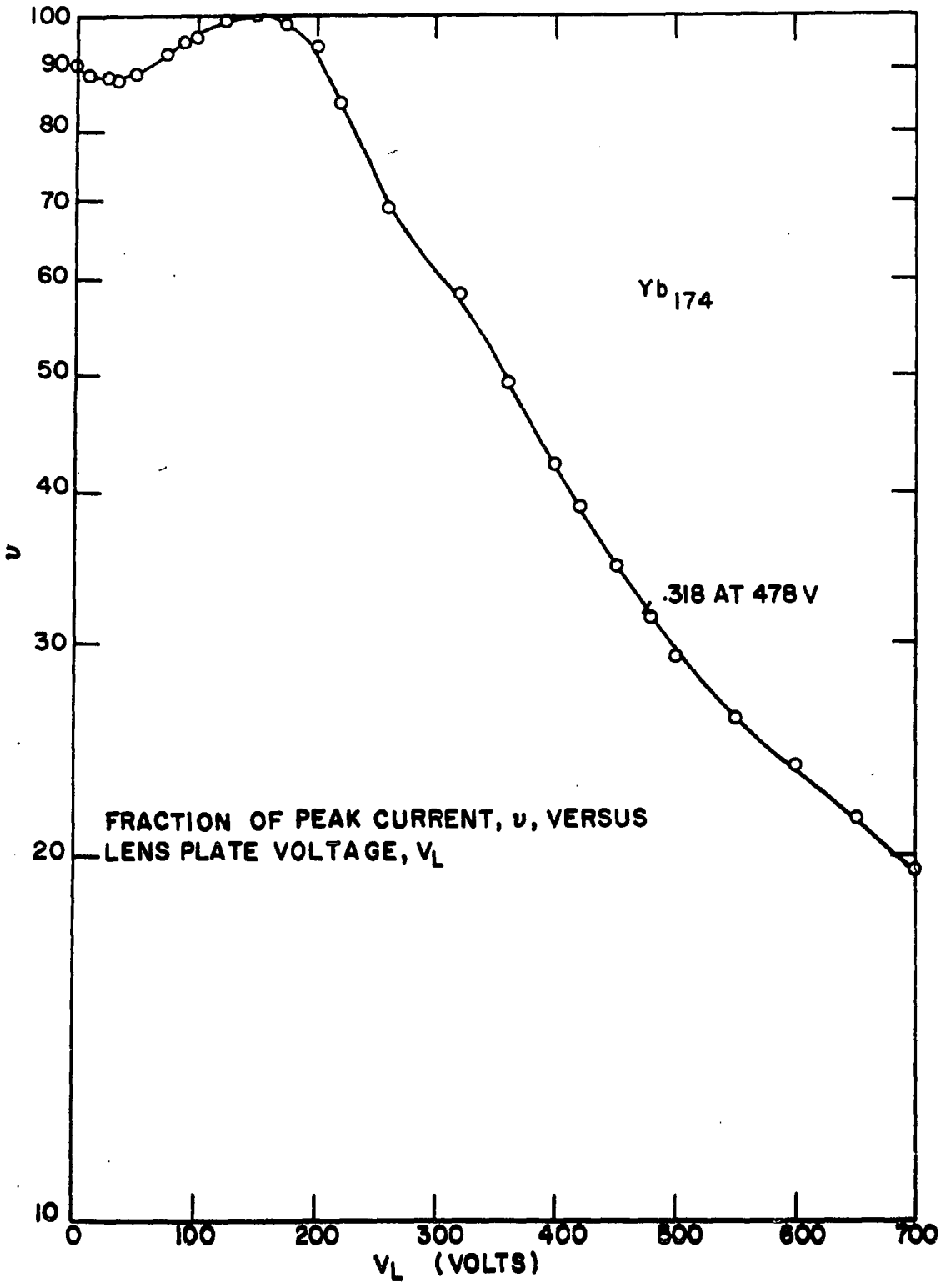
100
90
80
70
60
50
40
30
20
10
υ
Yb 174
.318 AT 478 V
FRACTION OF PEAK CURRENT, υ, VERSUS
LENS PLATE VOLTAGE, V_L
0
100
200
300
400
500
600
700
V_L (VOLTS)

XV. APPENDIX E: SAMPLE CALCULATION OF Q_+/Q_o FOR Gd

In this appendix we will summarize the calculation of Q_+/Q_o for gadolinium at 2500°K or kT = 0.215 eV. From Equation 18 we have Q_+ and Q_o defined as follows:

$$Q_+ = g_+ + \sum_j g_+^j \, e^{-E_j^+/kT}, \text{ and}$$

(18)

$$Q_o = g_o + \sum_j g_o^j \, e^{-E_j^o/kT}.$$

The values of g_o^j, g_+^j, E_j^o, and E_j^+ are given in Table 10. The result of the calculation of each term of these series is then listed in Table 16.

Table 16. The terms of Q_+ and Q_o

	Q_+		Q_o	
j	g_+^j	$e^{-E_j^+/kT}$	g_o^j	$e^{-E_j^o/kT}$
0	6	1.	5	1.
1	8	.8600	7	.8801
2	10	.6940	9	.736
3	12	.5116	11	.562
4	14	.3279	13	.372

We now have these terms summed to give the results

$Q_+ = 6 + 8\ (.8600) + 10\ (.6940) + 12\ (.5116) + 14\ (.3279)$

$= 30.56$ and

$Q_o = 5 + 7\ (.8801) + 9\ (.736) + 11\ (.562) + 13\ (.372) = 28.78.$

The coefficient A is then equal to 1.06.

Figure 32. Fraction of peak current, v, versus lens plate voltage, V_L, for ytterbium